Development of novel organic optoelectronic technologies for biomedical applications

Shahab Rezaei Mazinani


N°d'ordre NNT : 2017LYSEM028

THESE de DOCTORAT DE L'UNIVERSITE DE LYON

opérée au sein de

l'Ecole des Mines de Saint-Etienne

Ecole Doctorale N° 488
Sciences, Ingénierie, Santé

Spécialité de doctorat : Microélectronique
Discipline : Bioélectronique Organique

Soutenue publiquement le 16/10/2017, par :
Shahab REZAEI MAZINANI

Development of Novel Organic Optoelectronic Technologies for Biomedical Applications

---

Devant le jury composé de :

Président :	Christophe Bernard	Directeur de recherche 1, INSERM, Aix-Marseille Université
Rapporteurs :	John de Mello	Professor, Imperial College London
	Alexander Fleischmann	Chargé de recherche 1, INSERM, Collège de France
Examinateurs :	Andreas Offenhäusser	Professor, Forschungszentrum Jülich, Helmholtz-Gemeinschaft
	Paschalis Gkoupidenis	Group leader, Max Planck Institute for Polymer Research
Directeur de thèse :	George Malliaras	Professor, Ecole des Mines de Saint-Etienne
Co-encadrante :	Esma Ismailova	Associate Professor, Ecole des Mines de Saint-Etienne

Spécialités doctorales	Responsables :	Spécialités doctorales	Responsables
SCIENCES ET GENIE DES MATERIAUX	K. Wolski Directeur de recherche	MATHEMATIQUES APPLIQUEES	O. Roustant, Maître-assistant
MECANIQUE ET INGENIERIE	S. Drapier, professeur	INFORMATIQUE	O. Boissier, Professeur
GENIE DES PROCEDES	F. Gruy, Maître de recherche	SCIENCES DES IMAGES ET DES FORMES	JC. Pinoli, Professeur
SCIENCES DE LA TERRE	B. Guy, Directeur de recherche	GENIE INDUSTRIEL	X. Delorme, Maître assistant
SCIENCES ET GENIE DE L'ENVIRONNEMENT	D. Graillot, Directeur de recherche	MICROELECTRONIQUE	Ph. Lalevée, Professeur

EMSE : Enseignants-chercheurs et chercheurs autorisés à diriger des thèses de doctorat (titulaires d'un doctorat d'État ou d'une HDR)

ABSI	Nabil	CR	Génie industriel	CMP
AUGUSTO	Vincent	CR	Image, Vision, Signal	CIS
AVRIL	Stéphane	PR2	Mécanique et ingénierie	CIS
BADEL	Pierre	MA(MDC)	Mécanique et ingénierie	CIS
BALBO	Flavien	PR2	Informatique	FAYOL
BASSEREAU	Jean-François	PR	Sciences et génie des matériaux	SMS
BATTON-HUBERT	Mireille	PR2	Sciences et génie de l'environnement	FAYOL
BEIGBEDER	Michel	MA(MDC)	Informatique	FAYOL
BLAYAC	Sylvain	MA(MDC)	Microélectronique	CMP
BOISSIER	Olivier	PR1	Informatique	FAYOL
BONNEFOY	Olivier	MA(MDC)	Génie des Procédés	SPIN
BORBELY	Andras	MR(DR2)	Sciences et génie des matériaux	SMS
BOUCHER	Xavier	PR2	Génie Industriel	FAYOL
BRODHAG	Christian	DR	Sciences et génie de l'environnement	FAYOL
BRUCHON	Julien	MA(MDC)	Mécanique et ingénierie	SMS
CAMEIRAO	Ana	MA(MDC)	Génie des Procédés	SPIN
CHRISTIEN	Frédéric	PR	Science et génie des matériaux	SMS
DAUZERE-PERES	Stéphane	PR1	Génie Industriel	CMP
DEBAYLE	Johan	MR	Sciences des Images et des Formes	SPIN
DEGEORGE	Jean-Michel	MA(MDC)	Génie industriel	Fayol
DELAFOSSE	David	PR0	Sciences et génie des matériaux	SMS
DELORME	Xavier	MA(MDC)	Génie industriel	FAYOL
DESRAYAUD	Christophe	PR1	Mécanique et ingénierie	SMS
DJENIZIAN	Thierry	PR	Science et génie des matériaux	CMP
DOUCE	Sandrine	PR2	Sciences de gestion	FAYOL
DRAPIER	Sylvain	PR1	Mécanique et ingénierie	SMS
FAUCHEU	Jenny	MA(MDC)	Sciences et génie des matériaux	SMS
FAVERGEON	Loïc	CR	Génie des Procédés	SPIN
FEILLET	Dominique	PR1	Génie Industriel	CMP
FOREST	Valérie	MA(MDC)	Génie des Procédés	CIS
FRACZKIEWICZ	Anna	DR	Sciences et génie des matériaux	SMS
GARCIA	Daniel	MR(DR2)	Sciences de la Terre	SPIN
GAVET	Yann	MA(MDC)	Sciences des Images et des Formes	SPIN
GERINGER	Jean	MA(MDC)	Sciences et génie des matériaux	CIS
GOEURIOT	Dominique	DR	Sciences et génie des matériaux	SMS
GONDRAN	Natacha	MA(MDC)	Sciences et génie de l'environnement	FAYOL
GONZALEZ FELIU	Jesus	MA(MDC)	Sciences économiques	FAYOL
GRAILLOT	Didier	DR	Sciences et génie de l'environnement	SPIN
GROSSEAU	Philippe	DR	Génie des Procédés	SPIN
GRUY	Frédéric	PR1	Génie des Procédés	SPIN
GUY	Bernard	DR	Sciences de la Terre	SPIN
HAN	Woo-Suck	MR	Mécanique et ingénierie	SMS
HERRI	Jean Michel	PR1	Génie des Procédés	SPIN
KERMOUCHE	Guillaume	PR2	Mécanique et Ingénierie	SMS
KLOCKER	Helmut	DR	Sciences et génie des matériaux	SMS
LAFOREST	Valérie	MR(DR2)	Sciences et génie de l'environnement	FAYOL
LERICHE	Rodolphe	CR	Mécanique et ingénierie	FAYOL
MALLIARAS	Georges	PR1	Microélectronique	CMP
MOLIMARD	Jérôme	PR2	Mécanique et ingénierie	CIS
MOUTTE	Jacques	CR	Génie des Procédés	SPIN
NEUBERT	Gilles			FAYOL
NIKOLOVSKI	Jean-Pierre	Ingénieur de recherche	Mécanique et ingénierie	CMP
NORTIER	Patrice	PR1	Génie des Procédés	SPIN
O CONNOR	Rodney Philip	MA(MDC)	Microélectronique	CMP
OWENS	Rosin	MA(MDC)	Microélectronique	CMP
PERES	Véronique	MR	Génie des Procédés	SPIN
PICARD	Gauthier	MA(MDC)	Informatique	FAYOL
PIJOLAT	Christophe	PR0	Génie des Procédés	SPIN
PINOLI	Jean Charles	PR0	Sciences des Images et des Formes	SPIN
POURCHEZ	Jérémy	MR	Génie des Procédés	CIS
ROUSSY	Agnès	MA(MDC)	Microélectronique	CMP
ROUSTANT	Olivier	MA(MDC)	Mathématiques appliquées	FAYOL
SANAUR	Sébastien	MA(MDC)	Microélectronique	CMP
STOLARZ	Jacques	CR	Sciences et génie des matériaux	SMS
TRIA	Assia	Ingénieur de recherche	Microélectronique	CMP
VALDIVIESO	François	PR2	Sciences et génie des matériaux	SMS
VIRICELLE	Jean Paul	DR	Génie des Procédés	SPIN
WOLSKI	Krzystof	DR	Sciences et génie des matériaux	SMS
XIE	Xiaolan	PR1	Génie industriel	CIS
YUGMA	Gallian	CR	Génie industriel	CMP

Mise à jour : 03/02/2017

École Nationale Supérieure des Mines de Saint-Étienne

NNT°: 2017LYSEM028
Shahab REZAEI MAZINANI

DEVELOPMENT OF NOVEL ORGANIC OPTOELECTRONIC TECHNOLOGIES FOR BIOMEDICAL APPLICATIONS

Speciality: Microelectronics
Key words: Organic photodetector, bulk heterojunction, biomedical devices, bioelectronics, optical electrophysiology
Abstract:
Organic optoelectronic devices have many promising qualities for biomedical applications. Organic photodetectors (OPD), one type of such devices, have yet to be utilized for the detection of signals in the brain, to the best of our knowledge. The goal of this thesis was to explore the use of OPDs, based on different electron-donor and -acceptor materials in neuroscience applications. Different types of minimal-structure OPDs are presented, which have an excellent sensitivity and a high potential for incorporation into existing microfabrication methods. The organic sensors were utilized for monitoring the brain's intrinsic optical signals and fluorescent calcium dynamics. Additionally, another aspect of these devices is presented (in combination with organic electrochemical transistors (OECT)): neuroinspired electronics, electronics that mimic biology. This thesis establishes the promise of OPDs for monitoring brain activities, which would lead to their integration, as high-sensitive micron-scale optical sensors in organic neural probes. Such device would result in exploring optical biological activities in the deep brain on the cellular level and would push the frontiers of optical-electrophysiology by giving a better understanding of complex mechanisms of the brain function and neurodegenerative diseases.

École Nationale Supérieure des Mines de Saint-Étienne

NNT°: 2017LYSEM028
Shahab REZAEI MAZINANI

DEVELOPPEMENT DES TECHNOLOGIES OPTOELECTRONIQUES A BASE DES MATERIAUX ORGANIQUES POUR LES APPLICATIONS DANS LE BIOMEDICAL

Spécialité : Microélectronique
Mots clefs : Photodétecteur organique, bulk heterojunction, applications biomédicales, bioélectronique, électrophysiologie optique
Résumé:
Les dispositifs optoélectroniques organiques possèdent plusieurs avantages pour les applications dans le domaine du biomédical. Le photodétecteur organique (OPD) est un type de dispositif optoélectronique qui n'est pas encore utilisé pour la détection d'activité cérébrale. L'objectif de cette thèse a été d'explorer l'utilisation des OPD, constitués de différent matériaux donneur-accepteur d'électrons, dans le domaine des neurosciences. Nous avons présenté différent types d'OPD possédant une structure minimale, une excellente sensibilité et un grand potentiel d'intégration dans les méthodes de microfabrication existantes. Les détecteurs organiques ont été utilisés pour l'enregistrement de signaux optiques intrinsèques et de signaux fluorescents reflétant l'activité du calcium dans le cerveau. De plus, un autre aspect des OPD est présenté (en combinaison avec les transistors électrochimiques organiques (OECT)) : des systèmes électroniques biomimétiques basé sur une architecture électronique neuro-inspirée. Cette thèse démontre le potentiel des OPD pour enregistrer des activités cérébrales. Elle ouvre une nouvelle perspective, grâce à leur grande sensibilité, comme capteur optique en combinaison avec des dispositifs neuronaux implantables. Ceci élargira les frontières de l'électrophysiologie optique pour explorer les mécanismes complexes du cerveau et des maladies neurodégénératives.

Acknowledgements

I believe that the perception of time, in a sense that how fast or slow it passes is a personal point of view and depends on many factors, such as daily life or professional occupations and of course age. This rises two questions: Why when we are very young, sweet summer time is long and one hour waiting feels like one day? Why we're in the end of our third decade of life, one day can pass like one hour? There are many explanations on how the time accelerates by ageing to our vision, but I am not going in this direction.
My view about how the three years of my PhD life passed, is a paradox. I see it as the fastest slow-time of my life! A progressive accomplishment of aims, while practicing patience and exploring new horizons. Lights and shades passed and the passion of searching for knowledge *blowed me hither and thither in a wayward course* [Bertrand Russell]. A lot of events and changes happened so fast that I coud not find their time.
It was my pleasures to be among great scientists at the department of Bioelectronics (BEL), where I found my self always at home and at Traverse, where I found my home. I did my PhD in this exceptional department where there was a life going on beside work, because of the people who were part of it and the people who established it with their philosophy; George Malliaras and Roisin Owens.
I owe the greatest thanks to my supervisors, George Malliaras and Esma Ismailova for the best opportunities that they provided me during these three years. I am always thankful of Esma who, gave me the opportunity to join BEL; an occasion that changed my life. I am grateful of all the kind supports and attentions of George, who will be always a role-model for me in life. It was a unique chance to work with the philosophy of freedom in research in BEL.
It was a big change in my life to move from Vienna to Aix-en-Provence. This led to finding Aix-en-Provence my home with the enormous kindness of my French family "les Faillards".
Durant ces années, j'ai profité du soutien de l'Ecole des Mines, en particulier Esma, George, M. Lalevée, Mme. Villaréal, Mme. Jamen, M. Duflot, M. Ray.
I will always remember the presence of these people beside my supervisors, who gave shape to my PhD: Paschalis Gkoupidenis, Anton Ivanov, Alexandra Rutz and Rodney O'Connor. Pascalis taught me how to think when facing a problem and how to find the way to solve it, in nutshell academic thinking. This was not just limited to conducting a research, but also invaluable lessons in life and I will always be grateful. I thank Anton for all his supports during my PhD. He supervised me in neuroscience and electrophysiology and showed me how to find my way in this domain. I would like to thank Christophe Bernard, his research group and especially

Anton for always welcoming me warmly. Without this freedom at Christophe's lab it would not have been possible to achieve this work. Alexandra taught me scientific writing, how to see my research in different angles and how to present it. Scientific writing needs a lot of practice, corrections and patience. Incredibly, she never refused to put her valuable time to correct me. I am grateful of all the kind attentions of Rod shaping the final phase of my PhD by bringing new aspects and motivating me to push the project forward. I am always thankful that he presented me Paris Neuroscience School, which had a big influence on the final phase of my PhD and also my post-doctoral carrier. I would like to thank Esma, George and Rod for their invaluable supports, to send me to this school, where I found this opportunity to meet the excellent neuroscience community of Paris.
During these years in BEL, I had several precious occasions of meeting great professors who visited our department for sabbatical. Among them, I had the honour of working with Professor John de Mello, who supervised me in optoelectronics. I am grateful for his invaluable supports during the second year along with Kirsty Roy. It was my pleasure to meet Professor David Martin and his family, who taught me precious lessons in life.
I had the honour of being representative of PhD student at the graduate school, where I had the chance of meeting remarkable people, including M. Desrayaud, and to experience the French democratic system in fine details. For this, I should thank all the PhD students who chose me as their representative; Véronique for giving me the motivation to candidate myself and George for his supports. Going to Saint-Étienne, communicating thoughts and difficulties of PhD students and participating in important decisions were a unique experiences that I will always remember as a highlight in my activities during these three years.
The flowing life in BEL was of course was because of its amazing people. I would like to thank Jolien, my friend and amazing office-mate, for listening to always and for the best moments during three years. I will always remember my kind friends Anna-Maria and Mahmoudy, with whom we started our PhD together and finished together as well. I thank my friend Thomas for his helps during these three year and also for his kind attentions to improve my French. I would like to thank my friend Ilke for all the fun moments and all his helps. I thank my friend Gerwin for the best moments and for his patience to listen to me always. I thank Sophia for her input (page 52) during her one month internship with me and for the best moments. I would like to thank all my friends and colleagues for the best memories and fruitful discussions and good supports, Chris, Isabel, Sahika and Robert, Mary and Adam, Babis, Ana, Jake, Adel, Michel, Vincenzo and Viviana, Marcel, Seiichi, Johnathan and Liza, Eloïse, Yi, Donata, Marc, Susan, Miriam, Bastien, Séverine, Pierre, Dimitris, Magali, Aimie, Federica, Clemens, Carol and Amale.
I would like to thank the technical staff of the clean room at "Centre Charpak", in particular Gaëlle Rondeau, Thierry Camilloni, Sylvain Nolot, Cyril Calmes and Jessica Mazuir for all their works. Without their support BEL's scientific achievements would not have been possible. I would like to thank also the administrative staff of Centre Charpak, especially Michelle Gillet and Anaïs Balaguer for their works in the background of our research, which are crucial for the functioning of the system.
La vie est pleine de coïncidences. Si j'ai connu l'Ecole des Mines et BEL, c'est grâce à mon cher

ami Amir-Pasha. Je suis reconnaissant de toutes ses aides et attentions pendant mon doctorat. Je remercie infiniment mon cher professeur, Armand, pour m'avoir soutenu durant neuf ans et pour m'avoir enseigné l'excellence de la culture et de la pensée scientifiques.
Quand je contemple cette période, je trouve la présence de ma chère et adorable Lucie, qui a soufflé une nouvelle joie dans ma vie. Je suis reconnaissant de sa patience, de son attention et de son encouragement qui m'ont donné la force pour réussir la dernière année de mon doctorat. Je remercie également sa famille.
In the end, I dedicate this thesis to my family, who brought me their best support through all the stages to provide me the best conditions. Without them it would not have been possible to achieve PhD. All my love to my parents, aunts and uncle.

Connais-tu le pays où les citronniers fleurissent, où, dans la feuillée sombre, rougissent les oranges d'or ? Un vent léger descend du ciel bleu, le myrte croît discret, et le laurier superbe, le connais-tu bien ?
Johann Wolfgang von Goethe
Les années d'apprentissage de Wilhelm Meister
1796

Gardanne, 8 septembre 2017 S. RM.

Contents

List of Figures

Abstract

Optical measurement is one of the most widely-used methods in biology and medicine. The scope of the applications of this method is so broad that includes from monitoring different diseases in a whole organism like brain (e.g. MRI scan) to investigating biological mechanisms in one neuron. This method in biology has shown tremendous advancements for monitoring metabolism, gene expression, dynamics of free ions and ion channels. Optical measurement encompasses microscopy techniques and light detector devices such as built-in high affinity silicon photodetectors in commercially available cameras.
Generally in neuroscience, optical activities are reported using two methods, i.e. monitoring of label-free optical activities of the brain tissue exposed to a light source and visualizing dynamics of ions and ion channels using optical and fluorescent indicator dyes (genetically and chemically labeled). The first method reports the effect of cell swelling and shrinkage arising form different cellular mechanisms such as cell volume regulation and metabolism, which is still not completely known. The second method reports functional aspects of cellular and neuronal network signalling, indicating how electrical signals, such as action potentials integrate in cells and neuronal network. Among different types of ions, calcium $(Ca)^{2+}$ is almost involved in all the biological processes and generates versatile signals. Understanding its functions helps to broaden our knowledge about fundamental mechanisms in life science. Undoubtedly, light detector devices and sensors play an important role for presenting opt-electrophysiological activities. The widely used charge-coupled device (CCD) and metal-oxide-semiconductor (CMOS) cameras based on inorganic photodetectors have shown to have certain drawbacks, such as relatively high noise level (high dark current density (DCD) of silicon photodetectors) and relatively slow image scanning unit, which make them less suitable for detecting very fast and low-amplitude activities. On the other hand, the cost of optimizing these systems is high. This is why there are new trends in developing and employing organic photodetector (OPD) devices in imaging and sensor systems, since they are low-cost, highly sensitive and offer the tunability of their chemical and physical characteristics. These organic devices have shown important improvements in the critical parameters for optical detection, such low DCD, hence a better performance than their inorganic counterparts.
Investigation of the OPD performance for optical detection in biomedical applications, sets the aim of this PhD thesis.
The *first chapter* intends to present an overview on the related concepts of this work, from understanding of fundamentals of the dynamics of ions in the brain and organic optoelectron-

ics to the state-of-the art of highly-sensitive OPD devices, which are also used in imaging and sensor systems. A brief summery of critical criteria for reaching high sensitivity in OPD will be described, such as linear dynamic range (LDR) and low DCD. This will give the idea of how OPD devices are finding their place in optical sensor applications.
In the *second chapter* the great potential of widely-used and well-known active materials, i.e. poly(3-hexylthiophene-2,5-diyl) (P3HT) and [6,6]-Phenyl C61 butyric acid methyl ester ($PC_{60}BM$), in biomedical optical detection will be presented. After an overview on the instrumentation issues in label-free optical imaging and the state-of-the-art of the biomedical application of optoelectronic devices, it will be shown how OPD resolves the issue of real-time recording of electrophysiological and optical signals in pathophysiological and physiological conditions.
Then, the *third chapter* focuses on the application of a new polymer eXtra Large Bandgap Polymer (XPL6) blended with [6,6]-Phenyl C70 butyric acid methyl ester ($PC_{70}BM$) with tailored optoelectronic properties for the detection of near-UV fluorescent activities of Ca^{2+} ions. These ions were marked with a chemical fluorescent indicator dye. This chapter starts with an introduction to the state-of-the-art and the current methods of light detection in fluorescent microscopy. Then after giving an overview on the latest advancements in the biomedical applications of organic optoelectronic devices, the great potential of this highly sensitive device in detecting ultra-low amplitude $PC_{70}BM$ signals will be demonstrated both *in-vitro* and *ex-vivo*.
Furthermore, the *fourth chapter* aims to demonstrate the potential of neuro-inspired functions and architectures in designing electronic systems. Neuro-inspired electronics is a new trend, where the goal is to integrate models of the efficient data processing mechanisms of neuronal networks for their simplicity and efficiency for novel designs of electronic devices. This work shows the reproducing the neuromorphic function of orientation selectivity (a phenomenon in the visual cortex) by combining OPD and organic electrochemical transistor (OECT) for emulating the visual system's function. After an introduction to the current trends of OECT and neuro-inspired devices, it will be shown that OPD is used as a simple model of the retina in combination with OECT for emulating the receptive field and the visual cortex cell activity.
In the *final chapter*, the main results that were obtained during this PhD will be summerized and discussed, then future perspectives will be introduced.

Key words: Organic photodetector, bulk heterojunction materials, biomedical devices, bioelectronics, optical electrophysiology

1 Background and State-of-the-Art

1.1 The nervous system

The brain serves as the most sophisticated organ in the nervous system of all vertebrate animals. The nervous system (Figure 1.1) is a complex system, whose appropriate functionality depends on its elementary components, their interconnections and organization [1]. This system receives a big amount of information from sensory system then integrates them, in order to determine body reactions [2].

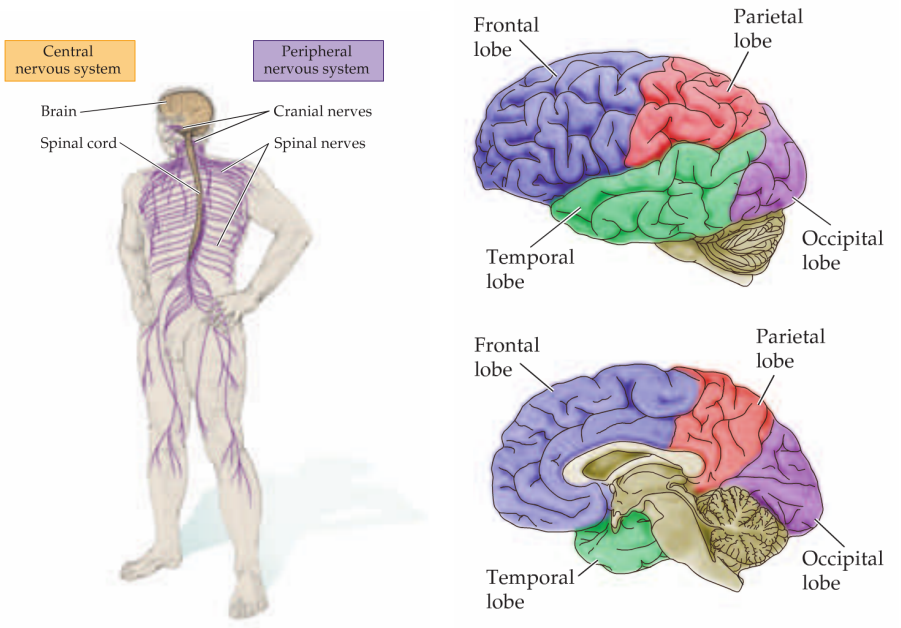

(a) Central Nervous System. (b) Human Brain.

Figure 1.1 – The the principal regions of human's Central Nervous System. Adapted from [3].

1.1.1 Neurons and glia cells and cellular diversity in the nervous system

The central nervous system consists of more than 100 billion neurons and several times as many supporting cells. In this system, cells can be divided into two broad categories: the nerve cells, neurons, and supporting cells called neuroglia (or glia) [2, 3]. A neuron (Figure 1.2a) receives incoming signals through synapses that are located majorly on the neuronal dendrites and cell body. Depending on the type of neurons, there might be a few hundreds to more than 200,000 synaptic connections (Figure 1.2b) from input fibers. Conversely, the output signal leaves the neuron from an axon. Then, the axon contains many branches to other cells and parts of the nervous system. Most synapses have the special feature that the signal normally propagates in the forward direction, from the preceding neuron's axon terminal to dendrites of subsequent neurons. This feature is crucial for specific nervous functions [2, 3]. In contrast to neurons, supporting cells are not capable of electrical signalling. There exists three kinds of glia cells: astrocytes, oligodendrocytes, microglial cells (Figure 1.2c). The major function of astrocytes is to conserve physiological chemical conditions for neurons. Oligodendrocytes function is to form myelin of neural axons. And microglial cells are involved in defence mechanism against external bodies. Neurons and glia have many similar typical cell compartments in common, including mitochondria and a variety of vesicular structures [3]. The diversity of cell types in the nervous system is wider than any other organ. This can be categorizied by physiological activity, morphology and molecular identity etc. Undoubtedly, the great cellular diversity of the nervous system is one of the most important factors of the capacity of its complicated networks that are mediated by sophisticated behaviours [3].

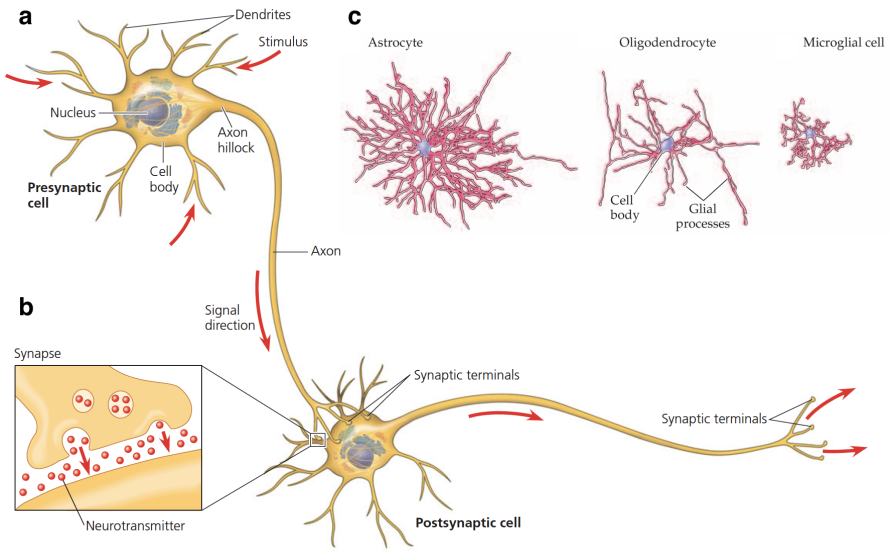

Figure 1.2 – **a)** Structure of a neuron, consisted of a cell body, an axon and multiple dendrites. **b)** Structure of a synapse, for connecting the axon of one neuron to the dendrite/soma of another. **c)** Different neuroglial cells in the Central Nervous System. Adapted from [3].

1.1.2 Synapses

The synapse is the junction point of consecutive neurons. It determines the spreading direction of neuronal signals though the nervous system. The synaptic transmission of signals can be easy or difficult, depending on the synapse type. Also synaptic transmission can be controlled by inhibitory or excitatory signals from other regions of the nervous system, such as opening and closing synapses in a specific neural circuit. In addition, the response of some postsynaptic neurons can be with a large or few number or output impulses. Therefore, the synaptic performance is highly selective and versatile, like often blocking of weak signals while passing strong ones and amplification of some weak signals and channeling them in different directions [2] (Figure 1.3). The two main types of synapses are chemical and electrical. In a chemical synaptic connection, one preceding neuron emits a chemical substance called a neurotransmitter, which bonds to receptor proteins in the next neuron's membrane for variety of functions, such as excitation, inhibition or modification of the sensitivity. More than 40 important neurotransmitters have been discovered thus far. Some of the best known are acetylcholine, norepinephrine, epinephrine, histamine, gamma-aminobutyric acid (GABA), glycine, serotonin, and glutamate [2]. Electrical synaptic connection functions based on allowing passive ionic current to flow through the gap junction pores in a neuronal network. The usual source of such current is the potential difference generated locally by the electrical signal. Gap junctions consist of hexameric complexes formed by the ensemble of subunits called connexons, which are present in both the pre- and postsynaptic membranes [3].

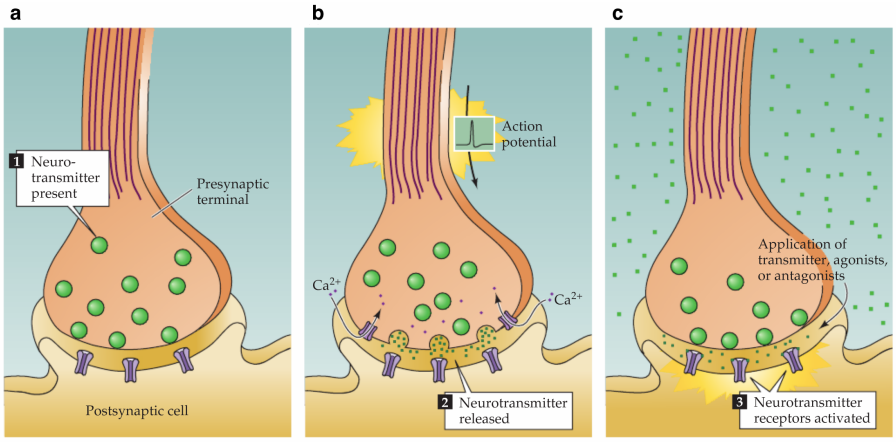

Figure 1.3 – Demonstration of a neurotransmitter at a synapse, showing **a)** its presence, **b)** release, and **c)** the postsynaptic presence of specific receptors. Adapted from [3].

1.1.3 Neuronal circuits

Neurons are organanized into ensembles of neuronal circuits for processing different and specific types of informations and providing sensation, perception and behaviour. The synaptic connection is the communication unit of such circuit and their structure varies according to

different functions [3].

1.2 Generation of electrical signals in nerve cells

Nerve cells transmit information by generating electrical signals. Intrinsically, neurons are not good electrical conductors, however they generate electrical signals based on the ion flow mechanism across their plasma membranes (Figure 1.4) and all kind of electrical signals arise from transmembrane ion fluxes [3].

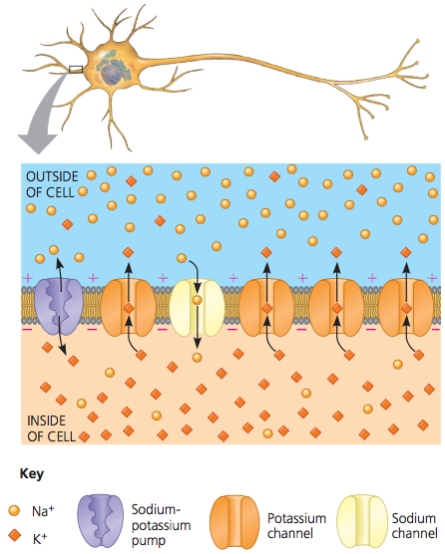

Figure 1.4 – Generation of electrical signals arising from transmembrane ion fluxes. Adapted from [4].

1.2.1 Ionic movements and generation of electrical signals

An electric potential is generated across the neuron's membranes due to difference in the cross-membrane ionic concentration, and the cell membranes' permeability to different ions in a selective way. These two facts underly two different kinds of proteins in the cell membrane and cross-membrane ion channels. Firstly, the gradient of ion concentration is organized by active transporter proteins, which actively transport ions across the cell membrane according to the concentration gradients. Secondly, cell membranes are selectively permeable due to ion channels, which are proteins that permit ions to pass the cell membrane in the direction of ionic concentration gradient. Therefore, ion transporters and channels' mechanism are in a contrary way, which results in the generation electrical signals based on potential difference between intra- and extra-cellular spaces [3, 5]. In the resting membrane potential state, neurons have a negative potential and between -40 to -90 mV. When action potential takes place, it leads to increasing the resting membrane potential in a transient manner and turns the transmembrane potential to positive potential [3].

1.2.2 Action potential

- **Resting state.** At the resting potential most of the voltage-gated sodium $(Na)^+$ channels of the axon membrane are closed (Figure 1.5.1) [4].

- **Depolarization.** As the result of a stimulus, Na^+ ion channels open and Na^+ ions diffuse into the cell. This leads to the reduction of the magnitude negative potential inside the membrane potential. This inflow of Na^+ results in depolarization and opening of more Na^+ channels and diffusion of more Na^+ ions. Action potential occurs when the depolarization level passes the threshold value (about -55mV) (Figure 1.5.2) [4].

- **Rising phase.** Once the action potential initiates, it gains a magnitude that is independent of the stimulus (Figure 1.5.3) [4].

- **Repolarization/Falling phase.** Inactivation of voltage-gated Na^+ channels happens shortly after their opening, which halts Na^+ inflow and most voltage-gated potassium $(K)^+$ channels open, leading to a fast outflow of K^+ ions. These two important events increase the membrane potential to under the threshold level. This is called falling phase (Figure 1.5.4) [4].

- **Hyperpolarization/Undershoot.** In this phase, Na^+ channels close, however some K^+ channels are still open. This results in the diffusion of K^+ out of the neuron, which leads to shift the membrane potential toward -90mV. Then the gated K^+ channels close and the membrane potential returns to the resting state (Figure 1.5.5) [4].

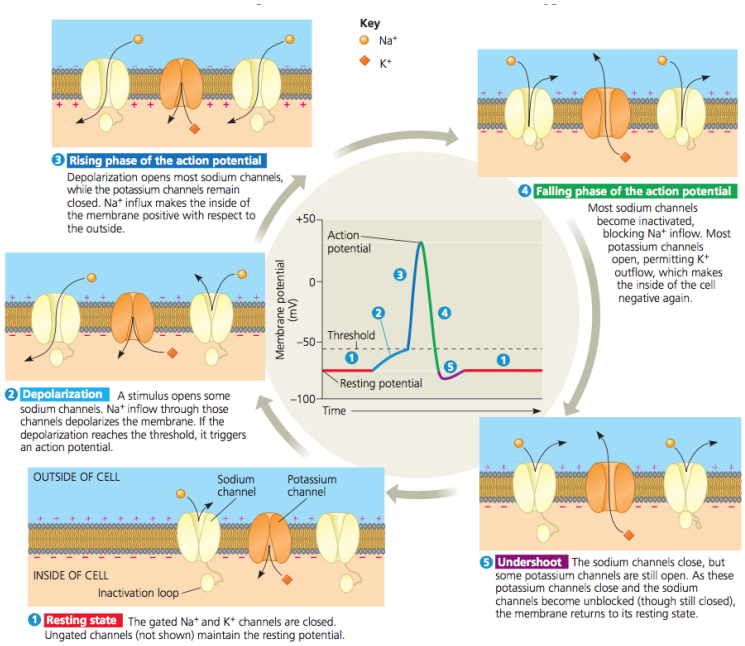

Figure 1.5 – Action potential. Adapted from [4].

1.2.3 The ionic basis of action potential

Hodgkin and Katz assessed the role of Na^+ in action potential generation by removing it from the external medium in their experiment. It was found out that lowering the concentration of external Na^+ results in the reduction of both the rate of rise of the action potential and its peak amplitude (Figure 1.6). [3, 6]. Therefore, the extra- and intra-cellular ionic exchange is the ionic basis of action potential.

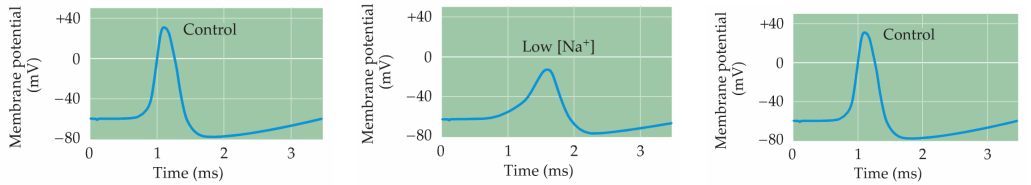

(a) An evoked action potential with the normal intra- and extracellular ionic concentration.

(b) Reduction of Na^+ concentration results in the reduction the signal's amplitude

(c) Action potential's recovery by rebalancing Na^+ concentration

Figure 1.6 – Effect of the reduction of Na^+ concentration on action potential [3].

1.2.4 Recording of intracellular electrical activity and local field potential

Two common approaches for measuring electrical signals of nerve cells are intracellular (Figure 1.7a) and extracellular recordings (Figure 1.7b). In extracellular electrophysiological measurement, an electrode is placed at the proximity of a cell for detecting its activities and in intracellular recording, the electrode is implanted in the cell [3]. Extracellular recording monitors the extracellular electric field, local field potential (LFP) with submillisecond temporal resolution and it can be used as a facet of the neuronal communication. A major benefit of this method is it well known biophysics of its measurements. Extracellular field results from the superposition of overall contributions of any excitable membrane such as dendrite, soma, axon etc., transmembrane currents and electrical signals. Therefore, any transmembrane current results in intracellular and extracellular voltage deflection. The waveform characteristics of LFP is proportional to the contribution of sources and and depend on the brain tissue's properties [5].

1.2.5 Rebalancing mechanism of ionic concentration

The movement of ions and organic molecules (osmolytes) across cell membranes results in imbalances; in other words, a change in osmotic pressure. By use of channels and transporters, osmolytes, and as a result water, move to rebalance the initial concentrations (Figure 1.8). The water flux to rebalance the cell, results in cell swelling or shrinkage and is referred to as the mechanism of cell volume regulation [7, 8].

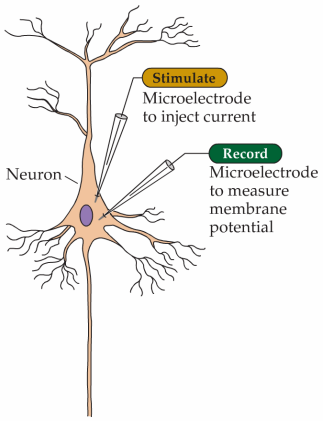

(a) Single neuron's internal recording and stimulation. Adapted from [3].

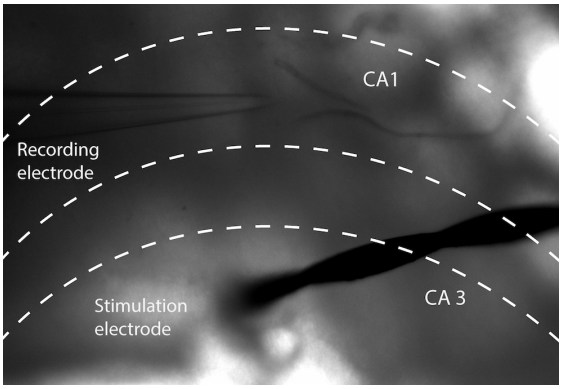

(b) Recording of LFP from mouse's hippocampus.

Figure 1.7 – Recording of single cell's activity and local field potential.

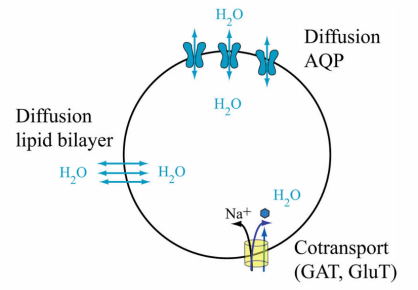

Figure 1.8 – Based on the osmotic pressure's level, water can diffuse though the cellular wall (lipid bilayer) or via the acquaporin channels, channels for cellular water exchange. In addition, it can be diffused against its gradient by cotransporters, such as glutamate using the driving force of Na^+ in order to move the water and the neurotransmitters against their gradient. Adapted from [7].

1.2.6 Visual cortex neurons and primary visual system's function

In the primary visual cortex, the majority of neurons are sensitive to the orientation of a visual stimulus [9]. Approximately every sensory neuron in this area is tuned selectively to the ensemble of visual inputs, whether it would be a simple image, such as oriented lines like in Figure 1.9 or a sophisticated visual scene. In primary visual cortex, neurons are responsive preferentially to edges or to particular orientations [10]. The receptive field (RF) is an area of the visual system influenced by the neuronal discharge. The RF is the main structure for studying the physiology of neurons with visual response, since it transforms the visual image to neuronal activity as an inherent function of space-time domain. The RF is mapped using the powerful technique of white-noise analysis to characterize RF for neurons spatio-temporally. In the visual system, the information is transferred from retina through the lateral neniculate nucleus (LGN) to the visual cortex, in a sequential manner. Figure 1.9b presents one of the main configurations of spiking neurons. The organization of retinal ganglion cells and LGN

neurons is approximately circular. In the center-surrounded configuration the polarities of center part and surrounding part are reversed. In this configuration, the RF center responds to bright stimuli (center ON, positive sign) and the surround responds to dark stimuli (center OFF, negative sign). In simple cells, most of the geniculate input is spatially oriented (Figure 1.9c) and is transferred to the primary visual cortex and the elongated subregions response to bright or dark stimuli [11, 12].

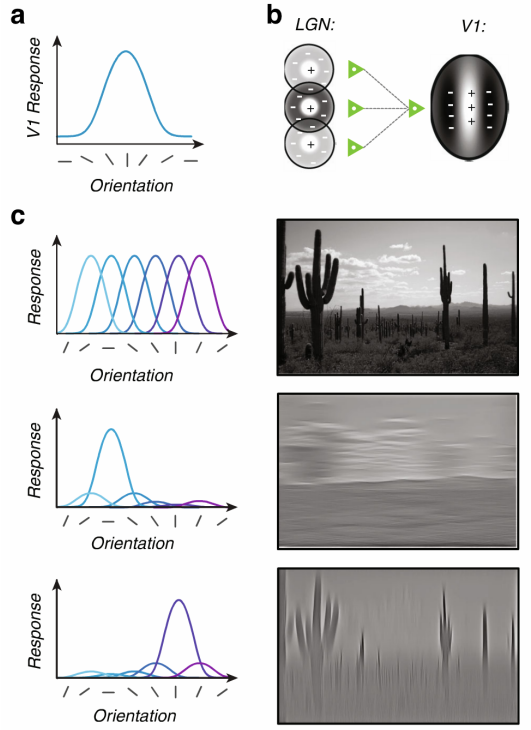

Figure 1.9 – **a)** An example of a typical model of orientation selectivity tuned to a specific function. In this example neuron has a preference of vertical orientations. The orientation tuning's bandwidth is in the range of 30–40°. **b)** Sensory neurons in V1, in all the possible ways of orientation are selective. The combination of their activities gives the ability of analyzing visual scenes. As an example, for the desert scene, channels that are selective to horizontal orientations respond to the clouds. Channels that are selective to vertical orientations respond to to the cacti. The combination of their activity, makes us enable to detect all the elements in the scene. **c)** A model presenting excitatory convergence of orientation selectivity. In this model, three LGN neurons and their circular RF are illustrated. They lie vertically next to each other. The afferents from LGN cells converge to a V_1 neuron; this effect shows the orientation selectivity. In this example, it applies for vertically oriented contours. Adapted from [10].

1.3 Label-free and fluorescent indicator-based optical recording in neuroscience

Optical recording of neurophysiological activity is done using imaging techniques (a.k.a. functional imaging), mainly using two methods; label-free method, including optical imaging of fast [13] and slow intrinsic signals recorded from changes in the optical properties of

brain tissue [14] and fluorescent imaging of different ions labeled with fluorescent indicator dyes [15].

1.3.1 Common imaging devices and light detectors

Figure 1.10 illustrates the major instrumentation types of imaging used in biology. The light sensing device is usually mounted on a microscope in combination with a light source. The type of light source combination depends indeed on the application. The light source is used for the excitation of fluorescent indicators and lightening samples. Two imaging approaches (Figures1.10a and b) involve wide-field microscopy [16, 17], one in combination with multi-pixel photodiode arrays (Figures1.10a) and other in combination with intensified CCD and CMOS cameras (Figure 1.10b) [16]. CCD cameras comprise of densely packed multi-pixel photodiode arrays and in contrast to classical multi-pixel photodiodes, they comprise of a serial signal read-out mechanism. The utilization of photodiode array method is rare, since they provide a relatively low spacial resolution, however they are characterized by a very high speed and dynamic range. On the other hand, modern cameras provide a high spatial and temporal resolution but the serial read-out mechanism limits their temporal resolution relatively and they have a high noise level [16,18]. In order to image the activities of fluorescent indicators deeply in the brain, confocal (Figure 1.10c) and two-photon microscopy (Figure 1.10d) are the most commonly used methods in fixed-position microscopy. There exists specialized tools for the fluorescent imaging of freely moving animals also, such as endoscopic and portable head-mounted microscopic approaches (Figures 1.10e,f) [16].

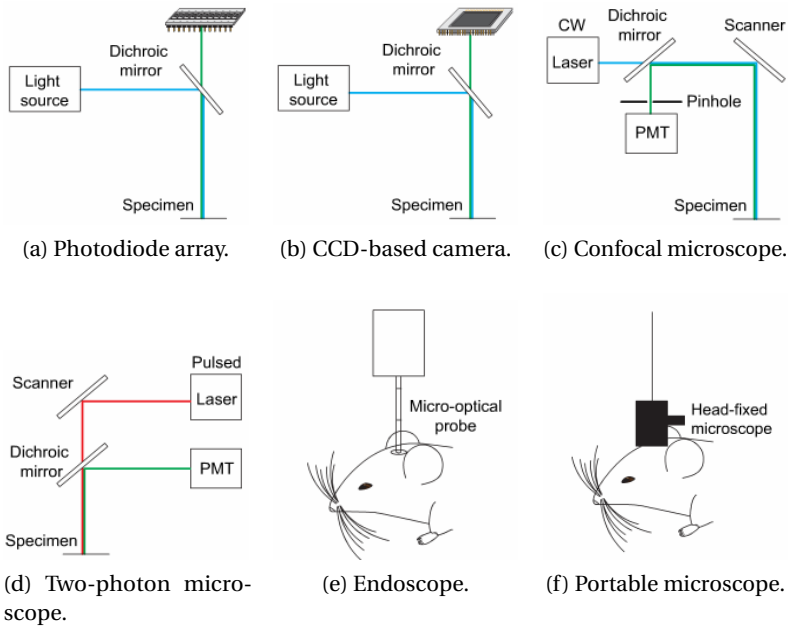

(a) Photodiode array. (b) CCD-based camera. (c) Confocal microscope.

(d) Two-photon microscope. (e) Endoscope. (f) Portable microscope.

Figure 1.10 – Common imaging approaches. Adapted from [16].

1.3.2 Optical and fluorescent indicator technology

One of the most important aims of neuroscience is the understanding of nervous system's information processing and encoding from cellular to circuit level. The tremendous development of optical and fluorescent indicators for reporting neuronal functions has enabled this field to monitor activities of ions and ion channels in any region of interest in the brain. The indicators can be divided into two groups, chemical and genetically encoded indicators. The chemical indicator, which is the traditional kind, has been developed initially for *in-vitro* application, then its utility was expanded to *in-vivo* application, giving the possibility of targeting a single cell by injection techniques. Genetically encoded indicators, broadened monitoring functional neuronal activities enormously by providing the possibility of targeting a specific type of cell or ion channel in any region interest in the brain for visualizing activities. These indicators can be grouped based on their target into two sets: optical and fluorescent indicators for monitoring ion channel activities such as voltage or Ca^{2+} channels and for visualizing concentration gradients of specific type of ions, such as Ca^{2+}, K^{+}, Na^{+} etc. [15, 16, 19].

1.3.3 Optical imaging of fast intrinsic signals

Hill et al. [20] in the pioneering description of fast intrinsic optical changes indicated that they take place coincidently with neuronal activity. These fast changes occur during the voltage changes (polarization changes) when action potential happens, which can be probably due to the reorientation of the membrane proteins. Light detection in label-free optical imaging is traditionally performed by CCD cameras in combination with a wide-field microscope [21]. This technique lets to image the functional mechanism of optical changes of the brain tissue with a spacial resolution of 50 μm. This current technology is still limited for doing more investigation of the optical changes of a single neuron during polarization [22].

1.3.4 Optical imaging of slow intrinsic signals

Slow intrinsic optical changes can be detected more easily using CCD cameras in any region of the brain. These signals arise from cell swelling and the superposition of several sources that contribute in their formation including electrical, majorly action potentials and multiple optical processes [6], such as metabolic activities that cause molecular oxidation, blood volume changes chromophore redox and light scattering etc. [14].

1.3.5 Comparison of label-free optical recording and fluorescent imaging

Fluorescent indicator imaging technique and label-free optical imaging method have their advantages and disadvantages. Their major difference is the time resolution of the signals, which concerns slow intrinsic optical changes and fast signals with submillisecond resolution arsing from fluorescent indicators. In addition, the constraints in the technology for studying fast intrinsic optical changes should be taken intro account. However, each of these signals

present different information about various kinds of neuronal and circuit functions; thus, replacing one by another is not the case. In addition, the advantage of optical imaging of the intrinsic optical changes is that in contrast to using dyes, problems such as photo-dynamic and -bleaching damages, as well as pharmacological secondary effects do not exist [22].

1.4 Organic optoelectronics

Organic optoelectronics field has received a tremendous attention for its plethora of applications in organic photovoltaics [23], light-emitting diodes, organic photodetector for imaging [24, 25] and biomedical utilizations [26]. This technology notably offers the possibility of low-cost fabrication, modifiability of chemical and physical characteristics through molecular synthesis and design. Also they provide the ease of fabrication, which is mainly due to the possibility of the solution deposition of active materials in the room temperature from very small (μm-feature) to large area flexible substrates [27]. One of the most innovative technologies of organic optoelectronics is sensors based on OPD [28], which has illustrated a high sensitivity. The active layer of such devices (like a typical architecture of organic photovoltaic devices) is composed of an electron donor and an electron acceptor material, where the electron donor is a semiconducting polymer with a low ionization potential (IP). In most cases, the electron acceptor material is a small molecule, such as fullerene derivatives with a high electron affnity (EA), but it can be also another conjugated polymer or a semiconducting metal-oxide, which is referred to hybrid devices [29–31]. Other photovoltaic device technologies use small organic molecule as electron donor material. Kallmann and Pope in their early work, back in 1959, presented an early organic photovoltaic made from anthracene [32]. Today, bulk heterojunction (BHJ) structures [23, 33, 34] based on small-molecule photovoltaics present a power conversion efficiency (PCE) above 10% in single-junction binary devices (comprising of single donor-acceptor (D-A) materials) [35–37]. These improvements in the device performance is due to the design and synthesis of novel D-A polymers, illustrating optimized energy levels and band-gaps in order to reach high PCE [38–44].

1.4.1 Conjugated polymers

Polymers used in photodetector applications consist of a fully conjugated backbone with single or double bonds that alter [45, 46]. Figure 1.11 shows the conjugated polymers used in this thesis. Single and double bonds' alterations enable the delocalization of electrons across the polymer's backbone, due to the overlap of π-orbitals. As result, semiconductors consist of a highest occupied molecular orbital (HOMO) and a lowest unoccupied molecular orbital (LUMO). The energy difference between HOMO and LUMO defines the minimum excitation energy of an electron and the semiconductor's band-gap. In conducting materials, such as metals, there is a small energetic difference between the valance and conduction band. Hence, they do not have band-gap. In insulating materials, the difference in the energy levels is too high. Therefore, the electron excitation form HOMO to LUMO is difficult [47]. Semiconduc-

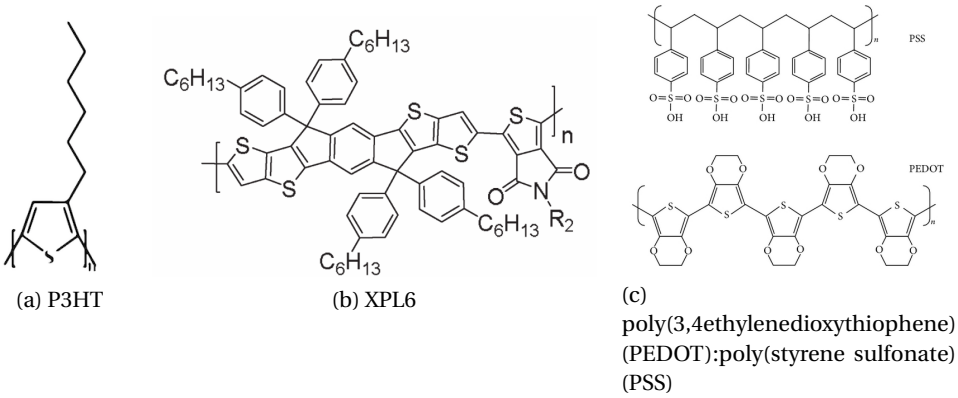

(a) P3HT (b) XPL6 (c) poly(3,4ethylenedioxythiophene) (PEDOT):poly(styrene sulfonate) (PSS)

Figure 1.11 – Conjugated polymers mentioned in this thesis.

tors, in natural state behave like insulator materials, but doping these materials makes them electrically conductive [48]. Development of polymers for photodetector applications has led to complicated chemical structures (Figure 1.11). Aromatic units is the basis of plenty of conjugated polymers. These units allow for the ease of chemical and physical modifications and other characteristics, such as stability and optoelectronic properties. Aromatic-based polymers possess two types of resonance forms, the aromatic and the quinoid form. The latter describes the polymer structure. For achieving the smallest band-gap, both resonance structures should describe the polymer in an equal manner. In this case, the bond-length difference between single and the double bonds should be small. In order to stabilize the quinoid form, electron donor and acceptor materials should co-polymerize to form the structure [49, 50]. Variations in the polymer's chemical structure affects several properties [51]. The chemical structure can be divided into two parts, conjugated backbone and the side-chains. These parts can be modified chemically in order to tune the properties. Properties from the point of view of OPD that can be influenced by structural modifications are indicated in below [51]:

- **Band-gap and optical absorption**. Smaller band-gap gives a higher overlap with the absorption spectra and consequently absorption of more photons. Most of the photons are absorbed in the active layer, which is crucial for the device performance [51]. In conjugated polymers absorption bands are very intense and small [52]. Figure 1.12 illustrates the optical absorption spectra of widely used polymers.
- **Energy levels**. Beside altering the energy levels in order to define the absorption spectra, these levels should be matched to the energy level of the electron-acceptor material in order to give a high potential difference during charge separation. Energy levels are important for the stability of polymers against photo-oxidation.

P3HT (Figure 1.11a) is a commonly used polymer that is appropriate for the absorption of full spectrum light. XPL6 (Figure 1.11b) is a newly synthesised polymer, which gives a wide bandgap and has a high absorption at blue and green wavelengths, which makes it an

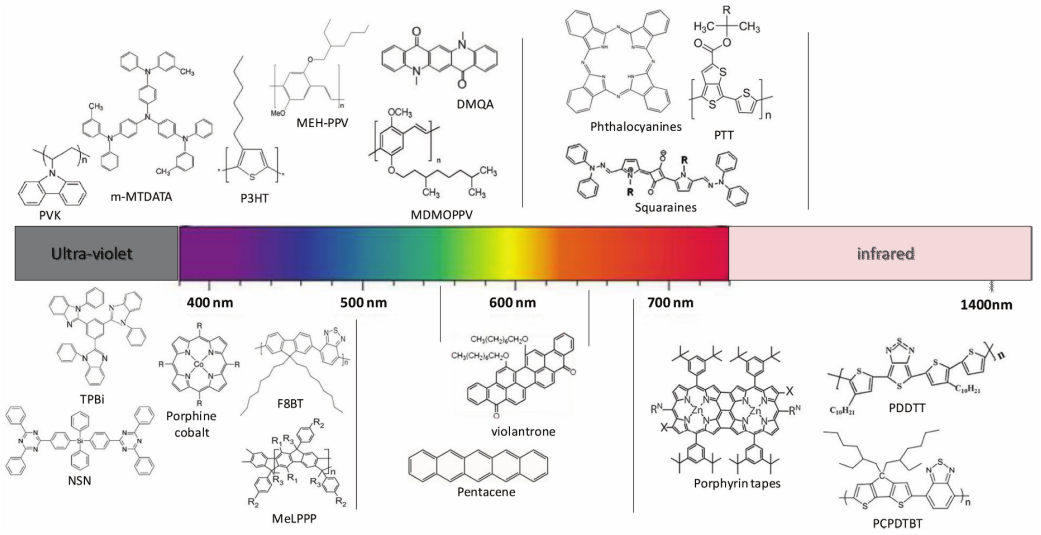

Figure 1.12 – Absorption spectra of widely used electron-donor polymers. Adapted from [53].

interesting polymer for detection application in near-UV light spectrum [54]. PEDOT:PSS is highly conducting polymer with a high work-function about $5.2eV$ that is important for interfacing the active layer and adjacent anode electrode for charge separation.

1.4.2 Fullerene derivatives

Fullerenes are very powerful electron acceptors with excellent electron transport characteristics, for this reason they are widely used in OPD technologies. Generally, fullerene derivatives illustrate a limited solubility. For this reason, different functionalized derivatives have been developed [55]. Therefore, this family with different levels of solubility and variety of physical characteristics should be co-polymered with novel low band-gap polymers [56]. $PC_{60}BM$ [55] and $PC_{70}BM$ [57] are the most frequently utilized fullerene electron-donor materials (Figure 1.13). Other than PCBM, there exists several other fullerene derivatives used in photovoltaic

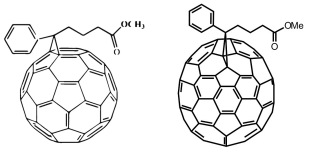

(a) $PC_{60}BM$ (b) $PC_{70}BM$

Figure 1.13 – Chemical structure of $PC_{60}BM$ and $PC_{70}BM$

technology, such as bis-PCBM [58, 59] and $I_{60}BA$ [23]. The chemical structure of $PC_{60}BM$ and $PC_{70}BM$ are different, due to different amount of carbon atoms comprising the cage. As Figure 1.14 illustrates, $PC_{70}BM$ has a broader spectrum than $PC_{60}BM$, for this reason, in some cases the device efficiency is increased due to a higher absorption [56, 58].

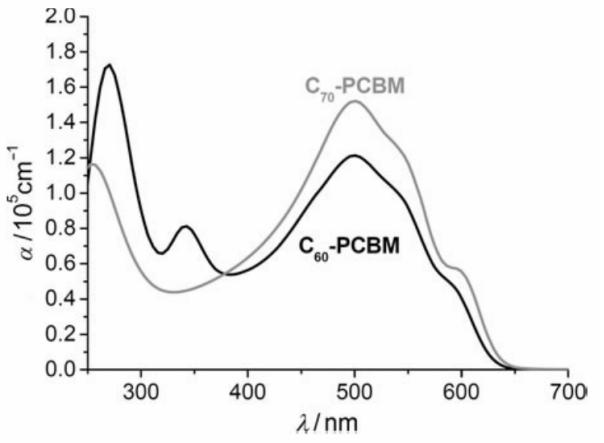

Figure 1.14 – Absorption spectra of $PC_{60}BM$ and $PC_{70}BM$. Adapted from [56].

1.4.3 Bulk heterojunction

General architecture of OPD device is a multilayer stack (sandwich form) similar to that showed by Tang et al. [60]. This structure (Figure 1.15) consists of a transparent electrode (anode), usually a conducting oxide like indium tin oxide (ITO) [23] or a polymer, such as PEDOT:PSS [34]; D-A light-absorbing layer and a second electrode (cathode). There exists other OPD structures, such as bilayer with the same architecture, but different in the active layer [60]. Figure 1.16a illustrates the energy level diagram of an organic BHJ under illumination. When the device is under illumination, photons are absorbed with an average photon energy, which is larger than the optical band-gap of BHJ (Figure 1.16a **step 1**). This step is followed by thermalization and the creation of excitons (Figure 1.16a **step 2**). The interface between D-A materials is responsible for exciton diffusion (Figure 1.16a **step 3**) and disassociation, which is the formation of electrons and holes. The electrons and holes are transported through D-A layer respectively (Figure 1.16a **step 4**) and are collected at the electrodes, thereby contributing to the generation of electrical current in the external circuit [52]. Organic semiconductors possess large extiction coefficient, which leads to harvesting light at relatively thin layers with a thickness range of 80–200 nm [52,54]. The organic layer is sandwiched between two electrodes with different work functions. This leads to the formation of a built-in potential and an electric field, which aides the transport of charges [61]. Therefore, after the illumination an interplay of drift and diffusion govern the electron and hole currents in the OPD device [62].
Two important challenges in OPD devices are, exciton dissociation and charge collection at electrode.

- **Exciton dissociation**. Excitons should be dissociated and diffused in D-A layer rapidly before that they decay to the ground state [63] (charge recombination). Hence, the D-A layer's thickness should be comparable to the exciton diffusion length [52]. Indeed, the efficiency of the device depends on transportation of holes in the donor component and and electrons in acceptor component of the phase-separated network. Furthermore,

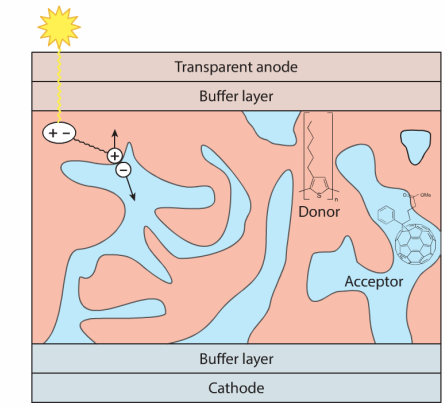

Figure 1.15 – General structure of organic photodetector. Adapted from [46].

control of the film's morphology [64–68] is crucial for the efficient extraction of excitons [52].

- **Charge collection**. The physics of the interface between D-A layer and the electrodes is complex and much remains to understand. The deposition of the active layer on electrode results in a charge-density redistribution at the interface and geometry modifications, which affects the alignment of electronic levels versus electrode's Fermi level at the organic layer's frontier (1.16b). Although these interfaces are not very well understood yet, but it has been shown that surface modification of electrode by depositing self-assembled monolayers [69] and the application of a monolayer of the polymer polyethylenimine ethoxylated (PEIE) [70] are different ways to enhance the interface of the electrical contact. A monolayer PEIE has shown the modification of the interface of electrode and D-A layer by arranging the charge distribution at the electrode surface [71], leading to the optimization of charge collection [70]. Furthermore, Kieler et al. have presented that the application of PEIE results in the decrease of dark current, hence leading to the increase of OPD device's detectivity [72].

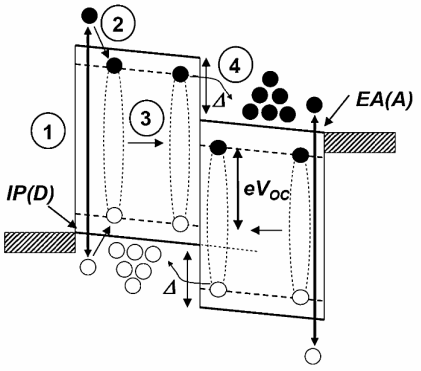

(a) Bulk heterojunction energy level diagram.

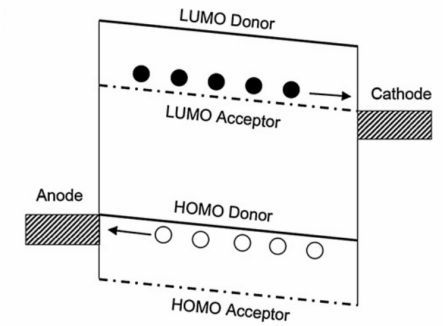

(b) Cross-sectional OPD geometry.

Figure 1.16 – Bulk heterojunction energy level diagrams. Adapted from [52].

1.4.4 Organic photodetector's electrical characteristics

In dark, the OPD functions as a standard diode, which can be approximated by an equivalent circuit (Figure 1.17a). The equivalent circuit is composed of [52, 73]:

I. A diode characterized with ideality factor n and reverse saturation current density J_0 in dark at reverse bias (studied using semi-logarithmic scale of current-voltage (I-V) curve as shown in Figure 1.17b), according to Shockley's p-n junction theory [74].

II. A photocurrent upon illumination, current source J_{ph}.

III. A series resistance, R_S, which should be minimized. This parameter is considered as the contact resistance between the D-A layer and the electrodes. The buffer layers can help to minimize R_S by matching the work functions at their interface.

IV. A shunt resistance, R_P, which should be maximized. This parameter is influenced by leakage paths in the BHJ structure. This involves structural defects, like pin-holes or impurities in the film that lead to charge recombination.

The latter is explained the following mathematical model [73], which describes the I-V behaviour of OPD:

$$J = J_0\left[exp\left\{\frac{e(V-JR_S)}{nk_BT}-1\right\}\right]+\frac{V-JR_S}{R_P}-J_{ph} \tag{1.1}$$

where, e the elementary charge, k_B is Boltzmann's contant and T is temperature [74]. In equation 1.1 [73], the first expression indicates the recombination current, the second expression explains the shunt current and the third one, the photocurrent. From the semi-logarithmic scale curve (Figure 1.17b), the dark current can be extracted, which is measured by applying negative bias (reverse) in dark conditions. Generally, the dark current in OPD devices is intrinsically low, since their conductivity is low, which makes them to reduce the noise dramatically [75]. This parameter should be reduced to increase the sensitivity of the device for detection (detectivity) and to minimize its power consumption. It has been reported that possessing a large offset between the D-A layer's HOMO level the electrode's Fermi level is a key parameter in order to minimize the hole injection, leading to decrease the dark current [53]. In the state-of-the-art, $5.5eV$ is one of the deepest offsets that has been reported [76]. From the linear scale of I-V curve (Figure 1.17c), under illumination, three important parameters can be extracted for device performance evaluation:

I. **Short circuit current** J_{SC}. Achieved photocurrent at zero volt.

II. **Open circuit voltage** V_{OC}. Achieved voltage at zero volt. This parameters depends on the energy difference between the HOMO of donor and LUMO of acceptor, as parameter Δ shows in Figure 1.16a.

III. **Fill factor** FF. Maximum value of this parameter is a function of V_{OC} and J_{SC} and the diode's ideality factor (Figure 1.17c) [52].

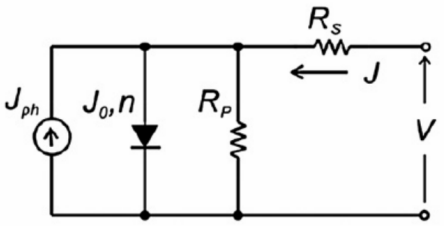

(a) Equivalant circuit for modelling organic photodetector.

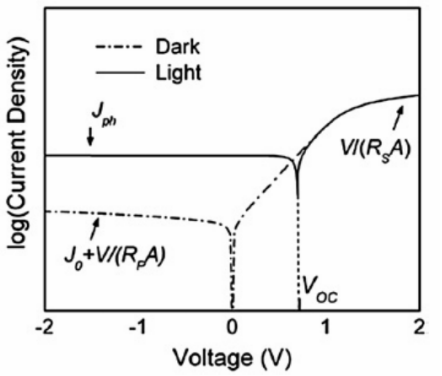

(b) Semi-logarithmic plot of the same electrical characteristics, in forward and reverse bias.

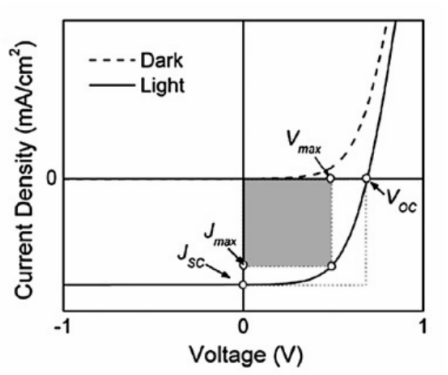

(c) Schematic of IV curves in the dark and under illumination.

Figure 1.17 – Electrical characteristics of organic photodetector. Adapted from [52].

1.4.5 Stability and life-time of organic photodetectors

One of the critical challenges that limits the application of OPD, especially in open air is the stability of these devices in presence of degrading elements, such as oxygen, humidity and light. Taking into account the tremendous growth of this field, more stable devices are highly demanding. One challenge in organic semiconductor-based devices is how to unify efficiency, stability and process for the same material [77]. Chemical degradation of OPDs can be mainly considered for the role of oxygen, water and the reaction between the D-A layer with electrode materials. The electron-donor materials used in this thesis are less susceptible to chemical degradation, since probably they do not possess many sensitive oxygen acceptor groups [54, 77]. On the other hand, fullerenes are known for their high degradation potential,

since they have a very high electron affinity [77]. Furthermore, it has been stated that the presence of impurities and moisture within the polymer increase the ionic conduction in the structure and results in corrosion acceleration. Here we divide some of the most important chemical degradation factors (Figure 1.18) into two groups:
Related to the environment:

- Oxygen and water diffusion. Oxygen and water are known to diffuse into the OPD and react with the active materials. Encapsulation impedes this procedure, but current encapsulation materials do not remove this process. There exist different sources of diffusion, such as through the outer electrode via microscope pinholes, release and diffusion of the oxygen from the oxidized sublayers into the active material. Therefore, it is important to remove the microscopic pinholes [77].

- Photo-oxidation. It has been explored that illumination accelerate the oxidation of the organic material's sublayer. Although several investigations has been carried out to understand the chemical degradation by photoaxidation, however its nature is fairly understood [77].

Related to the device structure:

- Metal electrode. Low work-function electrode tends to react with the oxygen, hence it leads to formation of an aluminium-oxide thin layer, with insulation properties. This thin layer tends to react with the fullerene molecules, hence it decreases the charge transport at the interface of D-A layer and the electrode. This leads to decrease in the device performance. In addition, during the metal evaporation, hot particles can penetrate within the polymer and oxidize it. This results in the reduction of the efficiency of charge transport within the D-A layer and also oxidation of the active material [77].

- ITO electrode. It has been observed that indium diffuses though the device structure and ends up at the cathode electrode's (aluminum (Al)) surface. The nature of this phenomenon is poorly understood, however it has been stated this is due to the interaction between the PEDOT:PSS layer and ITO. When the water is uptaken from this polymer, it becomes acidic. On the other hand, ITO is sensitive to acidic compounds, which etch it. Therefore, the etching process leads to the release of ITO molecules through the device structure [77].

- PEDOT:PSS interlayer. This layer is used as a hole transporter interfacing between the ITO electrode and the D-A layer. The PEDOT:PSS contains water and after being spin-coated on the electrode, the film is annealed to remove water. However, this polymer is hygroscopic and takes up water from the atmosphere. This leads to fast degradation of the device, by rapid oxidation of the active material and low-work function electrode [77].

Electrical stress is another parameter, which concerns applying of electrical stress in a repetitive manner to a device. This leads to inducing traps in the semiconductor, which results in changes in device behaviour [78] and hence its degradation [79]. Currently, one of the most widely-used encapsulation strategies is epoxy, which has been reported to be efficient up to several months [80]. Figure 1.18 illustrates the interaction of degradation parameters within the device structure.

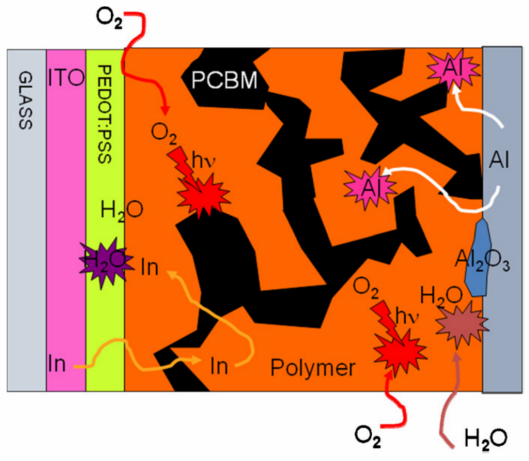

Figure 1.18 – Schematic showing a cross-sectional view of an OPD with possible processes that conspire the degradation of D-A layer. Adapted from [77].

1.5 State-of-the-art of optical detection using OPD

Applications of OPD for optical detection in sensor systems is gaining an increasing attention, especially since the publication of a landmark study by Gong et al. in 2009 [28] that reported an OPD with high sensitivity for detection. Since then, a few reports have focused on the development of OPDs as optical sensors with high sensitivity. Inorganic photodetectors have shown an optical detection capability (detectivity) limited to $\sim 10^{12}$ Jones [28] (1 Jones= $1cmHz^{1/2}W$). They have illustrated a relatively a higher dark current density ($10^{-7}mA/cm^2$) than what can be suitable for imaging purposes [24, 81] and a relatively small LDR (lower than $\sim 10^{-12}$) at ultra-low light intensities. Non-linearities in dynamic behaviours in response to ultra-low light intensities (pW/cm^2-$\mu W/cm^2$) has also been reported [28, 75]. These devices need a cooling system in order to increasing their dynamic range and to decrease their dark current to gain a higher sensitivity [18, 28]. A high dark current results in limitations in the sensor's detection ability. Linear dynamic range, which is defined as linear relationship between input and output signal of the device, is important in order to correlate them. These are considered as crucial parameters for the sensitivity/detectivity of any sensor. State-of-the-art of OPDs have presented ultra-low dark current densities ($10^{-15}A/cm^2$), lower than inorganic devices ($\sim 1nA/cm^2$) [24, 82] or have reported relatively high efficiency of more than 60%, which is directly correlated with the responsivity [83–85]. To date, the trade-off

of low dark-current and high device responsivity remains a challenge [72]. One of the most recent reports has tried to address this trade-off by using of PEIE for modifying the interlayer energy level between the D-A layer and electrode. They demonstrate an ultra-low DCD ($10^{-13} mA/cm^2$ [72]) and relatively high quantum efficiency. Furthermore, other works have reported DCD quantities between $\sim 10^{-8}$ [28] to $\sim 10^{-12} mA/cm^2$ [86]. All these quantities have been obtained for devices performing at a high reverse bias range of $-2V$. Application of reverse bias aims to enhance the device's charge collection and increasing the sensor's response time [72, 87]. However, stressing to the device by applying bias leads to increase of the DCD level, changes in the device behaviour and its degradation [78, 79]. Interestingly, it has been shown also that the organic devices present a large linear dynamic range up to $\sim 10^{-13} A/cm^2$ at ultra-low light intensity of $10^{-12} W/cm^2$ [28, 75]. This quantity of LDR is about 2 orders of magnitude larger than silicon photodetectors [28, 75]. These well-performing parameters have been achieved mainly through chemical modification of D-A layer materials (common approach), changing the device architecture by using a bilayer of active materials [75] and the manipulation of the ohmic contact using PEIE [72].

Another rising effort is to integrate OPDs with very low DCD to integrate in multi-pixel arrays for imaging purposes. Very low DCD is typical for very small active areas (lower than $1 mm^2$) as it has been reported in 2008 [24]. However, for relatively larger areas, obtaining a low dark current becomes challenging. A recent report have illustrated the imaging application of these devices for relatively large areas, $\sim 4 mm^2$, however the reported DCD ($10^{-4} mA/cm^2$ at reverse bias) is relatively high in comparison to other organic counterparts. The state-of-the-art of the biomedical applications of optoelectronic devices will be covered in Chapters 2 and 3. Although a good device performance is desirable in OPD applications, the structural simplicity of OPD should be considered as an important design aspect since it can offer an easy fabrication. This parameter can be achieved by minimizing the number of layers and manufacturing phases, such as annealing-free process or adapting organic active materials to in-air fabrication. To date, Gong and Kieler [28, 72] have reported a well performing minimal device structure, composed of 4 layers electrode/interlayer/BHJ/electrode.

1.6 Aim of the thesis

As indicated in the Abstract, investigation of the OPD performance for optical detection in biomedical applications sets the background of this PhD thesis. This thesis is the first step towards discovering the possibility of utlizing both established active materials and new polymers for optical detection in biomedical applications. We aimed to incorporate important parameters of structural simplicity and minimized number of layers for the simplicity of fabrication.

For this goal, in order to evaluate the device performance to measure a broad range of biological signals, label-free intrinsic optical changes with a wide spectral range and Ca^{2+} signals with a narrow green fluorescent emission profile were assessed.

Label-free and slow intrinsic optical changes of the brain, are a kind of signals known for their

low-amplitude optical changes. Established materials, P3HT and $PC_{60}BM$ were chosen for their low DCD, wide optical absorption and ease of fabrication. Then, the OPD performance was studied by detecting Ca^{2+} signals, which are known for their fast and ultra-low amplitude fluorescent emission. For this aim, a new polymer XPL6 was blended with $PC_{70}BM$. The resulting active layer gave a very high absorption spectra, fitting to the emission spectrum of Ca^{2+} signals. The OPD based on this active layer showed to have an ultra-low DCD with a very high detectivity. In addition to the simplicity of the OPD structure, the processing of this active material is enhanced too since it is annealing-free.
Furthermore, the application of OPD devices as a simplified model of the retina to emulate orientation selectivity in neuro-inspired electronics was studied.

2 Monitoring Intrinsic Optical Signals in Brain Tissue with Organic Photodetectors

2.1 Abstract

Optical methods utilized in studying living tissues are able to monitor biological activities such as metabolism, gene expression and variations in ionic concentration. Organic optoelectronic devices have numerous advantages over traditional inorganic technologies, yet limited examples exist in brain tissue assessment. An OPD with a simple structure acts as a highly sensitive optical sensor for detecting intrinsic optical signals of a living brain tissue. The signals are related to cell volume variations and are essential in studying biological events, such as metabolism and hypoxia. This work demonstrates for the first time the capability of organic photodetectors to assess opto-physiological events in neuroscience. Their simple fabrication and the capability for selective absorption of an optical event via tuneable chemistry paves the way for their integration in biomedical prostheses with broad applications.

2.2 Résumé

Les méthodes optiques utilisées dans l'étude des tissus vivants sont capables d'enregistrer des activités biologiques, telle que le métabolisme, l'expression génétique et des fluctuations des concentrations ioniques. Des dispositifs optoélectroniques organiques ont montré des avantages uniques en comparaison de ceux inorganiques, mais leurs applications sont encore limitées dans l'étude du cerveau. Un photodétecteur organique OPD possédant une structure simple démontre une haute sensibilité en tant que capteur optique pour détecter des signaux intrinsèques optiques (IOS) dans un tissu cérébral *ex-vivo*. Ces signaux sont reliés au volume cellulaire et ils sont essentiels pour étudier des événements biologiques comme le métabolisme et l'hypoxie cérébrale. Ce travail de recherche montre la capacité des photodétecteurs organiques pour enregistrer des événements opto-physiologiques en neuroscience. La fabrication simple de ces dispositifs et leurs capacités pour une absorption sélective par le réglage de leurs propriétés physico-chimiques ouvrent une nouvelle perspective pour leur

intégration dans les prothèses biomédicales avec des larges applications.

2.3 Introduction

Optical measurements are widely used to monitor biological activities such as changes in metabolism [88], gene expression [89] and ionic dynamics [16]. Essentially optical imaging is most commonly performed combining microscopy with optical sensors like the high affinity silicon photodetectors found in commercially available cameras [16]. Varity of methods been developed to report biological activities such as molecular probes [90], fluorescent indicator dyes (e.g. for Ca^{2+}, K^{+}) [16], bioluminescent sensors [91] and optogenetic tools that use genetically encoded fluorescence [92]. Intrinsic optical imaging is a label-free method that detects changes in the intrinsic optical properties of brain tissue [93, 94] and metabolic variations using optical stimulation of brain tissue and as result, imaging activities of NADH and FAD molecules [88]. It is a versatile method for measuring physiological and pathophysiological changes in brain function such as epileptiform discharges and disease progression [95]. The measurement of intrinsic optical signal (IOS) reflects cell volume changes [7, 8, 96, 97], which can be used to measure blood volume in the brain [98] and to track propagation of neuronal excitation, hypoxia, spreading depression [93, 94]. Therefore, devices measuring IOS can be used as an optical sensing platform for studying various physiological and pathological events. In the brain, ion exchange is the source of electrophysiological activities. Intracellular ionic concentration changes follow an action potential. The cell volume regulation (CVR) is the mechanism that rebalances the ionic concentration mainly by water flux to reach the physiological conditions. This leads to cell swelling or shrinkage [7, 8, 93, 94, 97, 99]. In this way, changes in cell volume result in changes in the scattering or in the transmittance of incident light (i.e. optical properties of the tissue) [93, 94]. Therefore, IOS is a measurement of changes in CVR and the detection of these signals as an optical assessment of biological events is important to gain a better understanding of their underlying mechanisms [96]. Functional magnetic resonance [98] allows imaging global activity of the brain function by recording changes in its optical properties, resulted from blood volume variations [98]. The most common method for detecting CVRs, in a specific region of the brain, involves exposing the tissue to a full spectrum light and measuring IOS using CCD camera [93, 94, 100]. Temporal resolution of optical detection in cameras does not allows to track electrophysiological and opto-electrophysiological events simultaneously. This comes from the high temporal resolution of analogue electrical signals and limited temporal resolution of images captured and processed by cameras [101]. Using standalone photodetectors approach, the optical activity is translated to current and it is directly transmitted to acquisition systems. This gives the possibility to real-time detection of electrical and optical signals with comparable time resolution. Multiple examples of successful fabrication of organic photodetectors (OPD), including on mechanically flexible substrates [102], and their outstanding application in biological sensing [103] stimulate novel ideas for their integration at the interface with life sciences. Indeed, organic materials have shown a great deal of potential for a plethora of

applications [104], owing to numerous advantages, including thin film architecture, easy and low-cost fabrication, high sensitivity, tunability of physical and chemical characteristics, and great mechanical properties for in vivo applications [105–112]. Optoelectronic devices, in particular have been used for neural interfacing [26] and photoactivation of blind retina [113–115]. In these examples, the generated photocurrent has been utilized for electrical stimulation of neural cells and damaged visual tissue. In terms of sensing applications, organic light emitting diodes and OPDs have also been integrated into a flexible substrate to measure blood oxygen levels through the skin [116]. To the best of our knowledge, OPDs have not been yet employed as optical sensor to address challenges in neurophysiology. In the present work, we aim to broaden the biomedical application of organic photodetectors by demonstrating their utility and temporal resolution for recording changes in brain tissue's optical properties caused by CVR during both pathophysiological and physiological conditions.

2.4 Device characteristics and experimental setup

In order to measure real-time changes in intrinsic optical signals in living tissue, a customized setup was designed featuring a brain tissue slice in a perfusion bath with electrodes for recording and stimulation electrophysiological activity (Figure 2.1a). During all experiments, the neuronal network activity was recorded as a change in LFP in CA1 region (Figure 2.1b) using an extracellular electrode. A halogen light source was placed underneath the perfusion bath for illuminating the brain slice. In order to record IOSs from the specific region of the tissue (14 mm2), the transmitted light was collected and focused on the OPD with a microscope, mounted on top of the setup (Figure 2.1a). The OPD was used to measure changes in the transmittance through the brain slice caused by cell volume changes due to ion fluxes in and out of the neuronal network's cells. The photodetector was designed to have minimal layers and low leakage current in order to simplify the fabrication process and maximize sensitivity (Figure 2.1c). The structure consisted of a thin semi-transparent gold (Au) electrode on a glass substrate, P3HT) blended with $PC_{60}BM$ as the photoactive layer and an Al as the cathode (Figure 2.1c). Finally, the device was encapsulated using epoxy and a glass cover-slip. The device presented a low dark-current and a linear response to incident light intensity as a typical high performing OPD (Figure 2.1d) [87].

2.5 Results

In the first experiment, we recorded IOS during epileptiform discharge, induced by 4-aminopyridine (4-AP), a non-specific inhibitor of voltage-gated potassium channels. This drug is widely used in the field of experimental epileptology, since it evokes long-lasting (> 3 hrs) and spontaneous epileptiform activity [117, 118]. The OPD's generated current was recorded simultaneously with electrophysiological activities (extracellular field potentials). Induction of the epileptiform activity took about 15 minutes (Figure 2.2a) after the application of 4-AP and lasted over the entire period of the drug application (about 25 minutes). A synchronous excitation

occurred spontaneously involving not only CA1 pyramidal cells but all the neurons of the slice's network. The initial phase consisted of a set of collective and regular LFPs, indicating the overall excitation of the network. The first phase, showing the highly intense epileptiform activity (Figure 2.2a) lasted approximately 1 min (time interval: 15-16), then the intensity and the amplitude of the activity gradually decreased. This second phase, the decreasing period (time interval: 16 to the end), consisted of group epileptiform discharges occurring every 0.5 to 2 seconds. The generated photocurrent started to rise 12 seconds after the epileptiform discharge onset and reached its maximum (7.5%) almost 2 minutes after the peak of the epileptiform activity (Figures 2.2b).

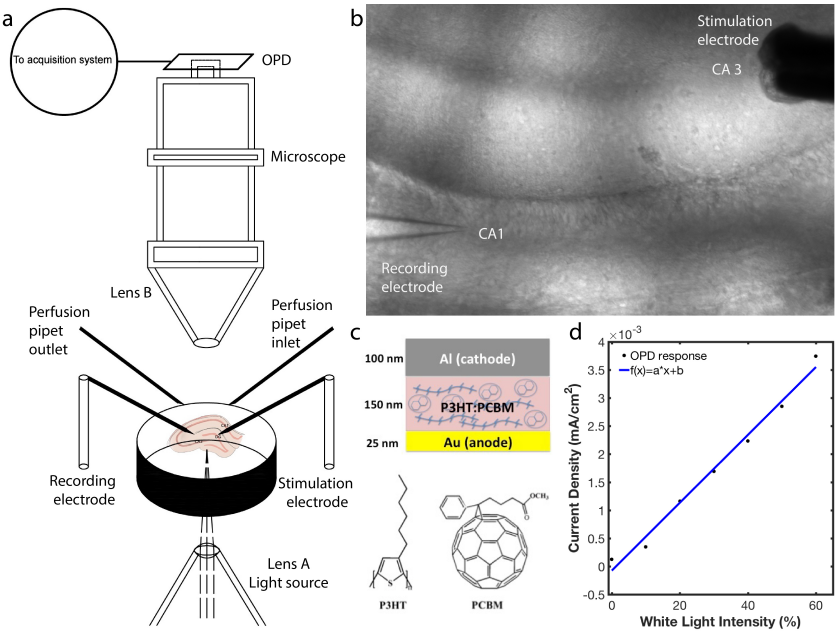

Figure 2.1 – **Schematics of the experimental setup and characteristics of the OPD device a)** Lens A focuses the light onto the region of interest and lens B collects the transmitted light from the tissue. The OPD was installed on top the microscope to detect optical changes and to avoid any optical perturbations caused by the perfusion solution flow. **b)** Optical image of the hippocampal slice, where the overall optical activity of the neuronal network was recorded. The stimulation electrode was implanted in the CA3 region to evoke synaptic response and the recording electrode was located in the CA1 region. **c)** OPD structure including a semi-transparent Au-anode, a P3HT:$PC_{60}BM$ blend film and Al as the cathode. **d)** Linear response of current density to the stepwise increase of illumination intensity shows the good performance of the OPD. The OPD was biased at -0.3V to maximize the photogenerated carrier.

IOS's temporal delay is probably due to the fact that the transmembrane water flow (CVR's effect), responsible for the cell swelling, is a slower process than the ion flux required for the generation of LFP changes. When the amplitude of the epileptiform activity decreased (Figure 2.2c), the transmittance of slice decreased as well (Figure 2.2d). Spectro-temporal analysis of the electrophysiological signal (Figure 2.2e) showed that the decrease of epileptiform activity's spectral power was followed by a decrease in transmittance (Figure 2.2d). Here, it was demonstrated that the epileptiform discharge caused significant changes in translucency

of the tissue due to cells swelling. This effect was clearly detected by the OPD. These results demonstrate the capability of OPD in studying strong signals (more than 5% optical changes) typical of pathophysiological events, e.g. epileptiform discharges.

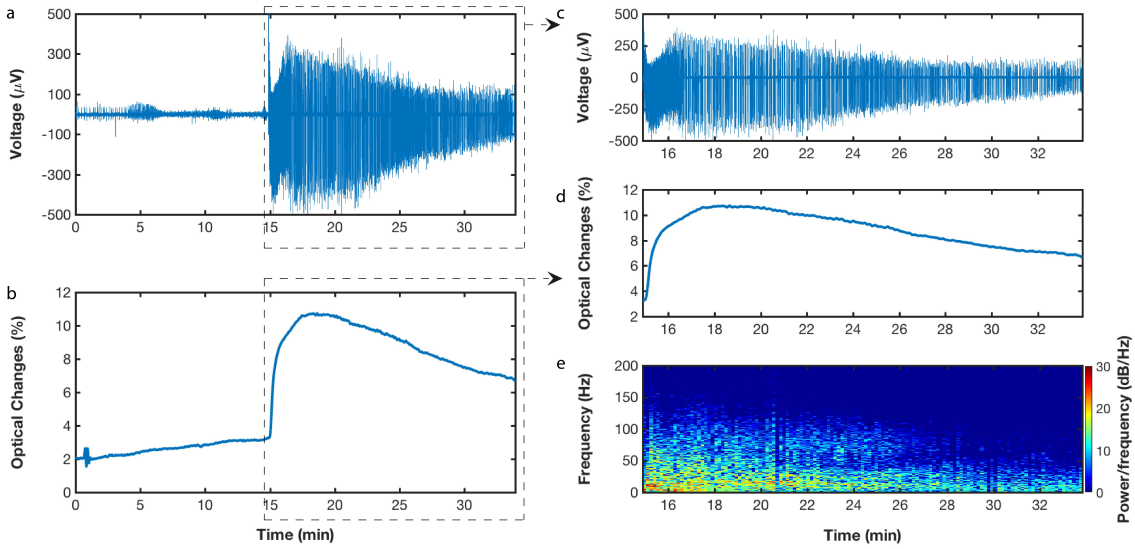

Figure 2.2 – **OPD detects optical changes with the same temporal resolution as simultaneously recordings electrophysiological signals during pathological epileptiform activity.** Inhibition of voltage-gated potassium channels by bath application of 4-AP induced epileptiform electrophysiological activity in hippocampal slices of an adult mouse. Epileptiform activity is associated with a dynamic change in the tissue optical properties. **a)** 4-AP induced activity is characterized by rapid oscillations of extracellular LFP. **b)** OPD generated current expressed as a percentage of the baseline value. OPD exposed to the white light transmitted through the tissue slice generates a current proportional to the light intensity. Variations in slice's optical properties modulate the transmitted light intensity that induces a variation of the electrical current generated by OPD. Note that cell swelling is already detectable as soon as 4-AP is washed in (between t=0 and t=15 min), whilst field oscillations are barely visible. At the beginning of 4-AP wash in, cells start to fire, but not in coordinated fashion. The latter occurs abruptly around t=15 min. **c)** Zoom in of the epileptiform activity of a. **d)** Zoom in on the variations of optical properties of the slice of b. Temporal comparison of the Figure c and d shows the delayed beginning of the augmentation of transmittance with respect to electrophysiological activity, which is due to the slow dynamics of cell swelling. **e)** Spectro-temporal representation of the LFP change illustrated on d. OPD generated current decreases simultaneously with a decay of electrophysiological activity power evaluated by spectro-temporal analysis of the LFP.

In the second experiment, the sensitivity of the OPD was investigated to detect lower-level IOSs (below 5% optical changes) generated by physiological events at tissue and even cellular levels (e.g. neuronal network activity). In this experiment, IOS was induced with physiological synaptic activation, which is much smaller than epileptiform activity. For this reason, a bipolar metal stimulation electrode was implanted in Stratum Radiatum close to the CA3 region (Figure 2.1b). The electrical stimulation of Schaffer collaterals induced synchronous excitation of hundreds of CA1 pyramidal cells. This network activity was evoked using two trains of electrical pulses generated with 10 Hz frequency (Figure 2.3a). The response to

synaptic stimulation was characterized by lower amplitude IOS. The duration of the first stimulation cycle was 30 seconds and the second cycle was 10 seconds. The maximum optical changes induced by both stimulation trains were approximately 3%, and the activities were significantly distinguishable from the noise level, 0.3% (root mean square of noise level expressed in percentage). In combination with the previous results, this signifies that the OPD can detect a high range of optical signals associated with neuronal activities of different ranges of intensity. When the network activity was induced, the transmittance started to increase to the maximum point (Figure 2.3b), which denotes that the CVR increases due to cell swelling. Both the trend and the magnitude of changes in IOS further confirm the OPD's performance and also validate its versatility for detecting both low and strong amplitude signals. The spontaneous activity that was detected in the slice before electrical stimulation persisted also after it. This suggests that the synaptic activation did not induce any depolarization block, and therefore, the evoked neuronal network activation remained in physiological range. In order to analyze the electrophysiological signal in the spectro-temporal domain, high-amplitude-bipolar stimulation artifacts were suppressed (Figure 2.3c) using a custom-made program. From the beginning of the first synaptic activation until the second, a comparison between the optical signal (Figure 2.3d) and spectro-temporal analysis of the same interval (Figure 2.3e) was conducted. During synaptic stimulation (interval A) the LFP's spectral power was high but decaying while IOS amplitude was low and slowly rising. The high spectral power of electrophysiological activities during stimulation in this interval led to blockade of the neuronal network and consequently, potentially blocked CVR's activity for a period of time, therefore cell swelling was not very pronounced. This phenomenon can be seen as slow changes of the IOS during a part of the synaptic activation period (interval A). After evoking the network activity (interval B), the LFP power decreased (Figure 2.3e), whereas IOS continued to rise. Afterwards, when the electrophysiological activity returned to its initial level (interval C), the IOS started to decay (Figure 2.3d). Thus, in the case of short lasting (seconds) physiological neuronal network activity, the IOS did not follow the LFP as it did in case of long lasting (minutes) epileptiform discharges. However, in both cases the OPD showed high sensitivity to detect the neuronal activation induced changes in the optical properties of the neuronal tissue. In order to examine the responsiveness of our OPD to physiological changes weaker than the first synaptic activation, an electrical stimulation of 10 seconds (Figure 2.3a) was applied before IOS reached the baseline (Figure 2.3b). It was observed that when stimulation was applied, the trend of the IOS that was decreasing halted, and immediately after the second synaptic activation, IOS increased towards the maximum level. Subsequently, the IOS decreased gradually until reaching the baseline. Thus, the OPD presented a high sensitivity and temporal resolution in such short-duration physiological events. This demonstrates that monitoring of optical properties using OPD could be a novel complementary approach to electrophysiology for detecting optical changes in brain tissue that may otherwise go unnoticed. To the best of our knowledge this is the first report of simultaneous, temporally-resolved recording of electrophysiological and IOS using OPD. These results indicate that OPD used in conjunction with electrophysiological recordings can provide a platform for studying how certain biological events and IOS are correlated thereby

leading to a better understanding of their mechanism.

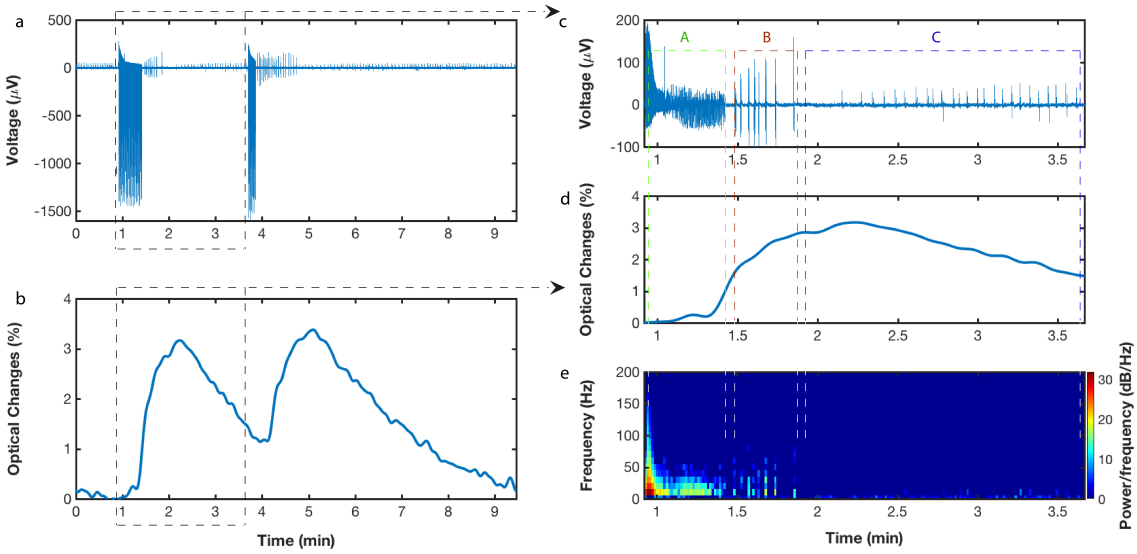

Figure 2.3 – **OPD can detect weak physiologically-relevant IOS evoked by neuronal activities.** Neuronal network activity induced by electrical stimulation is modulating the transmitted light, whose intensity changes were detected by the OPD. **a)** LFP responses to 10-Hz electrical stimulation for 30 and 10 sec recorded in hippocampal slice of adult mouse brain. Spontaneous activity detected in slice before electrical stimulation persisted also after it. This suggests that the stimulation did not induce a depolarization block and that induced neuronal network activation remained in physiological range. **b)** Responses to both stimulation events were accompanied by changes in the electrical current generated by the OPD. **c)** Zoom in on the first response to synaptic activation, where the stimulation artifacts are suppressed. **d)** Zoom in on the tissue's optical response to the first electrical stimulation. During the stimulation (interval A) the optical changes were slow but became faster at the end of stimulation train. Optical signal continued to rise during after-discharge (interval B) and started to decay slowly when network activity returned to its initial, before stimulation level (interval C). **e)** Time-frequency-power presentation of the LFP signals during and after the first cycle of synaptic activation. During synaptic stimulation, the LFP power was high and then decayed whereas IOS amplitude was low but slowly rising. After stimulation, the LFP power decreased whereas IOS continued to rise and started to decay when the electrophysiological activity returned to its initial level (Figure 2.2d). Thus, in the case of short lasting (seconds) physiological neuronal network activity the IOS did not follow the LFP as it did in case of long lasting (minutes) epileptiform discharges. However, in both cases the OPD showed sensitivity sufficient to detect the neuronal activation induced changes in optical properties of the neuronal tissue.

2.6 Conclusions

In conclusion, we presented an IOS recording platform using simple structure organic photodetector. We demonstrated the capability and potential impacts of this system for the detection of intrinsic optical signals, an important phenomenon caused by changes in cell volume in brain tissue. The OPDs revealed to have high sensitivity and high temporal resolution, allowing for simultaneous recording of electrophysiological and optical signals from the

brain and facilitating the understanding of their correlations. They demonstrated to detect a wide range of physiological, i.e. natural physiological activities and pathophysiological events, such as epileptiform activity. Though we focused on the detection of IOS here, the chemical tuning of the organic active materials constituting OPDs will allow this platform to be adapted for other optical sensing applications in living tissues in a discrete manner, including monitoring metabolic activity. Further improving its utility, we anticipate that this OPD-based platform can be miniaturized to make flexible implantable devices for in vivo applications. Their structural simplicity for tailored fabrication combined with their exceptional sensitivity and temporal resolution will prove an invaluable and versatile tool for numerous biological applications yet limited by complexity of commercially available technologies.

2.7 Materials and methods

Organic Photodiode Fabrication and Characterization: Fabrication of OPD was done using standard microfabrication procedure and in the open air, except last film annealing and encapsulation steps. This is due to the fact that film annealing accelerates the oxidation of the active material and trapping of oxygen during encapsulation procedure leads to the slow and long-term degradation of the device. At first, microscope glass slides of 25mm by 75mm were used as substrate. Transparent anode of 40 nm thicknesses was made using sequential thermal evaporation of 10 nm Cr and 30 nm Au on pre-patterned S1813 photoresist and a subsequent soaking in an acetone-isopropanol lift-off bath. The Cr layer was used to enhance the adhesion of Au to glass substrate. Active layer was spin-coated at 1000 RPM for 2 minutes to achieve 150 nm thicknesses (determined using optical profilometer Veeco) from solution blend of P3HT and $PC_{60}BM$ at a weight ratio of 1:1 in 1,2-dichlorobenzene and an overall concentration of 40 mg/ml. This solution was heated and stirred overnight at 90 °C prior to casting. The, film was annealed for 15 min at 110oC under inert atmosphere to drive off residual solvent and to stabilize the film. Cathode was deposited using thermal evaporation of 100 nm of Al using a shadow mask. The active area of the electrode was 14 mm2. For device encapsulation, epoxy (Ossila-E131) in conjunction with glass coverslip was UV-cured at the wavelength of 365nm for 2 min under inert atmosphere. Device characteristics were measured under dark conditions using Keithley 2612A source-meter.

Tissue Slice Preparation: A P21-56 OF1 male mice anaesthetized with isoflurane was decapitated; the brain was rapidly removed from the skull and placed in the ice-cold artificial cerebrospinal fluid (ACSF). The ACSF solution consisted of (in mmol/L): NaCl 126, KCl 3.50, NaH2PO4 1.25, NaHCO3 25, CaCl2 2.00, MgCl2 1.30, and dextrose 5, pH 7.4. ACSF was aerated with 95% O2/5% CO2 gas mixture. Saggital slices (350 µm) were cut using a tissue slicer (Leica VT 1200s, Leica Microsystem, Germany). During cutting, slices were submerged in an ice-cold (< 6°C) solution consisting of (in mmol/L): K-gluconate 140, HEPES 10, Na-gluconate 15, EGTA 0.2, NaCl 4, pH adjusted to 7.2 with KOH. Slices were immediately transferred to a multi-section, dual-side perfusion holding chamber with constantly circulating ACSF and allowed to recover for 2h at room temperature (22°C-24°C).

Synaptic Stimulation and Field Potential Recording: Ex-vivo LFP and patch-clamp recordings were performed on brain slices from P21-56 OF1 male mice. Slices were transferred to a recording chamber continuously superfused (15ml/min) with ACSF (33–34°C) with access to both slice sides. Schaffer collateral/commissures were stimulated using the DS2A isolated stimulator (Digitimer Ltd, UK) with a bipolar metal electrode. Stimulus current was adjusted using single pulses (40-170 μA, 200μs, 0.15 Hz) to induce LFP of about 50% maximal amplitude. LFPs were recorded using glass microelectrodes filled with ASCF, placed in stratum pyramidale of CA1 area and connected to a EXT-02F amplifier (npi electronic GMbh, Germany). Synaptic stimulation consisting of a stimulus train (200μs pulses) at 10 Hz lasting 30s was used to induce slice tissue optical response. To induce epileptiform activity a Kv1 channel blocker 4-aminopyridine (50 M) was added to ACSF.
Experimental setup: The illumination intensity was kept at 50% of the maximal power during the induction of both epileptiform and physiological activity. At this power, underneath the sample, a halogen lamp was used for the illumination of the brain slice with a stable intensity.
Data Analysis: Data analysis and signal processing were done using Matlab R2016b.

This chapter is based on the publication:
Rezaei-Mazinani S., Ivanov A.I., Proctor C. M., Gkoupidenis P., Bernard C., Malliaras G. G. & Ismailova E. (**2017**). Monitoring intrinsic optical signals in brain tissue with organic photodetectors. *Advanced Materials*, Submitted

3 Monitoring Fluorescent Calcium Signals with High Performance Organic Photodetectors

3.1 Abstract

Optical measurements are widely used to monitor biological activities, such as changes in metabolism, gene expression, and ionic concentrations. The main instruments to measure these optical activities, current approaches encompass microscopy and cameras equipped with high affinity inorganic sensors and image processing units. These light detection systems, due to their complex image processing, cause temporal delay in recording fast biological events. Organic photodetectors have numerous advantages for optical sensing applications recently, notably lower dark current level than inorganic counterparts and linear dynamic range in very low light intensities. These properties have shown that they are more sensitive than inorganic sensors. However, they have been limitedly investigated in biomedical applications, with no reported applications in the brain to date. In this chapter, an OPD with a simple structure and a ultra-low dark-current (10 fA/cm^2) is presented for detecting calcium activities via a fluorescent indicator. The active layer of the device consists of a novel wide-bandgap polymer XPL6 blended with $PC_{70}BM$, which results in high detectivity (10^{11} Jones) for green fluorescent wavelengths. The OPD acts as a highly sensitive sensor for the detection of low-intensity calcium fluorescent activities from living brain tissue. For the first time, this work presents the capability of organic photodetectors to measure fluorescent opto-electrophysiological events in neuroscience. The simplicity of fabrication and the capability of selective wavelength absorption via tunable chemistry paves the way for the integration of these devices in implantable biomedical devices with broad applications.

3.2 Résumé

Des méthodes optiques sont fréquemment utilisées pour enregistrer des activités biologiques comme des changements du métabolisme, des activités à l'origine des expressions génétiques et des concentrations ioniques. Des approches actuelles pour enregistrer ces activités optiques consistent de la microscopie et des caméras. Ces caméras sont équipées par des capteurs inorganiques de haute affinité et une unité de traitement d'images. La complexité de cette unité cause du retard dans l'enregistrement des événements biologiques rapides. OPD a montré récemment plusieurs avantages pour la détection optique, notamment un courant noir plus bas que leurs équivalents inorganiques, une gamme dynamique linéaire à la réponse des intensités de lumière très basses (100 pW/cm^2). Ces propriétés montrent que ces capteurs organiques sont plus sensibles que des dispositifs inorganiques. Cependant, l'investigation des applications biomédicales des OPD est limitée, et il n'existe aucun rapport concernant leurs applications en neuroscience. Dans ce chapitre, un OPD possédant une structure simple et un courant noir ultra-bas (10 fA/cm^2) est présenté afin de détecter des activités de calcium par un indicateur fluorescent. La couche active de cet OPD consiste en un accepteur d'électron $PC_{70}BM$, mêlé avec XPL6, un polymère possédant une large bande interdite. Cet OPD montre une haute détectivité (10^{11} Jones) pour enregistrer des activités fluorescentes en longueur d'onde verte. L'OPD démontre une haute sensibilité comme capteur optique pour détecter des activités fluorescentes à l'intensité basse du tissu cérébral vivant. Pour la première fois, ce travail de recherche présente la capacité de OPD pour enregistrer des événements opto-électrophysiologiques fluorescents en neuroscience. La simplicité de fabrication et la capacité de l'absorption dans une longueur d'onde d'une manière sélective ouvrent une nouvelle perspective pour l'intégration de ces OPD dans des dispositifs biomédicaux implantables.

3.3 Introduction

Optical measurement is one of the most widely-used methods in studying biological activities and signals, such as ion channels and signaling [15, 119], gene expression [89], metabolic activity [88] and intrinsic optical signals [21, 93, 94]. To record these optical activities, current techniques involve microscopy to shine light into tissue and imaging with cameras with high affinity inorganic sensors (CCD and CMOS) and image processing units [16]. Often, biological activities are visualized with the aid of fluorescent and luminescent molecular probes and genetically encoded indicators, both of which are available in a variety of wavelengths and can be used together for co-labeling [15, 90, 92]. Cameras record these activities by scanning in multiple frames, then these frames are transferred to an image processing unit. This is known as «read-out» process [101]. Afterwards, they are analyzed on a certain cell or region to measure the signal of ionic activity [16]. This process is known for limiting the time-resolution. By using a standalone photodetector unit combined with different types of microscopes, the optical signals can be recorded directly from any targeted cell or region. This approach will give the opportunity of removing scanning time delay and the real-time detection of signals from ions. On the other hand, it is known that inorganic photodetectors hardly distinguish

between different wavelengths, since their optical absorption band is wide and difficult to manipulate. Organic active materials and devices have shown great potential in the tunability of their chemical and physical properties, including absorption spectra. Various organic active materials have been introduced in the past illustrating different absorption spectral windows [53]. It has been shown that OPDs can be utilized for high quality imaging with high temporal resolution [25]. Organic materials have presented a linear dynamic range at very low light intensity [75], which distinguishes them from their inorganic counterparts that show non-linearity at very low intensity. They have demonstrated the possibility of having a lower noise level than inorganic devices because of the low conductivity of the bulk heterojunction layer [75]. This means that they give a lower dark current than their inorganic counterparts [28, 72], hence an enhanced sensitivity for optical detection [75, 75]. Recently, one promising report has shown the synthesis of a solution-processable set of organic active materials having a high-efficiency absorption in visible spectral range [54]. This is an example of the tunability of organic active materials. Therefore, these materials tend to be excellent candidates adaptable to the specificity of different biological problems for customized measurements, such as low-intensity fluorescent emission of metabolic activities or ion signals. Furthermore, organic materials employed in bioelectronic devices have presented mechanical flexibility, thin film architecture, easy and low-cost fabrication, high capacity for integration with living tissues and cells and great mechanical properties for in-vivo applications [105–112]. Organic optoelectronic devices interfacing living cells and biological tissues, particularly have been used for interfacing the neural system via the retina [26] and for treating blind retina using photoactivation [113–115]. These works focus on the electrical stimulation of damaged retina and neural cells. In the case of bio-optical optical sensing, organic light emitting diodes and OPDs have been combined into a flexible substrate in order to cutaneously measure oxygen levels of blood [116]. These works illustrate the broadness of the potential of organic optoelectronics for biomedical applications. To the best of our knowledge, OPDs have never been used as an optical sensor for studying biological activities in a specific spectral range. Among different types of ions, Ca2+ generates versatile signals that determine functional aspects of different cellular mechanisms [120]. In calcium imaging, fluorescent signals are recorded following the stimulation of biological sample, which can be a neuronal network or a single neuron [16, 120]. In the present work, we aim to broaden the biomedical utilization of organic photodetectors by demonstrating their high sensitivity and temporal resolution in the measurement of fluorescent calcium signals in vitro and ex vivo.

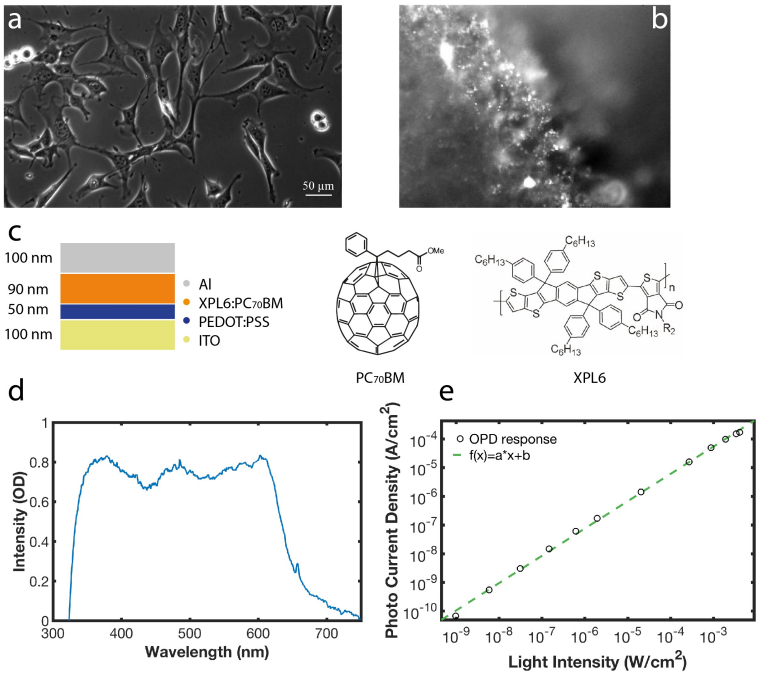

Figure 3.1 – **Calcium staining in *in-vitro* and *ex-vivo* and the OPD Characteristics**. **a)** Bright-field image of HT22 hippocampal cultured cells incubated in fluorescent Ca^{2+} indicator. **b)** Bright-field image of hippocampal slice incubated in the fluorescent indicator, bound to the cells over the neuronal network. **c)** OPD structure composed of a transparent ITO-electrode, a XPL6:$PC_{70}BM$ blend film and Al as the cathode. **d)** The device showed a very high absorption, especially at green wavelength. **e)** The device demonstrated a linear dynamic range at $0\,V$, under the illumination at the wavelength of $522\,nm$, in response to ultra-low light intensities.

3.4 Device characteristics and experimental aspect

In order to record Ca^{2+} signals *in vitro* and *ex vivo*, HT-22 hippocampal cultured cells (Figure 3.1a) and hippocampal slices (Figure 3.1b) were incubated in the fluorescent indicator $C_{51}H_{50}F_2N_2O_{23}$ (Fluo-4), which is Ca^{2+}-specific. After the indicator bound to the Ca^{2+} ions in solution, the cultured cells and hippocampal slices were exposed to a blue light source for triggering the fluorescent emission. The same experimental setup as section 2.4 was used for the measurements (Figure 2.1a). In order to initiate the inta- and extra-cellular ionic exchange, *in vitro*, potassium chloride (KCL) was applied to the cell media via μ-injection. During *ex vivo* experiments ionic exchange was induced in the neuronal network of hippocampal slice by electrical stimulation. The neuronal network activity was recorded as a change in LFP in CA1 region (Figure 2.1b) using an extracellular electrode. Fluorescent Ca^{2+} activities were measured in real-time, during all the experiments using the OPD was mounted on the setup for recording optical activities (Figure 2.1a). The OPD was designed to have minimal layers and low leakage current in order to simplify fabrication process and enhance the sensitivity, especially at fluorescent wavelength spectrum in order to detect low-amplitude Ca^{2+} signals from the cells and brain tissue. The structure composed of a thin transparet ITO electrode on a glass substrate, high work-function PEDOT:PSS as buffer layer, XPL6 blended with $PC_{70}BM$

for BHJ film and an Al as the cathode (Figure 3.1c). Finally, the OPD was encapsulated using epoxy and a glass cover-slip. Electro-donor XPL6 is a polymer that exhibits a high open circuit voltage ($\sim 1V$) and wide band-gap ($\sim 2eV$) [54]. Fullerene-based electron-acceptor $PC_{70}BM$ is known for enhanced low band-gap. The wide band-gap of XPL6 and the low band-gap of $PC_{70}BM$ in blend, improve the power conversion efficiency of the BHJ significantly, especially within fluorescent absorption spectrum. The active layer showed to have a very high absorption spectra (Figure 3.1d). The device presented an ultra-low dark current, $10fA/cm^2$ and an excellent detectivity of $10^{11} Jones$ which are important for a highly sensitive device. The OPD under $0V$ bias showed to have a stable behaviour and a linear dynamic range in response to ultra-low illumination intensities at $522nm$ wavelength (Figure 3.1e).

3.5 Results

In the *in vitro* experiment, high K^+ depolarization was induced using KCL. Following the injection, extra-cellular Ca^{2+} bound with the dye and diffused to the cells and was recorded by the OPD as a high fluorescent Ca^{2+} activity rising up to ~ 13% optical changes (Figure 3.2). After the sharp rise of the optical signal, the Ca^{2+} ions diffused in the cells by binding to the intracellular buffer, known to have slow dynamics. As result, the increasing trend of optical signal reached the plateau approximately at ~ 13% (Figure 3.2). Due to the photobleaching effect of Ca^{2+} because of being exposed to the stimulation light, the cells died and the signal did not reach the baseline. This signal is considered to be relatively strong because in *in-vitro* , cells are of the same type and the network is dense, which gives a pronounced fluorescent emission. This activity was detected successfully by the OPD. This experiment showed the high sensitivity of the OPD for recording the fluorescent activities from a population of cells. In *ex vivo* experiment, we recorded Ca^{2+} signals to determine whether the sensitivity of the OPD was high enough to detect weak activities from a brain slice. For inducing neuronal network activity, a bipolar metal stimulation electrode was implanted in Stratum Radiatum close to the CA3 region (Figure 2.1d). The synaptic activation of of Schaffer collaterals evoked synchronous excitation of hundreds of CA1 pyramidal cells. This network activity was evoked using a train of electrical pulses generated with 10 Hz frequency for 30 sec (Figure 3.3a). Using a home-built Matlab program, bipolar stimulation artefacts were suppressed and the signal was reconstructed. The response to synaptic stimulation was characterized by a lower amplitude Ca^{2+} signal than *in vitro* detected by OPD (Figure 3.2). Time-frequency-power presentation of the electrical signal (Figure 3.3b) showed that at the stimulation onset, the spectral power was at the maximum, $50-30dB$ at the frequency range of $30-10Hz$ (interval A). In the same interval, the optical signal (Figure 3.3c) demonstrated the Ca^{2+} diffusion over the network (interval A), with the maximum ~ 8% optical changes. Afterwards, the spectral power decreased to $30-20dB$, at the frequency range of $30-10Hz$ (interval B). In this interval, the Ca^{2+} signal reached the plateau, which means that the Ca^{2+} ions diffused inside the cells, over the neuronal network. The diffusion has slow dynamics due to the slow dynamics of the internal cellular buffer. At the final phase (interval C), the spectral power decreased to

$20-10dB$ at the frequency range of $30-10Hz$. This happened when the Ca^{2+} activity was at the final stage and was reaching the baseline. In *ex vivo* conditions, the fluorescent emitting cells that activate synchroniously are less dense than *in vitro* conditions, since they are propagated within an area. This leads to a less intense Ca^{2+} signal. The Ca^{2+} signal showed to be a surrogate of the electrical signal. These results presented the high sensitivity and temporal resolution of OPD for detecting real-time Ca^{2+} dynamics, induced by electrical stimulation of the neuronal network. While the electrical signal showed the overall activity of the neural network, the Ca^{2+} signal, simultaneously, demonstrated the functional physiological side of the neuronal network.

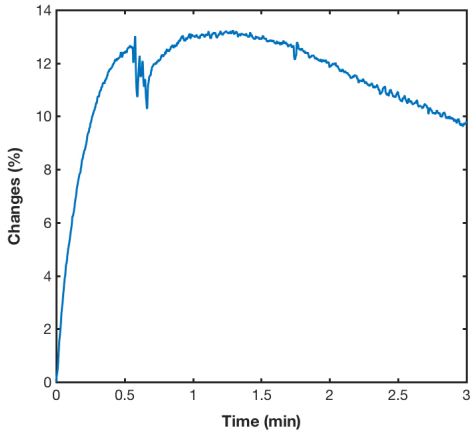

Figure 3.2 – **Optical signal due to high K^+ depolarization from cultured cells**. OPD can detect relatively strong K^+ signals, from high K^+ depolarization in cultured cells. Due to the injection of KCL to the media cells were depolarized and Ca^{2+} entered to the cells. As result, it gave a sharp rise of the signal up to ~ 13% of optical changes. Following entrance of the ions, they diffused in the cells, which has a slower dynamics, therefore there was a decrease in the slope of optical signal. The high K^+ depolarization caused photobleaching, which is toxic phenomenon, for this reason, the cells died shortly after the cellular ionic exchange. This signifies the high sensitivity and temporal resolution of the OPD for recording the fluorescent activities in a population of cells.

In the second *ex-vivo* experiment, we recorded fluorescent Ca^{2+} signals to evaluate the sensitivity and temporal resolution of OPD for detecting fast and low-intensity Ca^{2+} signals from the hippocampal slice. The spontaneous network activity was evoked using a train of electrical pulses generated with the same characteristics as above, with the duration of 1 sec at $100Hz$ (Figure 3.4a). Time-frequency-power presentation of the LFP signal (Figure 3.4b) showed a high amplitude Ca^{2+} shift in the neuronal network, lasted about 0.5 sec with the maximum of $50dB$ within the frequency range of $0-30Hz$. The optical signal (Figure 3.4c) showed the Ca^{2+} diffusion at this high spectral-power activity with with maximum optical changes of ~ 4%. Regarding the stimulation period was short, the spectral power decreased in the end of the stimulation, but the Ca^{2+} activity lasted for ~ 2.5 sec after it, then it reached the baseline.

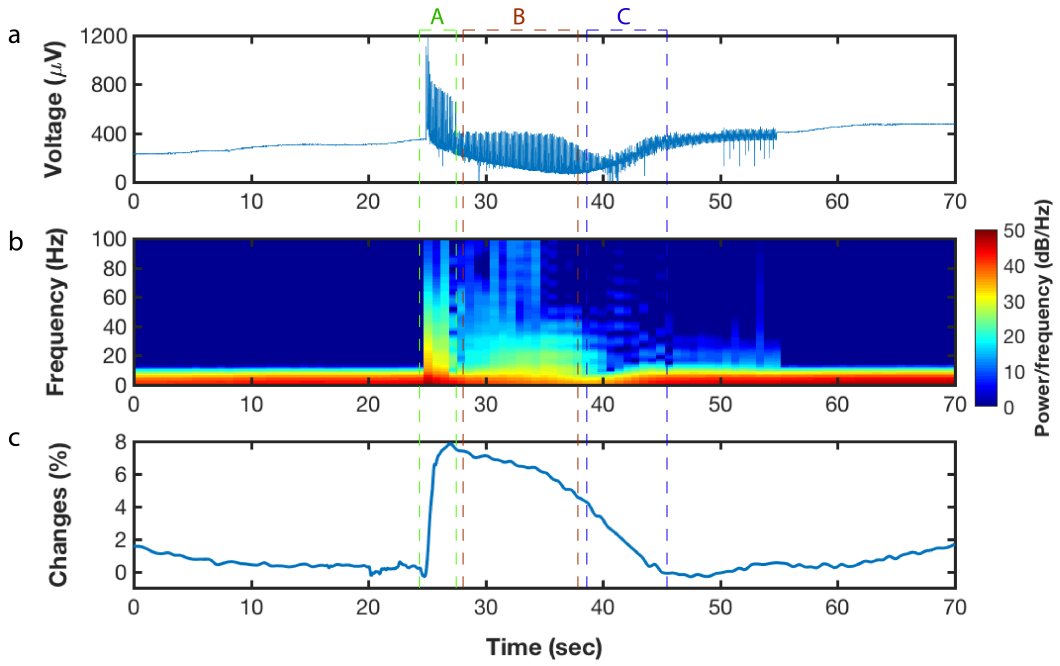

Figure 3.3 – **Fluorescent Ca^{2+} signal evoked by electrical stimulation**. OPD can detect relatively weak fluorescent Ca^{2+} signals from brain tissue in physiologically-relevant neuronal activities, evoked by 30 sec electrical stimulation. A hippocampal slice of adult mouse, incubated with a Ca^{2+}-specific fluorescent indicator was exposed to the blue light to trigger the fluorescent emission. The Neuronal network activity was evoked by electrical stimulation, which led to cell depolarization. The depolarization of the network cells resulted in the diffusion of Ca^{2+} ions bound with the fluorescent dye into the cells. This activity modulated the resulting fluorescent emission, which was recorded by the OPD. **a)** LFP response to $10Hz$ electrical stimulation. The evoked activity detected in the slice was spontaneous and afterwards it was persistant. This means that the stimulation did not evoke any depolarization block and that induced a neuronal network activity in physiological range. **b)** Time-frequency-power presentation of the LFP signal during stimulation. The activity started at the power-spectral density $50dB/Hz$ and it decreased to $10dB/Hz$ in the end of the stimulation due to exhaustion of the neurons. **c)** The optical signal showing the Ca^{2+} activities is a surrogate of electrical signal. The optical signal demonstrates the Ca^{2+} uptake over the network (interval A), which took place simultaneously with the start of the synaptic activation. The optical signal raised up to the maximum ~ 8% optical changes. This appears at the maximum of spectral power $50-20dB$ and at the frequency range of $10-80Hz$. Afterwards, the Ca^{2+} diffused through the cells over the network. The diffusion has slower dynamics due to the slow dynamics of the internal cellular buffer. This is where the optical signal reached the plateau and LFP's amplitude decrease and (interval B). The the spectral power was in the range of 35 to $20dB$ within the frequency range of $80Hz$ during plateau phase (interval B). Finally, the Ca^{2+} signal faded away, where the LFP's amplitude was at the minimum and the spectral power was about $20dB$ at the frequency range of $10-20Hz$ (interval C). This presents the high sensitivity and temporal resolution of OPD for detecting the Ca^{2+} dynamics due to the induced synaptic activation of neuronal network.

The short stimulation interval, led to the diffusion of lower amount of Ca^{2+} than the last case. Therefore, the Ca^{2+} signal did not reach the plateau level and faded after the maximum level. The Ca^{2+} signal demonstrated that upon each pulse, a series of burst of activities were triggered. Upon the burst, Ca^{2+} diffusion took place over the network, which led to the

accumulation of Ca^{2+} in the cells. This showed the integration of the spiking activity in the level of neuronal network. It can be observed that the duration and amplitude Ca^{2+} signal was proportional to the duration and intensity of the synaptic activation over the network. This means that the OPD demonstrated an exceptional sensitivity and temporal resolution for recording fast and low-intensity fluorescent activities.

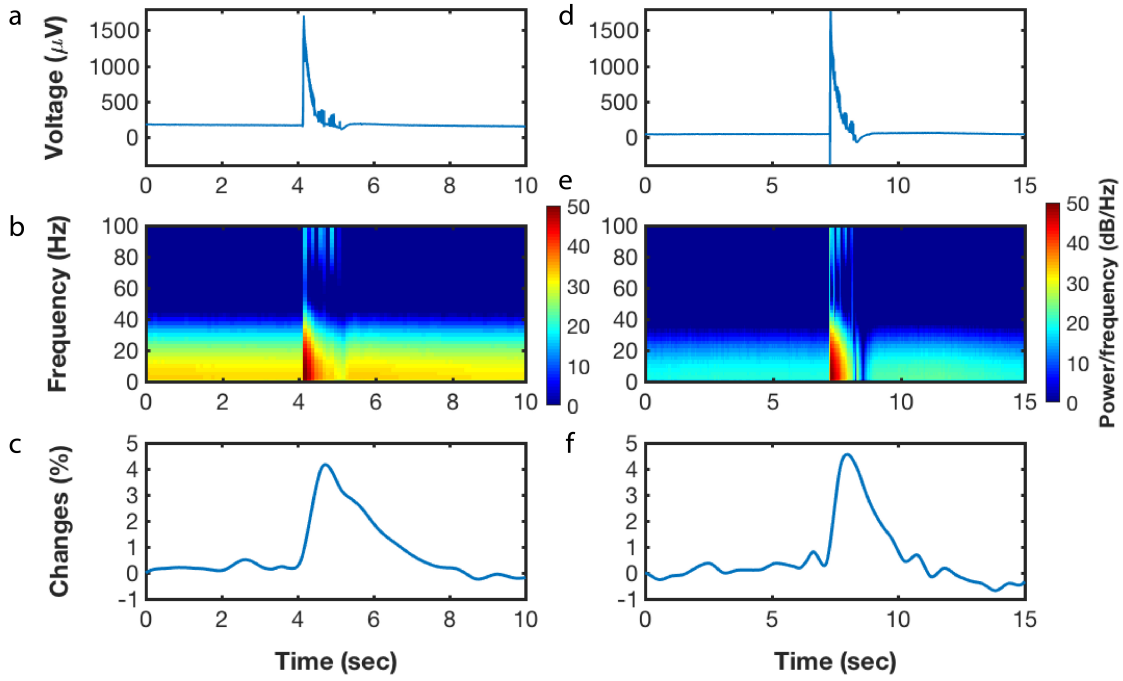

Figure 3.4 – **Fluorescent Ca^{2+} signal evoked by a short electrical stimulation**. OPD can detect weak fluorescent Ca^{2+} signals from brain tissue, evoked by 1 sec electrical stimulation. The neuronal network activity was evoked by electrical stimulation, which led to the diffusion of Ca^{2+} ions into the cells. **a)** LFP response to $100Hz$ synaptic activation for 1 sec. The induced activity detected in the slice was spontaneous and very short. **b)** Spectral power presentation of the LFP signal during electrical stimulation. The activity started at the power-spectral density of $50dB/Hz$ and it decreased to $20dB/Hz$ in the end of synaptic activation due to the short overall activity of neuronal network. **c)** The optical signal shows the Ca^{2+} uptake taking place approximately at $50dB$ within the frequency range of $0-50Hz$. This is where the optical signal approximately raised up to 4%. Afterwards, the signal showed a decreasing trend and tails off. This is due to the Ca^{2+} diffusion though the cells. This activity lasted almost 3 sec after the stimulation. This slow trend is due to the slow dynamics of the cellular buffer. This signifies that the dynamics of cellular buffer was slower than the stimulation period. In the end of the stimulation period the spectral-power decreases to $20-30dB$ within the frequency range $0-30Hz$. This signifies the high sensitivity and temporal resolution of the OPD for recording weak fluorescent activities in the brain tissue.

3.6 Conclusions

In conclusion, we demonstrated a platform for recording fluorescent ionic dynamics using a highly sensitive OPD. The capacity and promise of this system for the detection of Ca^{2+} signals was presented, which indicates the functional mechanism of neuronal network. We assessed versatility of device, by measuring the Ca^{2+} signal *in vitro* and *ex-vivo*, giving different intensities of Ca^{2+} signals. In this way, the OPD demonstrated a high sensitivity and high temporal resolution, which allows the detection of a wide range of Ca^{2+} signals. Though we focused on Ca^{2+} signal here, the tuneable properties of OPD will allow this platform to be adapted for other optical based sensing applications in living tissues including monitoring dynamics of other types of ions, ion channels, metabolic activities, gene expression and optogenetics. Detection of such events in specific regions of the brain, from a population to individual cells, will improve our understanding of metabolic and physiological activities, as well as optogenetic events and disease progression. Further improving its utility, we anticipate that this OPD-based platform can be miniaturized to make flexible implantable devices allowing for *in vivo* sensing. We anticipate that the structural simplicity of this OPD combined with its exceptional sensitivity and temporal resolution will prove an invaluable tool for numerous biological applications.

3.7 Materials and Methods

Organic Photodiode Fabrication and Characterization: All fabrication steps of OPD were done in open-air. Microscope glass slides of $25mm$ by $75mm$, featuring pre-patterned ITO were purchased from Ossila (S251). Transparent ITO film of $100nm$ was treated under O_2 plasma at $80Watts$ for $1min$ prior to the deposition of PEDOT:PSS (Heraeus AL 4083) interlayer by spin-coating. The PEDOT:PSS solution was sonicated for $15min$, then it was spin-coated at $5000RPM$ for $30sec$. This step was followed by annealing the film at 150^oC for $5min$. This gave a thickness of $\sim 50nm$. Active layer was spin-coated at $1300RPM$ for $180sec$ to obtain thickness of $\sim 85nm$ from solution blend of XPL6 and at a weight ratio 1:2 diluted in a mixture of 1,2-dichlorobenzene and 1-chloronaphthalene, 97:3 with concentration of $20mg/ml$. Processing active layer is annealing-free and this solution was heated and stirred overnight at 90^oC prior to casting. Cathode was deposited using thermal evaporation of $100nm$ of using a shadow mask. The active area of the OPD was $14mm^2$. For device encapsulation, epoxy (Ossila-E131) was covered with a glass coverslip was UV-cured at the wavelength of 365nm for 2 min under inert atmosphere. Device characteristics were measured under dark conditions using Unisense A/S, PA2000 pico source-meter.

Tissue Slice Preparation: A P21-56 OF1 male mice anaesthetized with isoflurane was decapitated; the brain was removed from the skull rapidly and placed in the ice-cold artificial cerebrospinal fluid (ACSF). The ACSF solution composed of (in $mmol/L$): sodium chloride (NaCl) 126, 3.50, NaH_2PO_4 1.25, $NaHCO_3$ 25, $CaCl_2$ 2.00, $MgCl_2$ 1.30, and dextrose 5, pH 7.4. ACSF was aerated with 95% O_2 5% CO_2 gas mixture. Saggital slices (350) were cut using a tissue slicer (Leica VT $1200sec$, Leica Microsystem, Germany). During slicing, brain slices

were submerged in an ice-cold ($< 6^oC$) solution consisting of (in $mmol/L$): K-gluconate 140, HEPES 10, Na-gluconate 15, EGTA 0.2, NaCl 4, pH adjusted to 7.2 with KOH. Slices were immediately transferred to a multi-section, dual-side perfusion holding chamber with constantly circulating ACSF and allowed to recover for 2h at room temperature ($22-24^oC$).

Labeling for calcium: HT-22 mouse hippocampal neuronal cells (Millipore Sigma) and brain slices were loaded with Fluo-4 AM, a labeled calcium indicator. HT-22 cells were cultured according to supplier's instructions. Brain slices are explained in latter. Fluo-4 AM (ThermoFisher Scientific) was prepared according to manufacturer's instructions. Briefly, a stock solution of Fluo-4 was prepared in DMSO. The working solution for cells was 5 in phosphate buffered saline (PBS) and for brain slices was 10 in ACSF. Cells and tissue slices were then incubated for 45 minutes-1 hour and subsequently washed with fresh PBS or ACSF.

Synaptic Stimulation and Field Potential Recording: *Ex-vivo* LFP and patch-clamp recordings were performed on brain slices from P21-56 OF1 male mice. Slices were transferred to a recording chamber continuously superfused ($15ml/min$) with ACSF ($33–34^oC$) with access to both slice sides. Schaffer collateral/commissures were stimulated using the DS2A isolated stimulator (Digitimer Ltd, UK) with a bipolar metal electrode. Stimulus current was adjusted using single pulses ($40-170$, 200, $0.15Hz$) to induce LFP of about 50% maximal amplitude. LFPs were recorded using glass microelectrodes filled with , placed in stratum pyramidale of CA1 area and connected to a EXT-02F amplifier (npi electronic GMbh, Germany). Synaptic stimulation consisting of a stimulus train (200 pulses) at $10Hz$ lasting $30sec$ was used to induce slice tissue optical response.

Experimental setup: The excitation light intensity was kept at 50% of the maximal power during the induction of physiological activity. At this power, underneath the sample, a blue light ($480nm$) was used for the excitation of Fluo-4 calcium indicator, bound to the cultured cells and brain slice with a stable intensity. During the measurements, a sharp long-pass dichroic filter at $520nm$ was used for sharp transition between the transmitted and reflected bands (Comar Optics-520 IY25). The measurement were performed over two weeks under ambient air. The devices showed an stable performance during this period.

Data Analysis: Data analysis and signal processing were performed using Matlab R2017a.

This chapter is based on the publication:
Rezaei-Mazinani S., Ivanov A.I., Rutz, AL., Chochos, C.L., Bernard, C., Malliaras, G.G., O'Connor, R., & Ismailova E. (**2017**). Monitoring fluorescent calcium signals in brain tissue with high performance organic photodetectors. *Advanced Materials*, In prepration

4 Orientation Selectivity with Organic Photodetectors and An Organic Electrochemical Transistor

4.1 Abstract

Neuroinspired device architectures offer the potential of higher order functionalities in information processing beyond their traditional microelectronic counterparts. In this chapter, we demonstrate a neuromorphic function of orientation selectivity, which is inspired from the visual system, with a combination of organic photodetectors and a multi-gated organic electrochemical transistor based on PEDOT:PSS . The device platform responds preferably to different orientations of light bars, a behavior that resembles orientation selectivity of visual cortex cells. These results pave the way for organic-based neuromorphic devices with spatially correlated functionalities and potential applications in the area of organic bio-electronics.

4.2 Résumé

Les dispositifs ayant l'architecture neuro-inspirée offrent le potentiel d'un ordre plus élevé des fonctionnalités dans le traitement des informations en comparaison avec leurs équivalents en microélectronique traditionnelle. Dans ce chapitre, la fonction neuromorphique de la sélectivité à l'orientation est présentée. Cette fonction est inspirée du système visuel. Nous la démontrons par la combinaison de l'OPD avec un OECT à multigrille à base de PEDOT:PSS. Le dispositif répond avec une certaine préférence aux différentes orientations des barres lumineuses. C'est un comportement qui se ressemble au phénomène, la sélectivité à l'orientation des cellules du cortex visuel. Ces résultats ouvrent la voie pour des dispositifs neuromorphiques à base des matériaux organiques ayant des fonctionnalités en corrélation avec des informations spatiales et des variétés d'applications dans le domaine bioélectronique organique.

4.3 Introduction

Nowadays, it is becoming apparent that traditional computing systems encounter limitations regarding their potential to process daily life information in real-time and to create patterns in order to solve unfamiliar problems [121]. A promising approach to overcome this limitation, is the functional imitation of the information processing ability of the brain with neuromorphic devices [122]. Over the past years, various forms of neuroplasticity and neural processing functions have been demonstrated with inorganic neuromorphic devices [123–128].
Within the area of organic electronics, the field of organic bioelectronics has emerged over the past few years [104, 112], offering a variety of applications such as biosensors and neural interfaces [109, 129]. Due to the facile interactions with biology, organic bioelectronics have also entered the realm of neuromorphic devices, offering neuromorphic functions at the interface with biological substances [130–132], thereby extending the functionality of existing neuromorphic devices. The attractive characteristics of organic electronic materials such as compatibility with low-cost fabrication processes and large-area, mechanically flexible substrates, as well as tunability of their electronic properties via chemical synthesis [133] promises the possibility of even further developments in neuromorphic devices. Various forms of neuro-inpired processing functions have already been implemented with organic-based transistors [134], nanowires [135], and resistive devices [136]. A prominent example of organic bioelectronic device is the OECT [137]. It consists of a conducting polymer channel and an electrolyte between the channel and the gate, which acts as the gating medium [138]. By applying a gate voltage, ions from the electrolyte are injected into the channel, modifying the doping level of the organic material and thus modulating the electronic current through the channel. Various neuromorphic functions have been recently reported in OECTs, such as short- and long-term plasticity and orientation selectivity [139–141]. Among the above mentioned neuromorphic functions, orientation selectivity is of particular interest, because it opens the door for novel, spatial concepts of information processing in organic bioelectronic devices [141].
Orientation selectivity has been studied extensively in the past decades and is related to visual perception. Hubel and Wiesel laid the foundation for understanding orientation selectivity of visual cortex cells [142–144]. According to their theory, visual cortex cells respond preferably (in terms of activity) to light bars with different orientations. Orientation selectivity is an important function of visual cortex that is responsible for first-level image processing of the everyday environment, and for its "deconstruction" into low-level information such as the edge detection [3]. In combination with other low-level functionalities (spatial, contrast filters, etc), edge detection forms then the basis for high-level perception such as image recognition [3, 145]. An "electrical" analogue of orientation selectivity was previously reported with a multi-gated OECT, in which a spatially oriented input voltage, was selectively correlated with the output of the transistor [141]. In this work we demonstrate an optoelectronic device platform that displays selectivity with respect to input light bars of different orientations, in analogy to the visual cortex cells. These results demonstrate the potential of organic neuromorphic devices for introducing spatial concepts in processing and sensing.

4.4 Materials and Methods

The device consists of two parts: **(a)** a grid of 3×3 organic photodetectors (OPD(x, y)) and **(b)** a multi-gated OECT with 3×3 gate electrodes (G(x, y)) (the device geometry is depicted in Figure 4.1a). The OPDs are commercially available [146] and fabricated on semi-flexible substrates, while the OECT was made using standard microfabrication techniques. As substrates for the fabrication of the OECT, $26mm \times 76mm$ glass slides were used. The contact lines were defined by evaporating a 10 nm chromium (Cr) and a 100 nm Au layer on top of pre-patterned photoresist used in a standard lift-off process and subsequently removed in a solvent bath.The Cr layer here is needed to promote the surface adhesion of Au to the glass substrate. To protect the contact lines from the electrolyte and to define the OECT's active areas, two parylene C layers were deposited on top, with 2 μm thickness each. The first layer was deposited on a surface treated with silane to enhance adhesion with the substrate and a thin 2% soap solution was spin-coated to form an anti-adhesive layer before the second deposition. This allows to peel-off the upper layer, thereby defining the device active area using consecutive photoresist patterning and reactive ion etching steps. The conducting polymer used in this communication was PEDOT:PSS [Clevios PH 1000 from Heraeus Holding GmbH, with 5 wt% ethylene glycol, 0.1 wt% dodecyl benzene sulfonic acid and 1 wt% of (3-glycidyloxypropyl)trimethoxysilane)]. It was used both as the channel and as the gate material. The desired film thickness ($\approx 500nm$) was obtained by three subsequent spin-coating steps with varying rotation speeds of 1500, 650, and 650 rpm respectively. PEDOT:PSS spin-coating was followed by a hard-bake step at 140 °C for $60min$. The gate electrodes had an area of $9mm$ while the channel had nominal dimensions of $15mm \times 0.5mm$ (length x width, L x W). Metal interconnects, insulated from contact with the electrolyte by parylene C, were used to establish electrical contacts. Detailed gate - channel distance mapping is described elsewhere [141]. After the fabrication of the OECT, the 3×3 grid of the gate electrodes, was connected one-to-one to the corresponding 3×3 grid of organic photodetectors with metal wires. The photodetector's active area as well as the spacing between each device was similar to that of the gate electrodes.

The photodetectors were used in order to capture the optical input stimuli that were projected on them with LEDs, and the resulting photocurrent was then used as a secondary input for the gate electrodes of the OECT (Figure 4.1a). The resulting output drain current ID was recorded, and from I_D the amplitude I_0 was defined in each experiment. The anode of the OPD was grounded and the cathode of each device was connected to each gate electrode of the OECT , in order to gate each pad with the resulting photocurrent of the OPD. The light bars ware generated by using 3 green LEDs that were simultaneously driven using a voltage pulse ($V_{OPD} = 3.2V, t_{OPD} = 100ms$). The LEDs had the appropriate spacing in order to generate a light bar with homogeneous spatial intensity and a shape that was similar to that of 3 OPDs in a row. Single gate measurements were performed with one LED using the same voltage and time conditions. The OECT was gated with ($x = 1-3, y = 1-3$) lateral Au electrodes covered with PEDOT:PSS (secondary inputs), and NaCl electrolyte ($100mM$) in deionized water. The drain current was measured using a National Instrument PXIe-1062Q

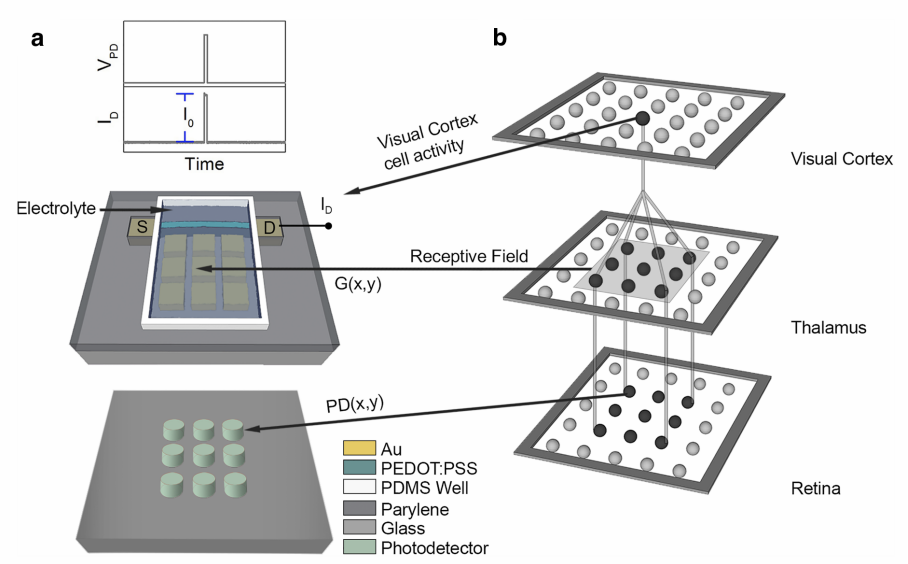

Figure 4.1 – **a)** Simplified schematic of the proposed device. The device consists of a 3 × 3 grid of OPD (OPD(x, y)) and a multi-gated OECT with a grid of 3 × 3 gate electrodes (G(x, y)). Every photodetector is connected in one-to-one fashion with every gate electrode (connections not shown here for simplicity). Top inset shows the measurement procedure: a voltage pulse is applied at the light emitting diode (LED)s (V_{OPD}) and spatial light patterns are projected on the photodetectors (through LEDs) and their resulting photocurrent drives the OECT through the gate electrodes. The amplitude I_0 of the output drain current I_D is defined in each experiment.

system. The OECT was biased with a PXIe-4145 source measure unit (SMU) (at $V_D = 0V$) that was simultaneously recording the drain current with a sampling rate of $1kHz$. The pulses at the LED were generated by a National Instrument USB-6259. Both LED pulses and drain current measurements were internally triggered by the PXIe system. The acquisition system was monitored by custom-made LabVIEW software.

4.5 Results

Figure 4.1 presents a simplified analogy of the proposed device and the orientation selectivity in the visual system. In the case of the visual system, the optical information that is projected on the retina, is transmitted through optical nerves of the thalamus, into a group of LGN cells, which is also known as the receptive field. The receptive field is then projected to visual cortex cells and triggers their firing rate activity, which is orientation-dependent. In the case of the proposed device, the 3 × 3 grid of the OPDs captures spatial forms of optical stimuli (for example light bars that are emitted by LEDs) and is thus regarded as the retina of the system. The resulting photocurrent of the 3 × 3 OPD grid is subsequently transmitted in a one-to-one fashion into the 3 × 3 grid of gate electrodes of the OECT, and is regarded as the receptive field. This secondary electrical input of the gate's grid, modulates the drain current of the OECT and is "projected" into the output drain current. In analogy to the orientation selectivity of the visual system, the orientation of a spatial optical stimulus is projected into a scalar quantity,

the amplitude I_0 of the output current of the OECT (in analogy to the firing rate activity of cortical cells).
Initially, input light pulses were projected at every (x, y) photodetector separately by applying a voltage pulse to a single LED ($V_{OPD} = 3.2V, t_{OPD} = 100ms$). The resulting photocurrent is driven to the gate electrodes of the OECT and subsequently modulated the channel current I_D of the OECT (that is measured for $V_D = 0V$). Following this procedure, the resulting output current amplitude I_0 of the OECT is defined for every optical input and a spatial map of I_0 can be constructed. Figure 4.2 shows the normalized spatial map of current amplitude, $I_0/I_{0,MAX}$, where $I_{0,MAX}$ is the maximum amplitude at $(x = 1, y = 1)$ coordinates (i.e., the gate that is closest the drain electrode). When compared to the maximum amplitude $I_{0,MAX}$, I_0 decreases up to 30% for the highest gate-drain distance at coordinates $(x = 3, y = 3)$. Similarly with the case of a multi-gated OECT (with voltage inputs) [141], the amplitude I_0 displays a spatial inhomogeneity towards the drain electrode. This behaviour is attributed to the decrease of the electrolyte resistance as the distance between the gate-drain is decreased, which results in an enhancement of the transient current of the channel for smaller gate-drain distances [141]. As will be presented thereafter, this spatial inhomogeneity of I_0 towards the drain electrode, can be utilized to demonstrate orientation selectivity with spatially oriented input light pulses.

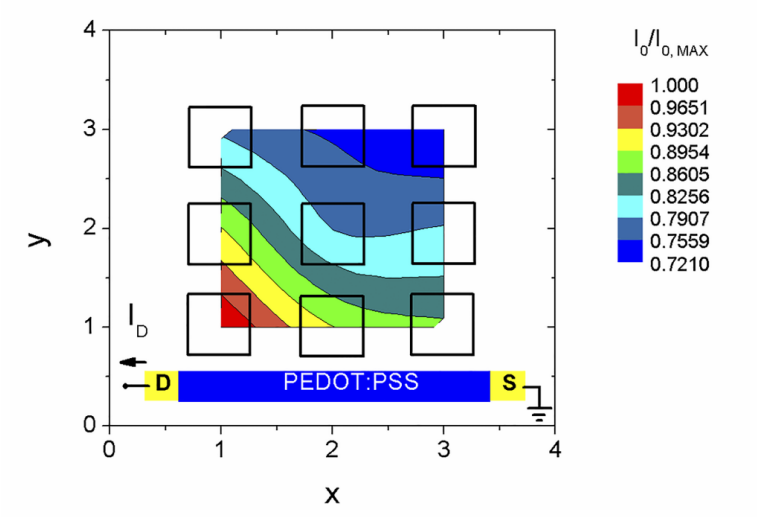

Figure 4.2 – Spatial map of the normalized output current amplitude $I_0/I_{0,MAX}$ of the OECT (for $VD = 0V$) for projecting a light pulse at each OPD separately through the LED (biasing conditions for the LED: $V_{OPD} = 3.2V, t_{OPD} = 100ms$). I_0 exhibits spatial inhomogeneity towards the drain electrode.

Light bars of homogeneous spatial intensity (i.e., spatial input light pulses) were defined by applying concurrently a voltage pulse at 3 LEDs ($V_{OPD} = 3.2V, t_{OPD} = 100ms$). "Optical" orientations were created by rotating the light bar, and projected on top of the (x, y) grid of the OPD. For example, the orientation of 45° can be defined by directing the input light bar at the photodetectors with coordinates $(x = 1-3, y = x)$. Various light bar orientations were created from 0° to 180° with a step of 45° and the resulting output amplitude I_0 of the OECT was defined in each case. It should be mentioned that here only light bars that define orientations

in respect to the central photodetector cell at coordinates ($x = 2, y = 2$) were used. In Figure 4.3a, the results are presented as the increasing percentage of $I0 = ((I_0 – I_{0,R}) / I_{0,R})$ in respect to the lowest reference amplitude $I_{0,R}$ (at orientations of 0° or 180°), and as a function of the orientation of the light bar. The amplitude of the output current I_0 depends on the orientation of the optical input and has a maximum at 45°. Figure 4.3b shows the orientation selectivity behaviour in a more comprehensive way, as a polar diagram of $(I_0 – I_{0,R}) / I_{0,R}$. Similarly to Figure 4.3a, the device displays selectivity to the diagonal orientation of the light bar towards the drain electrode (45°). This behaviour is consistent with our previous results in multi-gated OECTs with spatial voltage inputs [141]. Briefly, this behaviour is a direct consequence of the spatial map of I_0 (Figure 4.2), which exhibits an inhomogeneity towards the drain electrode. Therefore, the orientation of the light bar that includes the ($x = 1, y = 1$) photodetector (i.e., 45°), results in the highest output current amplitude I_0.

We have demonstrated a simplified analogy of orientation selectivity of the visual system using a combination of a grid of organic photodetectors and a multi-gated OECT. In the present device architecture, the grid of the OPD is used to discretize a continuous / spatial form of optical input (e.g., a light bar). This information is then driven to the multi-gated OECT, in which the functionality of orientation selectivity is realized and projected into a scalar quantity, namely the output amplitude I_0. A simple organic-based neural network topology is constructed with the multi-gated OECT that consists of multiple (secondary) inputs (i.e., the multiple gates), and weighted "soft" connections between the input gates and the output of the OECT thought the electrolyte continuum with minimal hardwired connections. Although this work is focused on processing of optical inputs, similar concepts might be extrapolated in biosensing in order to spatially map a biological substance (or an activity) and correlate it with a simple read-out, scalar quantity such as the output of an OECT.

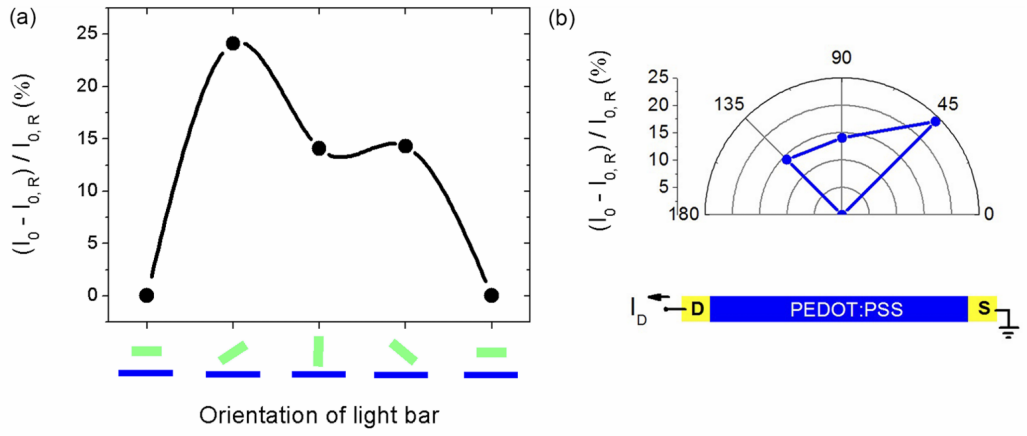

Figure 4.3 – **a)** Increasing percentage of $I_0 = ((I_0 – I_{0,R}) / I_{0,R})$ in respect to the lowest reference amplitude $I_{0,R}$ (at orientations of 0° or 180°), and as a function of the orientation of the light bar that is projected on the photodetectors. Spatial light pulses (bars) with homogeneous intensity and variable orientations were generated by using 3 LEDs (biasing conditions for the LEDs: $V_{OPD} = 3.2V$, $t_{OPD} = 100ms$). **b)** Polar diagram of $(I_0 – I0, R) / I_{0,R}$. The device exhibits selectivity for light bars with orientation of 45°.

4.6 Conclusions

In conclusion, the neuromorphic function of orientation selectivity was demonstrated in this work using organic-based devices. This function is inspired from the visual system. In particular, the proposed device exhibits selectivity with respect to input light bars with different orientations, in analogy to the visual cortex cells. The results may pave the way for introducing spatial concepts of information processing and sensing in organic bioelectronic devices.

This chapter is based on the publication:
Gkoupidenis P.*, **Rezaei-Mazinani S.***, Proctor C. M., Ismailova E. & Malliaras G. G. (**2016**). Orientation selectivity with organic photodetectors and an organic electrochemical transistor. *AIP Advances*, 6(11), 111307 - * *Authors contribute equally to this work.*

5 Conclusions and Future Perspectives

5.1 Conclusions

Optical electrophysiological signals, depending on their nature, can have unpredictable behaviour with fluctuations, whose intensities (amplitude) vary as a function of time. The dynamics of these signals can be fast or slow. Their emission spectral window is diverse, depending on for instance, the type of molecule in the metabolic system or a fluorescent indicator dye. Furthermore, electrophysiological measurements are performed in ambient conditions or in a humid environment, where there exists different degradation parameters, e.g. oxygen diffusion that challenge the device stability. Therefore, optical detection of low-amplitude biological signals demands highly sensitive light detectors that would also be capable of matching with the signals' specificity. Also, devices for such type of measurements should be resistant enough to degradation to have a stable behaviour.
This thesis demonstrates the capability of OPDs in biomedical applications, in general and in neurophysiological applications in particular. OPDs based on established active materials and novel polymers were utilized to measure a variety of label-free and fluorescent indicator-based activities from the brain. The versatility of these devices was shown by recording these optical signals, which gave a broad range of amplitude and temporal resolution. These OPDs were designed with simple structure and fabricated in ambient partially (Chapter 2) and entirely (Chapter 3) to apply the idea of simple manufacturing. These devices were shown to have a very low dark-current, important for the device sensitivity, and a linear dynamic range, crucial for the correlation of input and output signal in very low light intensities. These devices, depending on the type of the active layer's composing materials were assessed in different operational modes. The P3HT:$PC_{60}BM$ device was operated under a small reverse bias in order to enhance the photon absorption and have a stable output current over time. The XPL6:$PC_{70}BM$ device was operated at $0V$ and it showed a very stable performance over time with an excellent sensitivity. The active materials were chosen according to the emission profile of the optical signals. The first D-A materials were chosen for IOS, which are recorded when tissue is exposed to full spectrum light. The second set of materials were chosen to optimally detect near-UV calcium signals. This shows the versatility of organic active materials,

giving the possibility of employing them based on the specificity of biological problems. Therefore, narrow and wide absorption band OPDs can have a plethora of applications, tailored for detecting optical signals in biology. Furthermore, this thesis showed that utilization of these devices results in real-time recording of optical biological signals with enhanced temporal resolution and electrophysiological activities (local field potentials).

5.2 Discussion and future perspectives

5.2.1 Short-term technical perspectives

This short-term technical perspective includes the validation of necessary steps towards μ-scale and multi-pixel array OPDs combined with mechanical flexibility. In the case of OPDs, these devices have shown to have the capacity of flexibility in the past. However, multi-pixel arrays need photolithographic patterning of active materials for enhancing the scalability of devices and the integration of high density . The feasibility of flexible solar cells and OPDs have been shown in the past [102, 106]. However, these works do not discuss encapsulation strategies and the device durability for in-air applications. In addition, thin-film encapsulation approach is beneficial for fabricating devices with smaller thicknesses, which is another step towards greater mechanical flexibility.

Towards photolithographic patterning of active materials

Introduction to photolithographic patterning using orthogonal processing Photolithography is an established and cost-effective technique that has shown to give high resolution in patterning different types of materials. This method is a standard technique for inorganic semiconductors with well-established fabrication protocols in patterning technology. With respect to organic semiconductors, the application of this method still remains limited for many organic materials. Organic materials are incompatible with many resists, etchants, and developers used in conventional lithography processing [147]. For the compatibility of lithography processing steps with organic materials, orthogonality (Figure 5.1) is necessary for the protection of underlying layers from the deposition of a solution, such as deposition or removal of a photoresist film. State-of-the-art fluorinated photoresists, developers and etchers have shown the potential of solving this problem tremendously by their orthogonality with respect to certain organic materials, such as PEDOT:PSS, P3HT and some organic materials used in organic light-emitting diode (OLED)s [147, 148]. These fluorinated photolithographic materials would therefore have a great potenital in future works.

Photolithographic patterning of active materials for OPD As mentioned in Chapter 1, organic semiconductor materials are sensitive to oxygen, mostly because of the high affinity of electron-acceptor materials, e.g. PCBM to oxygen. Although successful orthogonal patterning of P3HT [148] has been shown in the past for the fabrication of organic transistors, it has not

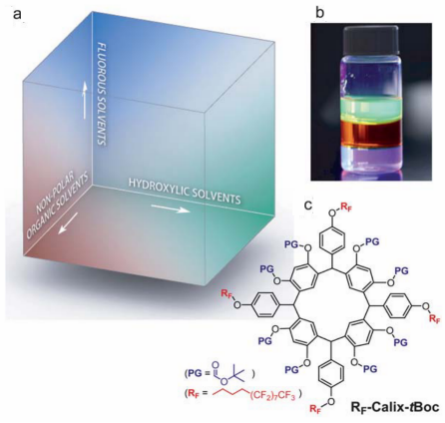

Figure 5.1 – **Principle of Orthogonal processing**. **a)** Schematic presentation of three classes of orthogonal materials. **b)** An example of three phase-separated solutions. **c)** An example of resorcinarene-based fluorinated photoresist. Adapted from [148].

been the case of P3HT:PCBM, probably due to the fast oxidation of PCBM. In the photolithography steps, baking thin-films after deposition is common for the evaporation of solvent or cross-linking of materials. As it was shown it this thesis, the spin-coating of the active layer in open-air does not decrease its performance significantly. However, in photolithography, baking the photoresist layer is done for establishing it. If we assume that lithography materials are orthogonal to PCBM, heating the active layer in ambient air results in the fast oxidation of PCBM. Here, it would be necessary to perform such steps with a high potential of oxidation under an inert atmosphere for minimizing the oxidation. Furthermore, wet-etching using orthogonal materials would be a promising approach for avoiding damages associated with dry-etching using oxygen-plasma. The Orthogonal patterning of conjugated polymers such as P3HT and PEDOT:PSS [149], have been shown in the past.

Application of PEIE for surface energy modifications

As it was introduced in Chapter 1, PEIE enhances the electron transport in the D-A layer [70]. Kielar et al. [72] showed that its application also leads to lowering the dark current, which results in decreasing the dark-current and OPD's efficiency. The application of PEIE thin-films will be beneficial for increasing the device efficiency for multi-pixel OPD arrays.

Mechanically flexible encapsulation approaches

Different organic and inorganic approaches for encapsulating devices against oxygen diffusion have been proposed [150]. In this section, organic and inorganic flexible approaches are listed in tables 5.1 and 5.2. It should be taken into account that moisture barrier is also necessary, especially for biomedical applications. Parelyne C, due to having pin-holes, is not an oxygen barrier, but it could serve as a barrier against humidity and moisture [150].

Table 5.1 – Mechanically flexible organic oxygen-barriers

Materials	Method	Cracks	Thickness	Flexibility	Cost	Durability
PVA [151]	Evaporation of aqueous solution	N.I	N.I	N.I	N.I	Long term
EVA [152]	UV-exposure	Cracks	N.I	Very flexible	Low cost	Long term
Cytop [153]	Spin-coating	N.I	N.I	Flexible	N.I	N.I
TiOx [153]	Evaporation	N.I	N.I	Flexible	N.I	N.I

† PVA = Polyvinyl alcohol, EVA = poly(ethylene-co-vinylacetate), Cytop, TiOx, N.I = No information

Table 5.2 – Mechanically flexible inorganic oxygen-barriers

Materials	Method	Cracks	Thickness	Flexibility	Cost	Durability
A2O3/ZrO2 [154]	ALD:A_2O_3 or ZrO_2+H_2O	N.I	$100-130nm$	Flexible	N.I	Long term
SiOx/SiNx/Paralyne [155]	ICPCVD & PECVD	Enhanced with plasma	50nm/50nm/300nm	Flexible	N.I	75 days
SiNx/Paralyne [150]	PECVD	Possible	$\sim 70nm$	Flexible	N.I	Long term

† ICPCVD = Inductively coupled plasma chemical vapour deposition, PECVD = Plasma-enhanced chemical vapor deposition, SiOx/SiNx/Paralyne stack: Three SiOx/SiNx stacks /encapsulated parylene / three SiOx/SiNx stacks , N.I = No information

5.2.2 Short-term application perspectives

Further investigations on intrinsic optical signlas

Several mechanisms, such as metabolic activities and CVR [8,21] underly IOS. One way to have a better understanding of how these mechanisms couple with each other is to simultaneously record IOS with individual signals. The simultaneous recording of IOS and LFPs was shown in this thesis and demonstrated the great potenital of these devices. More investigations could explore correlation of metabolism with IOS through measuring auto-fluorescent NADH and FAD in real-time with IOS. A grid of miniaturized OPD pixels could be beneficial to study the propagation of IOS in a small neuronal network and to also study a single neuron with simultaneously recording of action-potentials. Such optical recording could be done using a combination of narrow-band OPD pixels, sensitive to blue fluorescent emission and wide-band pixels sensitive to full-spectrum light.

Further investigations on ionic signals

This thesis demonstrated the possibility of recording Ca^{2+} signals with high sensitivity. Aspects of such applications could be broadened by recording fluorescent activities from multiple dyes (co-labeling) using narrow-band OPDs selective to a specific wavelength. Such types of recording could decrease the interference between excitation and emission wavelengths or two close fluorescent emission wavelengths in a multi-expressed molecular probes. For example, this could improve our understanding of the interactions of multiple ions or ion channels during action-potentials. Furthermore, these aspects could be expanded to study the correlation of different ions and auto-fluorescent metabolic molecules NADH and FAD by using devices equipped with narrow-band OPD arrays sensitive to blue, violet and green emission windows.

5.2.3 Long-term technical perspectives

Towards integrating organic photodetectors in implantable devices

The use of implantable devices featuring arrays of OPDs is not so distant. Such devices could be considered miniaturized optical-sensors for detecting various types of activities of a small population of cells or a single cell. The efforts towards integrating different types of narrow-band OPDs for detecting a specific wavelength is not only limited to tailoring their chemical and physical structure. The deposition of thin-film optical filters [156, 157] could also be an option to use optical filters on semi-narrow band OPDs.
For optical-recording in the deep brain, the delivery of a light source is crucial. Optogenetics [158] is an application field that has given various possibilities to develop such devices. However, to date, the state-of-the-art in biomedical devices has not included the development of photodetectors as biomedical optical sensors. In one report [159], their application is limited to assess the stimulation intensity of inorganic light-emitting diode (ILED)s.

State-of-the-art organic devices have shown the novel possibility of multicolour OLEDs. We can envision that implantable devices can feature multicolour μ-scale OLEDs and arrays of μ-scale OPDs for studying the dynamics of ions and ion channels co-labeled genetically, in a real-time, where there is the possibility of selective optical-stimulation with a specific wavelength and optical-recording in a specific spectral window.
Such promising devices will broaden the utilization of these devices by integrating them in the same platform in variety of biomedical applications.

Potential of thin-film optical filters

A variety of works have reported the optical properties of TiO_2 and SiO_2 [156, 157]. It has been shown that by using sol-gel spin-coating [156] and other chemical processing [157], these materials can be used as multilayer thin-film optical filters. Many sol-gel coatings present reflective and antireflective properties, which depend on properties such as central wavelength, number of layers, optical thickness arrangements, etc. This method is inexpensive, processable in ambient conditions and controllable by temperature through chemical contents [156]. Such thin-film optical filters will be powerful tools for direct optical filtering integrated on sensor devices.

Light delivery in the deep brain

Introduction to optogenetics In 1979, Francis Crick presented the idea of controlling one type of cell without altering the rest, for facing challenges in neuroscience [160]. This level of targeted controlling is not achievable with electrical stimulation, since an electrode will trigger other cells in network. On the other hand, traditional genetic methods for manipulating cells, are designed for activation or inhibition of a population of neurons that have the same temporal resolution [158].
Optogenetics refers to the integration of genetic and optical methods for achieving gain or loss of functions for a well-defined event in specific cells of a living tissue with very high temporal and spatial resolution. In a broad sense it means that optogenetic encompasses targetable and controllable tools for responding to light and delivering effector functions. This also enables technologies for light delivery to a specific target and obtaining read-outs for different analysis such as imaging [158]. This field in its actual form was demonstrated in 2005 by Boyden et al. [162].
The principle is based on using light-gated channels, such as rhodopsins, which are found in prokaryotes and light-sensitive algae. The gene coding for the formation of this type of protein is linked to a promoter and implanted in a virus. The genetic modification is applied through the virus injection in an animal by targeting a specific neuronal population. These neurons will express the algea gene and exhibit the opsin on surface. Figure 5.2.3a shows different types of opsins. These opsins, depending on their type are sensitive to a specific wavelength. When the light is emitted, the late-gate ion channels (Figure 5.2.3b) will be triggered and opened or their activation would be prevented. These wavelength-dependent opsins would induce an

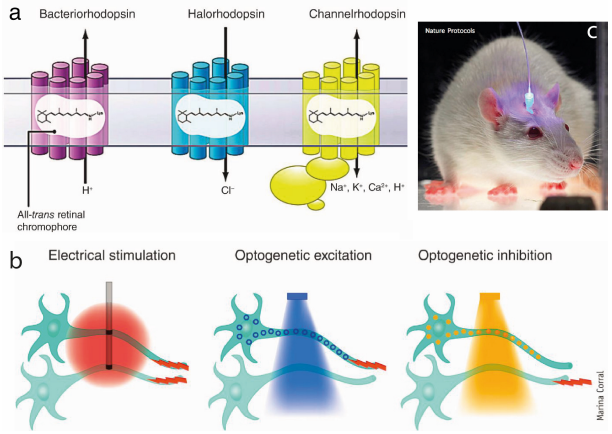

Figure 5.2 – **Operating principle of optogenetics in neuroscience**. **a)** The three main categories of microbial proteins used in single-component optogenetics. Adapted from [92]. **b)** Targeted excitation (blue-light excitation for channelrhodopsin) and inhibition (yellow light for activating halorhodopsin) conferring cellular specificity. This is not feasible with electrodes (action-potenitial) for maintaining high temporal resolution. Adapted from [158]. **c)** Optical deep-brain stimulation of neurons expressing microbial opsin genes. Adapted from [161].

excitation or inhibition along a neuronal pathway. An schematic of this process is shown in figure 5.2.3b [158, 162, 163].
This method provides a milli-second temporal resolution with a single cell spatial resolution, which will help to lead to a better understanding of brain disorders and fundamental mechanisms [162]. Furthermore, it provides the possibility of optogenetic control in *in-vivo* studies in freely-moving-animals (Figure 5.2.3c). This field is growing rapidly and various genetic toolkits, including microbes and molecules [164, 165] for studying diseases and biological mechanisms. Devices for highly sensitive detections [166–169] has also been developed.

Inorganic light-emitting diodes: An important device for optogenetics To date, one of the most common tools for optogenetic optical-stimulation is optical-fibers. The major drawback of this tool is that it is fragile and has a limited bending capacity. These drawbacks limit freely-moving animal experiments. For this reason, integrated light sources in flexible probes are being developed by the community. Multifunctional optogenetics probe [159] is one of the most advanced devices in this field. These flexible probes have shown the possibility of integrating multiple electronic components including μ-ILEDs and μ-inorganic photodetector (IPD).
Taking into account the high sensitivity and temporal resolution of OPDs, these devices could broaden new aspects of high-precision optical detection in neuroscience along with precise optogenetic control. The state-of-the-art works in inorganic biomedical devices illustrate broad possibilities of integrating electrical compartments in organic devices. Development of such multifunctional devices based on organic materials will aid to incorporate their exceptional sensitivity while having modifiable chemical and physical properties for more powerful tools.

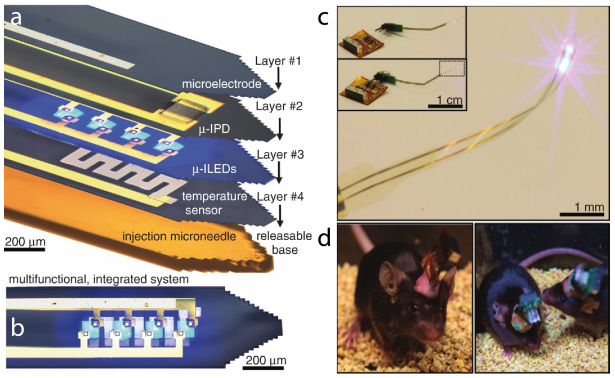

Figure 5.3 – **Multifunctional optogenetic probe**. **a)** Cross sectional view, from bottom the device involves: injection microneedle, temperature sensor, μ-inorganic light emitting diodes, μ-inorganic photodetector and microelectrode. **b)** Integrated system. **c)** Functional device. **d)** Implanted wireless device. Adapted from [159].

Micropatterned and colour tunable organic light emitting diodes: Promising technologies for organic devices for all-organic multifunctional probes One high potential method that has expanded the scalability of OLEDs is Orthogonal patterning of phosphorescent active materials. This promising method, which can be applicable to OPDs too, has resulted in μ-scale OLEDs (Figure 5.4a) [147]. Another promising technology for integrating all-organic multifunctional probes in the future is colour tuneable OLEDs (Figure 5.4) [170]. This device has shown to operate in different AC/DC modes for switching between different colours. These technologies demonstrate that the patterning of organic materials and technical variability of organic devices are developing. This means that potentially this direction would lead to integrating μ-scale OPDs and OLEDs in multifunctional organic probes.

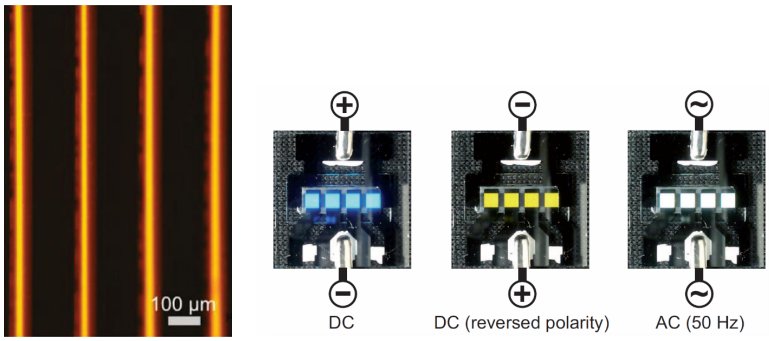

(a) Patterned μ-scale OLED. Adapted from [147].

(b) Colour tuneable OLEDs, operating in different AC/DC modes. Adapted from [170].

Figure 5.4 – Promising technologies for future all-organic multifunctional probes.

5.2.4 Long-term application perspectives

We anticipate that the integration of OPDs along with OLEDs and other electronic compartments such as organic electrodes and transistors in all-organic multifunctional probes will have a huge impact on investigations in several fields such as *In-vivo* studies of IOS in the deep brain that need a relatively long-term illumination for studying fast IOS in cellular level. Also, this concept will add new aspects to optical detection of optogenetic events along with the precise control of ion channels in cells. Furthermore, this concept will offer a novel advantage of deep-brain light delivery for the stimulation of different types of dyes in parallel with optical detection. This is a method that is limited from many aspects to date, such as the limited penetration of light (laser) in brain tissue and the actual limitations of inorganic light detectors. Such implantable and flexible multifunctional devices will improve our understanding in a broad range of fields, from the fundamental aspects of biology to the most complicated brain disorders.

Bibliography

[1] JF Vibert, A Sébille, M C Lavallard-Rousseau, F Boureau, and L Mazières. *Neurophysiologie: de la physiologie à l'exploration fonctionnelle*. Elsevier Health Sciences, 2011.

[2] JF Vibert, A Sébille, M C Lavallard-Rousseau, F Boureau, and L Mazières. *Guyton and Hall Textbook of Medical Physiology E-Book*. Elsevier Health Sciences, 2011.

[3] D Purves, GJ Augustine, D Fitzpatrick, LC Katz, AS LaMantia, JO McNamara, and SM Williams. *Neuroscience*. Sunderland. MA, 2003.

[4] JF Vibert, A Sébille, M C Lavallard-Rousseau, F Boureau, and L Mazières. *Campbell biology*. Pearson, Boston, 2011.

[5] György Buzsáki, Costas Anastassiou, and Christof Koch. The origin of extracellular fields and currents — EEG, ECoG, LFP and spikes. *Nat Rev Neurosci*, 13(6):407–420, 2012.

[6] LB Cohen. Changes in neuron structure during action potential propagation and synaptic transmission. *Physiological reviews*, 1973.

[7] Tiziana Cesetti, Francesca Ciccolini, and Yuting Li. GABA not only a neurotransmitter: Osmotic regulation by GABAAR signaling. *Front Cell Neurosci*, 6:3, 2012.

[8] Thomas Jentsch. VRACs and other ion channels and transporters in the regulation of cell volume and beyond. *Nat Rev Mol Cell Bio*, 17(5):293–307, 2016.

[9] David Ferster and Kenneth D Miller. Neural mechanisms of orientation selectivity in the visual cortex. *Annual review of neuroscience*, 23(1):441–471, 2000.

[10] Sam Ling, Janneke Jehee, and Franco Pestilli. A review of the mechanisms by which attentional feedback shapes visual selectivity. *Brain Struct Funct*, 220(3):1237–1250, 2015.

[11] DeAngelis, Gregory, Izumi Ohzawa, and Ralph Freeman. Receptive-field dynamics in the central visual pathways. *Trends Neurosci*, 18(10):451–458, 1995.

[12] Cristopher Niell. Cell types, circuits, and receptive fields in the mouse visual cortex. *Annu Rev Neurosci*, 38(1):1–19, 2015.

[13] MacVicar, Brian and Daryl Hochman. Imaging of synaptically evoked intrinsic optical signals in hippocampal slices. *The Journal of Neuroscience*, 11(5):1458, 1991.

[14] Angelica Zepeda, Clorinda Arias, and Frank Sengpiel. Optical imaging of intrinsic signals: recent developments in the methodology and its applications. *J Neurosci Meth*, 136(1):1–21, 2004.

[15] Hai-bo Yu, Min Li, Wei-ping Wang, and Xiao-liang Wang. High throughput screening technologies for ion channels. *Acta Pharm Sinic*, 37(1):34–43, 2015.

[16] Christine Grienberger and Arthur Konnerth. Imaging calcium in neurons. *Cell*, 73(5):862–885, 2012.

[17] Ryota Homma, Bradley Baker, Lei Jin, Olga Garaschuk, Arthur Konnerth, Lawrence Cohen, Chun Bleau, Marco Canepari, Maja Djurisic, and Dejan Zecevic. *Wide-Field and Two-Photon Imaging of Brain Activity with Voltage and Calcium-Sensitive Dyes*, volume 489. Springer, 2009.

[18] Klaus Suhling, Liisa M Hirvonen, James A Levitt, Pei-Hua Chung, Carolyn Tregidgo, Alix Marois, Dmitri A Rusakov, Kaiyu Zheng, Ameer-Beg, Simon, Simon Poland, Simao Coelho, Robert Henderson, and Nikola Krstajic. Fluorescence lifetime imaging (FLIM): basic concepts and some recent developments. *Medical Photonics*, 27:3–40, 2015.

[19] Michael Lin and Mark Schnitzer. Genetically encoded indicators of neuronal activity. *Nat Neurosci*, 19(9):1142–1153, 2016.

[20] D. Hill and R. Keynes. Opacity changes in stimulated nerve. *J Physiology*, 108(3):278–281, 1949.

[21] MacVicar, Brian A. REVIEW: Mapping neuronal activity by imaging intrinsic optical signals. *Neurosci*, 3(6):381–388, 1997.

[22] A Grinvald, D Shoham, D Shmuel, I Glaser, E Vanzetta, E Shtoyerman, H Slovin, C Wijnbergen, R Hildesheim, and A Arieli. *In-vivo Optical Imaging of Cortical Architecture and Dynamics*. Springer, 1999.

[23] Letian Dou, Jingbi You, Ziruo Hong, Zheng Xu, Gang Li, Robert Street, and Yang Yang. 25th anniversary article: A decade of Organic/Polymeric photovoltaic research. *Adv Mater*, 25(46):6642–6671, 2013.

[24] Tse Ng, William Wong, Michael Chabinyc, Sanjiv Sambandan, and Robert Street. Flexible image sensor array with bulk heterojunction organic photodiode. *Appl Phys Lett*, 92(21):213303, 2008.

[25] Tobias Rauch, Michaela Böberl, Sandro Tedde, Jens Fürst, Maksym Kovalenko, Günter Hesser, Uli Lemmer, Wolfgang Heiss, and Oliver Hayden. Near-infrared imaging with quantum-dot-sensitized organic photodiodes. *Nat Photonics*, 3(6):332–336, 2009.

[26] Maya-Vetencourt, José, Diego Ghezzi, Maria Antognazza, Elisabetta Colombo, Maurizio Mete, Paul Feyen, Andrea Desii, Ambra Buschiazzo, Mattia Paolo, Stefano Marco, Flavia Ticconi, Laura Emionite, Dmytro Shmal, Cecilia Marini, Ilaria Donelli, Giuliano Freddi, Rita Maccarone, Silvia Bisti, Gianmario Sambuceti, Grazia Pertile, Guglielmo Lanzani, and Fabio Benfenati. A fully organic retinal prosthesis restores vision in a rat model of degenerative blindness. *Nat Mater*, 2017.

[27] Oksana Ostroverkhova. Organic optoelectronic materials: Mechanisms and applications. *Chem. Rev.*, 116(22):13279–13412, 2016.

[28] Xiong Gong, Minghong Tong, Yangjun Xia, Wanzhu Cai, Ji Moon, Yong Cao, Gang Yu, Chan-Long Shieh, Boo Nilsson, and Alan Heeger. High-Detectivity polymer photodetectors with spectral response from 300 nm to 1450 nm. *Science*, 325(5948):1665–1667, 2009.

[29] JJM Halls, CA Walsh, NC Greenham, EA Marseglia, RH Friend, SC Moratti, and AB Holmes. Efficient photodiodes from interpenetrating polymer networks. *Nature*, 376(6540):498–500, 1995.

[30] G Yu and A Heeger. Charge separation and photovoltaic conversion in polymer composites with internal donor/acceptor heterojunctions. *J Appl Phys*, 78(7):4510–4515, 1995.

[31] Waldo Beek, Martijn Wienk, and René Janssen. Hybrid polymer solar cells based on zinc oxide. *J Mater Chem*, 15(29):2985–2988, 2005.

[32] H Kallmann and M Pope. Photovoltaic effect in organic crystals. *J Chem Phys*, 30(2):585–586, 1959.

[33] C. Brabec, N. Sariciftci, and J. Hummelen. Plastic solar cells. *Adv Funct Mater*, 11(1):15–26, 2001.

[34] Gang Li, Rui Zhu, and Yang Yang. Polymer solar cells. *Nat Photonics*, 6(3):153–161, 2012.

[35] Yuhang Liu, Jingbo Zhao, Zhengke Li, Cheng Mu, Wei Ma, Huawei Hu, Kui Jiang, Haoran Lin, Harald Ade, and He Yan. Aggregation and morphology control enables multiple cases of high-efficiency polymer solar cells. *Nat Commun*, 5:5293, 2014.

[36] Varun Vohra, Kazuaki Kawashima, Takeshi Kakara, Tomoyuki Koganezawa, Itaru Osaka, Kazuo Takimiya, and Hideyuki Murata. Efficient inverted polymer solar cells employing favourable molecular orientation. *Nat Photonics*, 9(6):403–408, 2015.

[37] Sunsun Li, Long Ye, Wenchao Zhao, Shaoqing Zhang, Subhrangsu Mukherjee, Harald Ade, and Jianhui Hou. EnergyLevel modulation of SmallMolecule electron acceptors to achieve over 12% efficiency in polymer solar cells. *Adv Mater*, 28(42):9423–9429, 2016.

[38] J. Roncali. Molecular engineering of the band gap of Conjugated systems: Facing technological applications. *Macromol Rapid Comm*, 28(17):1761–1775, 2007.

[39] Pierre-Luc Boudreault, Ahmed Najari, and Mario Leclerc. Processable Low-Bandgap polymers for photovoltaic applications†. *Chem Mater*, 23(3):456–469, 2011.

[40] Pierre Beaujuge and Jean Fréchet. Molecular design and ordering effects in -Functional materials for transistor and solar cell applications. *J Am Chem Soc*, 133(50):20009–20029, 2011.

[41] Christos L Chochos and Stelios A Choulis. How the structural deviations on the backbone of conjugated polymers influence their optoelectronic properties and photovoltaic performance. *Progress in Polymer Science*, 36(10):1326–1414, 2011.

[42] Xin Guo, Martin Baumgarten, and Klaus Müllen. Designing -conjugated polymers for organic electronics. *Prog Polym Sci*, 38(12):1832–1908, 2013.

[43] Jhong-Sian Wu, Sheng-Wen Cheng, Yen-Ju Cheng, and Chain-Shu Hsu. Donor–acceptor conjugated polymers based on multifused ladder-type arenes for organic solar cells. *Chem Soc Rev*, 44(5):1113–1154, 2014.

[44] Xugang Guo, Antonio Facchetti, and Tobin J Marks. Imide- and Amide-Functionalized polymer semiconductors. *Chem Rev*, 114(18):8943–9021, 2014.

[45] Masahiro Hatano, Shu Kambara, and Shigeharu Okamoto. Paramagnetic and electric properties of polyacetylene. *J Polym Sci*, 51(156):S26–S29, 1961.

[46] Andriy Zhugayevych and Sergei Tretiak. Theoretical description of structural and electronic properties of organic photovoltaic materials. *Annu Rev Phys Chem*, 66(1):305–330, 2015.

[47] Rolf E Hummel. *Electronic Properties of Materials*. Springer, 2011.

[48] Mark Geoghegan and Georges Hadziioannou. *Polymer Electronics*. Oxford University Press, 2013.

[49] Sabine Ludwigs, editor. *P3HT Revisited – From Molecular Scale to Solar Cell Devices*, volume 265. springer, 2014.

[50] EE Havinga, W ten Hoeve, and H Wynberg. A new class of small band gap organic polymer conductors. *Polymer Bulletin*, 29(1-2):119–126, 1992.

[51] Renee Kroon. Synthesis and properties of -conjugated polymers for organic photovoltaics, 2013.

[52] Bernard Kippelen and Jean-Luc Brédas. Organic photovoltaics. *Energy Environ Sci*, 2(3):251–261, 2009.

[53] KangJun Baeg, Maddalena Binda, Dario Natali, Mario Caironi, and YongYoung Noh. Organic light detectors: Photodiodes and phototransistors. *Advanced Materials*, 25(31):4267–4295, 2013.

[54] Christos L Chochos, Athanasios Katsouras, Nicola Gasparini, Chrysanthos Koulogiannis, Tayebeh Ameri, Christoph J Brabec, and Apostolos Avgeropoulos. Rational design of HighPerformance WideBandgap (2 eV) polymer semiconductors as electron donors in organic photovoltaics exhibiting high open circuit voltages (1 v). *Macromol Rapid Comm*, 38(2):1600614, 2017.

[55] Jan Hummelen, Brian Knight, LePeq, F, Fred Wudl, Jie Yao, and Charles Wilkins. Preparation and characterization of fulleroid and methanofullerene derivatives. *J Org Chem*, 60(3):532–538, 1995.

[56] Pavel Troshin, Harald Hoppe, Alexander Peregudov, Martin Egginger, Sviatoslav Shokhovets, Gerhard Gobsch, N. Sariciftci, and Vladimir Razumov. [70]FullereneBased materials for organic solar cells. *Chemsuschem*, 4(1):119–124, 2011.

[57] Martijn Wienk, Jan Kroon, Wiljan Verhees, Joop Knol, Jan Hummelen, Paul Hal, and René Janssen. Efficient Methano[70]fullerene/MDMOPPV bulk heterojunction photovoltaic cells. *Angewandte Chemie Int Ed*, 42(29):3371–3375, 2003.

[58] Martijn Lenes, GertJan Wetzelaer, Floris Kooistra, Sjoerd Veenstra, Jan Hummelen, and Paul Blom. Fullerene bisadducts for enhanced OpenCircuit voltages and efficiencies in polymer solar cells. *Adv Mater*, 20(11):2116–2119, 2008.

[59] Martijn Lenes, Steve Shelton, Alex Sieval, David Kronholm, Jan Hummelen, and Paul Blom. Electron trapping in higher adduct FullereneBased solar cells. *Adv Funct Mater*, 19(18):3002–3007, 2009.

[60] C Tang. Twolayer organic photovoltaic cell. *Appl Phys Lett*, 48(2):183–185, 1986.

[61] I Campbell, T Hagler, D Smith, and J Ferraris. Direct measurement of conjugated polymer electronic excitation energies using Metal/Polymer/Metal structures. *Phys Rev Lett*, 76(11):1900–1903, 1996.

[62] P.W.M. Blom, V.D. Mihailetchi, L.J.A. Koster, and D.E. Markov. Device physics of Polymer:Fullerene bulk heterojunction solar cells. *Adv Mater*, 19(12):1551–1566, 2007.

[63] Christopher M Proctor, Chunki Kim, Dieter Neher, and ThucQuyen Nguyen. Nongeminate recombination and charge transport limitations in DiketopyrrolopyrroleBased SolutionProcessed small molecule solar cells. *Adv Funct Mater*, 23(28):3584–3594, 2013.

[64] Ellen Moons. Conjugated polymer blends: linking film morphology to performance of light emitting diodes and photodiodes. *J Phys Condens Matter*, 14(47):12235–12260, 2002.

[65] F. Padinger, R.S. Rittberger, and N.S. Sariciftci. Effects of postproduction treatment on plastic solar cells. *Adv Funct Mater*, 13(1):85–88, 2003.

[66] Gang Li, Vishal Shrotriya, Jinsong Huang, Yan Yao, Tom Moriarty, Keith Emery, and Yang Yang. High-efficiency solution processable polymer photovoltaic cells by self-organization of polymer blends. *Nat Mater*, 4(11):864–868, 2005.

[67] W. Ma, C. Yang, X. Gong, K. Lee, and A.J. Heeger. Thermally stable, efficient polymer solar cells with nanoscale control of the interpenetrating network morphology. *Adv Funct Mater*, 15(10):1617–1622, 2005.

[68] J. Peet, J. Kim, N. Coates, W. Ma, D. Moses, A. Heeger, and G. Bazan. Efficiency enhancement in low-bandgap polymer solar cells by processing with alkane dithiols. *Nat Mater*, 6(7):497–500, 2007.

[69] S. Khodabakhsh, B.M. Sanderson, J. Nelson, and T.S. Jones. Using SelfAssembling dipole molecules to improve charge collection in molecular solar cells. *Adv Funct Mater*, 16(1):95–100, 2006.

[70] Yinhua Zhou, Fuentes-Hernandez, Canek, Jaewon Shim, Jens Meyer, Anthony Giordano, Hong Li, Paul Winget, Theodoros Papadopoulos, Hyeunseok Cheun, Jungbae Kim, Mathieu Fenoll, Amir Dindar, Wojciech Haske, Ehsan Najafabadi, Talha Khan, Hossein Sojoudi, Stephen Barlow, Samuel Graham, Jean-Luc Brédas, Seth Marder, Antoine Kahn, and Bernard Kippelen. A universal method to produce Low–Work function electrodes for organic electronics. *Science*, 336(6079):327–332, 2012.

[71] Stephan van Reenen, Sandra Kouijzer, René AJ Janssen, Martijn M Wienk, and Martijn Kemerink. Origin of work function modification by ionic and amine-based interface layers. *Advanced Materials Interfaces*, 1(8), 2014.

[72] Marcin Kielar, Olivier Dhez, Gilles Pecastaings, Arnaud Curutchet, and Lionel Hirsch. Long-Term stable organic photodetectors with ultra low dark currents for high detectivity applications. *Sci Reports*, 6(1):39201, 2016.

[73] Jonathan Servaites, Mark Ratner, and Tobin Marks. Organic solar cells: A new look at traditional models. *Energy Environ Sci*, 4(11):4410–4422, 2011.

[74] W Shockley. The theory of p-n junctions in semiconductors and p-n junction transistors. *The Bell System Technical Journal*, 28(3):435–489, 1949.

[75] Fawen Guo, Zhengguo Xiao, and Jinsong Huang. Fullerene photodetectors with a linear dynamic range of 90 dB enabled by a CrossLinkable buffer layer. *Adv Opt Mater*, 1(4):289–294, 2013.

[76] Serge Beaupré and Mario Leclerc. PCDTBT: en route for low cost plastic solar cells. *J Mater Chem*, 1(37):11097–11105, 2013.

[77] Mikkel Jørgensen, Kion Norrman, and Frederik Krebs. Stability/degradation of polymer solar cells. *Sol Energ Mat Sol C*, 92(7):686–714, 2008.

[78] Kenji Harafuji, Hiroaki Sato, Takahiro Matsuura, Yuta Omoto, Toshihiko Kaji, and Masahiro Hiramoto. Degradation in organic solar cells under illumination and electrical stresses in air. *Japanese Journal of Applied Physics*, 53(12):122303, 2014.

[79] Munish Jassi, R Gurunath, and Sundar S Iyer. Degradation study of organic semiconductor devices under electrical and optical stresses. *IEEE Electron Device Letters*, 29(5):442–444, 2008.

[80] Amir Asadpoordarvish, Andreas Sandström, Shi Tang, Jimmy Granström, and Ludvig Edman. Encapsulating light-emitting electrochemical cells for improved performance. *Appl Phys Lett*, 100(19):193508, 2012.

[81] J. Blakesley and R. Speller. Modeling the imaging performance of prototype organic xray imagers. *Med Phys*, 35(1):225–239, 2008.

[82] Ardalan Armin, Ross D Jansen-van Vuuren, Nikos Kopidakis, Paul L Burn, and Paul Meredith. Narrowband light detection via internal quantum efficiency manipulation of organic photodiodes. *Nat Commun*, 6:6343, 2015.

[83] Il Kim, Xin Li, Mujeeb Ullah, Paul Shaw, Robert Wawrzinek, Ebinazar Namdas, and ShihChun Lo. HighPerformance, FullereneFree organic photodiodes based on a SolutionProcessable indigo. *Adv Mater*, 27(41):6390–6395, 2015.

[84] G. Azzellino, A. Grimoldi, M. Binda, M. Caironi, D. Natali, and M. Sampietro. Fully InkjetPrinted organic photodetectors with high quantum yield. *Adv Mater*, 25(47):6829–6833, 2013.

[85] Ardalan Armin, Mike Hambsch, Il Kim, Paul Burn, Paul Meredith, and Ebinazar Namdas. Thick junction broadband organic photodiodes. *Laser Photonics Rev*, 8(6):924–932, 2014.

[86] Riming Nie, Xianyu Deng, Lei Feng, Guiguang Hu, Yangyang Wang, Gang Yu, and Jianbin Xu. Highly sensitive and broadband organic photodetectors with fast speed gain and large linear dynamic range at low forward bias. *Small*, 13(24):1603260, 2017.

[87] Christopher Proctor and Thuc-Quyen Nguyen. Effect of leakage current and shunt resistance on the light intensity dependence of organic solar cells. *Appl Phys Lett*, 106(8):083301, 2015.

[88] Kelley A Foster, Francesca Galeffi, Florian J Gerich, Dennis A Turner, and Michael Müller. Optical and pharmacological tools to investigate the role of mitochondria during oxidative stress and neurodegeneration. *Progress in neurobiology*, 79(3):136–171, 2006.

[89] Shav-Tal, Yaron, Robert Singer, and Xavier Darzacq. Imaging gene expression in single living cells. *Nat Rev Mol Cell Bio*, 5(10):855–862, 2004.

[90] Bishnu Joshi and Thomas Wang. Exogenous molecular probes for targeted imaging in cancer: Focus on multi-modal imaging. *Cancers*, 2(2):1251–1287, 2010.

[91] Rudolf Griss, Alberto Schena, Luc Reymond, Luc Patiny, Dominique Werner, Christine Tinberg, David Baker, and Kai Johnsson. Bioluminescent sensor proteins for point-of-care therapeutic drug monitoring. *Nat Chem Biol*, 10(7):598–603, 2014.

[92] Karl Deisseroth. Optogenetics: 10 years of microbial opsins in neuroscience. *Nat Neurosci*, 18(9):1213–1225, 2015.

[93] Dmitriy Fayuk, Peter Aitken, George Somjen, and Dennis Turner. Two different mechanisms underlie reversible, intrinsic optical signals in rat hippocampal slices. *J Neurophysiol*, 87(4):1924–1937, 2002.

[94] PG Aitken, D Fayuk, GG Somjen, and DA Turner. Use of intrinsic optical signals to monitor physiological changes in brain tissue slices. *Methods*, 18(2):91–103, 1999.

[95] Michael M Haglund, George A Ojemann, and Daryl W Hochman. Optical imaging of epileptiform and functional activity in human cerebral cortex. *Nature*, 358(6388):668, 1992.

[96] Florian Lang. Effect of cell hydration on metabolism. *Nestle Nutr Inst Workshop Ser*, 69:115–26; discussion 126–30, 2011.

[97] B Friedrich, I Matskevich, and F Lang. Cell volume regulatory mechanisms. *Contrib Nephrol*, 152:1–8, 2006.

[98] Ying Ma, Mohammed Shaik, Mariel Kozberg, Sharon Kim, Jacob Portes, Dmitriy Timerman, and Elizabeth Hillman. Resting-state hemodynamics are spatiotemporally coupled to synchronized and symmetric neural activity in excitatory neurons. *Proc National Acad Sci*, 113(52):E8463–E8471, 2016.

[99] Knut Holthoff and Otto W Witte. Intrinsic optical signals in rat neocortical slices measured with near-infrared dark-field microscopy reveal changes in extracellular space. *The Journal of Neuroscience*, 16(8):2740, 1996.

[100] R.D. Andrew and Macvicar. Imaging cell volume changes and neuronal excitation in the hippocampal slice. *Neuroscience*, 62(2):371–383, 1994.

[101] Jacob Fraden. *Handbook of Modern Sensors. Physics, Designs, and Applications*. springer, 2010.

[102] Martin Kaltenbrunner, Matthew S White, Eric D Głowacki, Tsuyoshi Sekitani, Takao Someya, Niyazi S Sariciftci, and Siegfried Bauer. Ultrathin and lightweight organic solar cells with high flexibility. *Nat Commun*, 3:770, 2012.

[103] Xuhua Wang, Oliver Hofmann, Rupa Das, Edward Barrett, deMello, Andrew, deMello, John, and Donal Bradley. Integrated thin-film polymer / fullerene photodetectors for on-chip microfluidic chemiluminescence detection. *Lab Chip*, 7(1):58–63, 2006.

[104] M. Berggren and RichterDahlfors, A. Organic bioelectronics. *Adv Mater*, 19(20):3201–3213, 2007.

[105] Takao Someya, Zhenan Bao, and George G Malliaras. The rise of plastic bioelectronics. *Nature*, 540(7633):379–385, 2016.

[106] Takao Someya, Siegfried Bauer, and Martin Kaltenbrunner. Imperceptible organic electronics. *Mrs Bull*, 42(2):124–130, 2017.

[107] Dion Khodagholy, Jennifer N Gelinas, Zifang Zhao, Malcom Yeh, Michael Long, Jeremy D Greenlee, Werner Doyle, Orrin Devinsky, and György Buzsàki. Organic electronics for high-resolution electrocorticography of the human brain. *Science Advances*, 2(11):e1601027, 2016.

[108] Dion Khodagholy, Jennifer N Gelinas, Thomas Thesen, Werner Doyle, Orrin Devinsky, George G Malliaras, and György Buzsáki. NeuroGrid: recording action potentials from the surface of the brain. *Nat. Neurosci.*, 18(2):310–5, 2015.

[109] Dion Khodagholy, Thomas Doublet, Pascale Quilichini, Moshe Gurfinkel, Pierre Leleux, Antoine Ghestem, Esma Ismailova, Thierry Hervé, Sébastien Sanaur, Christophe Bernard, and George G Malliaras. In vivo recordings of brain activity using organic transistors. *Nat Commun*, 4:1575, 2013.

[110] Dion Khodagholy, Thomas Doublet, Moshe Gurfinkel, Pascale Quilichini, Esma Ismailova, Pierre Leleux, Thierry Herve, Sébastien Sanaur, Christophe Bernard, and George G Malliaras. Highly conformable conducting polymer electrodes for in vivo recordings. *Adv. Mater. Weinheim*, 23(36):H268–72, 2011.

[111] Adam Williamson, Jonathan Rivnay, Loïg Kergoat, Amanda Jonsson, Sahika Inal, Ilke Uguz, Marc Ferro, Anton Ivanov, Theresia A Sjöström, Daniel T Simon, Magnus Berggren, George G Malliaras, and Christophe Bernard. Controlling epileptiform activity with organic electronic ion pumps. *Adv. Mater. Weinheim*, 27(20):3138–44, 2015.

[112] Jonathan Rivnay, Róisín Owens, and George Malliaras. The rise of organic bioelectronics. *Chem Mater*, 26(1):679–685, 2014.

[113] Diego Ghezzi, Maria Antognazza, Marco Maschio, Erica Lanzarini, Fabio Benfenati, and Guglielmo Lanzani. A hybrid bioorganic interface for neuronal photoactivation. *Nat Commun*, 2:166, 2011.

[114] Diego Ghezzi, Maria Antognazza, Rita Maccarone, Sebastiano Bellani, Erica Lanzarini, Nicola Martino, Maurizio Mete, Grazia Pertile, Silvia Bisti, Guglielmo Lanzani, and Fabio Benfenati. A polymer optoelectronic interface restores light sensitivity in blind rat retinas. *Nat Photonics*, 7(5):400–406, 2013.

[115] Vini Gautam, David Rand, Yael Hanein, and K. Narayan. A polymer optoelectronic interface provides visual cues to a blind retina. *Adv Mater*, 26(11):1751–1756, 2014.

[116] Tomoyuki Yokota, Peter Zalar, Martin Kaltenbrunner, Hiroaki Jinno, Naoji Matsuhisa, Hiroki Kitanosako, Yutaro Tachibana, Wakako Yukita, Mari Koizumi, and Takao Someya. Ultraflexible organic photonic skin. *Sci Adv*, 2(4):e1501856, 2016.

[117] RD Traub, SB Colling, and JG Jefferys. Cellular mechanisms of 4-aminopyridine-induced synchronized after-discharges in the rat hippocampal slice. *J. Physiol. (Lond.)*, 489 (Pt 1):127–40, 1995.

[118] HJ Luhmann, VI Dzhala, and Ben-Ari, Y. Generation and propagation of 4-AP-induced epileptiform activity in neonatal intact limbic structures in vitro. *Eur. J. Neurosci.*, 12(8):2757–68, 2000.

[119] Thomas Knöpfel. Genetically encoded optical indicators for the analysis of neuronal circuits. *Nat Rev Neurosci*, 13(10):687–700, 2012.

[120] David Clapham. Calcium signaling. *Cell*, 131(6):1047–1058, 2007.

[121] Robert F Service. The brain chip. *Science*, 345(6197):614–616, 2014.

[122] Duygu Kuzum, Shimeng Yu, and H-S Wong. Synaptic electronics: materials, devices and applications. *Proc Spie*, 24(38):382001, 2013.

[123] Takeo Ohno, Tsuyoshi Hasegawa, Tohru Tsuruoka, Kazuya Terabe, James K Gimzewski, and Masakazu Aono. Short-term plasticity and long-term potentiation mimicked in single inorganic synapses. *Nat Mater*, 10(8):591–595, 2011.

[124] Sung Jo, Ting Chang, Idongesit Ebong, Bhavitavya B Bhadviya, Pinaki Mazumder, and Wei Lu. Nanoscale memristor device as synapse in neuromorphic systems. *Nano Lett*, 10(4):1297–1301, 2010.

[125] Tomas Tuma, Angeliki Pantazi, Manuel Gallo, Abu Sebastian, and Evangelos Eleftheriou. Stochastic phase-change neurons. *Nat Nanotechnol*, 11(8):693–699, 2016.

[126] André Chanthbouala, Vincent Garcia, Ryan O Cherifi, Karim Bouzehouane, Stéphane Fusil, Xavier Moya, Stéphane Xavier, Hiroyuki Yamada, Cyrile Deranlot, Neil D Mathur, Manuel Bibes, Agnès Barthélémy, and Julie Grollier. A ferroelectric memristor. *Nat Mater*, 11(10):860–864, 2012.

[127] Steven Lequeux, Joao Sampaio, Vincent Cros, Kay Yakushiji, Akio Fukushima, Rie Matsumoto, Hitoshi Kubota, Shinji Yuasa, and Julie Grollier. A magnetic synapse: multilevel spin-torque memristor with perpendicular anisotropy. *Sci Reports*, 6(1):31510, 2016.

[128] Li Zhu, Chang Wan, Li Guo, Yi Shi, and Qing Wan. Artificial synapse network on inorganic proton conductor for neuromorphic systems. *Nat Commun*, 5, 2014.

[129] Xenofon Strakosas, Manuelle Bongo, and Róisín M Owens. The organic electrochemical transistor for biological applications. *J Appl Polym Sci*, 132(15):n/a–n/a, 2015.

[130] G Tarabella, D'Angelo, P, A Cifarelli, A Dimonte, A Romeo, T Berzina, V Erokhin, and S Iannotta. A hybrid living/organic electrochemical transistor based on the physarum polycephalum cell endowed with both sensing and memristive properties. *Chem Sci*, 6(5):2859–2868, 2015.

[131] Agostino Romeo, Alice Dimonte, Giuseppe Tarabella, D'Angelo, Pasquale, Victor Erokhin, and Salvatore Iannotta. A bio-inspired memory device based on interfacing physarum polycephalum with an organic semiconductor. *Apl Mater*, 3(1):014909, 2015.

[132] Simon Desbief, Michele di Lauro, Stefano Casalini, David Guerin, Silvia Tortorella, Marianna Barbalinardo, Adrica Kyndiah, Mauro Murgia, Tobias Cramer, Fabio Biscarini, and Dominique Vuillaume. Electrolyte-gated organic synapse transistor interfaced with neurons. *Org Electron*, 38:21–28, 2016.

[133] George Malliaras and Richard Friend. An organic electronics primer. *Phys Today*, 58(5):53–58, 2005.

[134] Fabien Alibart, Stéphane Pleutin, David Guérin, Christophe Novembre, Stéphane Lenfant, Kamal Lmimouni, Christian Gamrat, and Dominique Vuillaume. An organic nanoparticle transistor behaving as a biological spiking synapse. *Adv Funct Mater*, 20(2):330–337, 2010.

[135] Wentao Xu, Sung-Yong Min, Hyunsang Hwang, and Tae-Woo Lee. Organic core-sheath nanowire artificial synapses with femtojoule energy consumption. *Sci Adv*, 2(6):e1501326, 2016.

[136] Yan Lei, Yi Liu, Yidong Xia, Xu Gao, Bo Xu, Suidong Wang, Jiang Yin, and Zhiguo Liu. Memristive learning and memory functions in polyvinyl alcohol polymer memristors. *Aip Adv*, 4(7):077105, 2014.

[137] Henry S White, Gregg P Kittlesen, and Mark S Wrighton. Chemical derivatization of an array of three gold microelectrodes with polypyrrole: fabrication of a molecule-based transistor. *J Am Chem Soc*, 106(18):5375–5377, 1984.

[138] DA Bernards and GG Malliaras. SteadyState and transient behavior of organic electrochemical transistors. *Adv Funct Mater*, 17(17):3538–3544, 2007.

[139] Paschalis Gkoupidenis, Nathan Schaefer, Benjamin Garlan, and George G Malliaras. Neuromorphic functions in PEDOT:PSS organic electrochemical transistors. *Adv Mater*, 27(44):7176–7180, 2015.

[140] Paschalis Gkoupidenis, Nathan Schaefer, Xenofon Strakosas, Jessamyn A Fairfield, and George G Malliaras. Synaptic plasticity functions in an organic electrochemical transistor. *Appl Phys Lett*, 107(26):263302, 2015.

[141] Paschalis Gkoupidenis, Dimitrios A Koutsouras, Thomas Lonjaret, Jessamyn A Fairfield, and George G Malliaras. Orientation selectivity in a multi-gated organic electrochemical transistor. *Sci Rep*, 6:27007, 2016.

[142] DH Hubel and TN Wiesel. Receptive fields of single neurones in the cat's striate cortex. *J Physiology*, 148(3):574–591, 1959.

[143] DH Hubel and TN Wiesel. Receptive fields, binocular interaction and functional architecture in the cat's visual cortex. *J Physiology*, 160(1):106–154, 1962.

[144] DH Hubel and TN Wiesel. Receptive fields and functional architecture of monkey striate cortex. *J Physiology*, 195(1):215–243, 1968.

[145] David Marr. *Vision: A Computational Investigation into the Human Representation and Processing of Visual Information*. MIT Press Scholarship Online, 2010.

[146] www.isorg.fr.

[147] Simonas Krotkus, Fabian Ventsch, Daniel Kasemann, Alexander A Zakhidov, Simone Hofmann, Karl Leo, and Malte C Gather. Photopatterning of highly efficient StateoftheArt phosphorescent OLEDs using orthogonal hydrofluoroethers. *Advanced Optical Materials*, 2(11):1043–1048, 2014.

[148] Alexander Zakhidov, Jin-Kyun Lee, DeFranco, John, Hon Fong, Priscilla Taylor, Margarita Chatzichristidi, Christopher Ober, and George Malliaras. Orthogonal processing: A new strategy for organic electronics. *Chem Sci*, 2(6):1178–1182, 2011.

[149] Shiming Zhang, Elizabeth Hubis, Camille Girard, Prajwal Kumar, John DeFranco, and Fabio Cicoira. Water stability and orthogonal patterning of flexible microelectrochemical transistors on plastic. *J. Mater. Chem. C*, 4:1382–1385, 2016.

[150] Jakaria Ahmad, Kateryna Bazaka, Liam J Anderson, Ronald D White, and Mohan V Jacob. Materials and methods for encapsulation of opv: A review. *Renewable and Sustainable Energy Reviews*, 27:104–117, 2013.

[151] Julien Gaume, Pascal Wong-Wah-Chung, Agnès Rivaton, Sandrine Thérias, and Jean-Luc Gardette. Photochemical behavior of pva as an oxygen-barrier polymer for solar cell encapsulation. *RSC Advances*, 1(8):1471–1481, 2011.

[152] EE Van Dyk, A Audouard, EL Meyer, and CD Woolard. Investigation of the degradation of a thin-film hydrogenated amorphous silicon photovoltaic module. *Solar Energy Materials and Solar Cells*, 91(2):167–173, 2007.

[153] J Granstrom, JS Swensen, JS Moon, G Rowell, J Yuen, and AJ Heeger. Encapsulation of organic light-emitting devices using a perfluorinated polymer. *Applied physics letters*, 93(19):409, 2008.

[154] Jens Meyer, Patrick Görrn, Franz Bertram, Sami Hamwi, Thomas Winkler, Hans-Hermann Johannes, Thomas Weimann, Peter Hinze, Thomas Riedl, and Wolfgang Kowalsky. Al2o3/zro2 nanolaminates as ultrahigh gas-diffusion barriers—a strategy for reliable encapsulation of organic electronics. *Advanced Materials*, 21(18):1845–1849, 2009.

[155] Eddy Lay, Dong-Sing Wuu, Shih-Yung Lo, Ray-Hua Horng, Hsiao-Fen Wei, Liang-You Jiang, Hung-Uang Lee, and Yu-Yang Chang. Permeation barrier coatings by inductively coupled plasma cvd on polycarbonate substrates for flexible electronic applications. *Surface and Coatings Technology*, 205(17):4267–4273, 2011.

[156] D. Hinczewski, M. Hinczewski, F.Z. Tepehan, and G.G. Tepehan. Optical filters from SiO2 and TiO2 multi-layers using sol–gel spin coating method. *Sol Energ Mat Sol C*, 87(1-4):181–196, 2005.

[157] Manuella Russo. Titanium oxide hydrates: Optical properties and applications, 2009.

[158] Karl Deisseroth. Optogenetics. *Nat Methods*, 8(1):26–29, 2010.

[159] Tae-il Kim, McCall, Jordan G, Yei Jung, Xian Huang, Edward R Siuda, Yuhang Li, Jizhou Song, Young Song, Hsuan Pao, Rak-Hwan Kim, Chaofeng Lu, Sung Lee, Il-Sun Song, GunChul Shin, Al-Hasani, Ream, Stanley Kim, Meng Tan, Yonggang Huang, Fiorenzo G Omenetto, John A Rogers, and Michael R Bruchas. Injectable, Cellular-Scale optoelectronics with applications for wireless optogenetics. *Science*, 340(6129):211–216, 2013.

[160] Francis Crick. The impact of molecular biology on neuroscience. *Philosophical Transactions Royal Soc Lond B Biological Sci*, 354(1392):2021–2025, 1999.

[161] Massimo Scanziani and Michael Häusser. Electrophysiology in the age of light. *Nature*, 461(7266):930–939, 2009.

[162] Edward S Boyden, Feng Zhang, Ernst Bamberg, Georg Nagel, and Karl Deisseroth. Millisecond-timescale, genetically targeted optical control of neural activity. *Nat. Neurosci.*, 8(9):1263–8, 2005.

[163] Kay Tye, Julie Mirzabekov, Melissa Warden, Emily Ferenczi, Hsing-Chen Tsai, Joel Finkelstein, Sung-Yon Kim, Avishek Adhikari, Kimberly Thompson, Aaron Andalman, Lisa Gunaydin, Ilana Witten, and Karl Deisseroth. Dopamine neurons modulate neural encoding and expression of depression-related behaviour. *Nature*, 493(7433):537–541, 2012.

[164] Melissa Warden, Jessica Cardin, and Karl Deisseroth. Optical neural interfaces. *Annu Rev Biomed Eng*, 16(1):103–129, 2014.

[165] Andre Berndt and Karl Deisseroth. Expanding the optogenetics toolkit. *Science*, 349(6248):590–591, 2015.

[166] R. Pashaie, P. Anikeeva, Jin Lee, R. Prakash, O. Yizhar, M. Prigge, D. Chander, T.J. Richner, and J. Williams. Optogenetic brain interfaces. *Ieee Rev Biomed Eng*, 7:3–30, 2014.

[167] Sung Park, Daniel Brenner, Gunchul Shin, Clinton Morgan, Bryan Copits, Ha Chung, Melanie Pullen, Kyung Noh, Steve Davidson, Soong Oh, Jangyeol Yoon, Kyung-In Jang, Vijay Samineni, Megan Norman, Grajales-Reyes, Jose, Sherri Vogt, Saranya Sundaram, Kellie Wilson, Jeong Ha, Renxiao Xu, Taisong Pan, Tae-il Kim, Yonggang Huang, Michael Montana, Judith Golden, Michael Bruchas, IV, Robert, and John Rogers. Soft, stretchable, fully implantable miniaturized optoelectronic systems for wireless optogenetics. *Nat Biotechnol*, 33(12):1280–1286, 2015.

[168] György Buzsáki, Eran Stark, Antal Berényi, Dion Khodagholy, Daryl R Kipke, Euisik Yoon, and Kensall D Wise. Tools for probing local circuits: high-density silicon probes combined with optogenetics. *Neuron*, 86(1):92–105, 2015.

[169] Polina Anikeeva. Optogenetics unleashed. *Nat Biotechnol*, 34(1):43–44, 2016.

[170] Markus Fröbel, Tobias Schwab, Mona Kliem, Simone Lenk, Karl Leo, Sebastian Reineke, and Malte C Gather. 32: Invited paper: Color on demand – ColorTunable OLEDs for lighting and displays. *SID Symposium Digest of Technical Papers*, 48(1):5–8, 2017.

Acronyms

$PC_{60}BM$ [6,6]-Phenyl C61 butyric acid methyl ester. x, 13, 14, 21, 25, 26, 30, 51

$PC_{70}BM$ [6,6]-Phenyl C70 butyric acid methyl ester. x, 13, 14, 21, 33, 34, 36, 37, 51

4-AP 4-aminopyridine. 25, 27

ACSF artificial cerebrospinal fluid. 41, 42

Al aluminum. 18, 25, 36, 37

Au gold. 25, 45

BHJ bulk heterojunction. 11, 14, 16, 20, 37

Ca calcium. ix, x, 10, 20, 21, 24, 36–41, 55

CCD charge-coupled device. ix, 9, 10, 24, 34

CMOS metal-oxide-semiconductor. ix, 9, 34

Cr chromium. 45

CVR cell volume regulation. 24–26, 28, 55

D-A donor-acceptor. 11, 14–20, 51, 53

DCD dark current density. ix, x, 20, 21

EA electron affnity. 11

HOMO highest occupied molecular orbital. 11, 16

I-V current-voltage. 16

ILED inorganic light-emitting diode. 55, 57

IOS intrinsic optical signal. 24–30, 51, 55, 59

IP ionization potential. 11

IPD inorganic photodetector. 57

ITO indium tin oxide. 14, 18, 36, 41

K potassium. 5, 10, 24, 37, 38

KCL potassium chloride. 36–38

LDR linear dynamic range. x, 19, 20

LED light emitting diode. 45–48

LFP local field potential. 6, 7, 25–29, 31, 36, 38–40, 42, 55

LGN lateral neniculate nucleus. 7, 8, 46

LUMO lowest unoccupied molecular orbital. 11, 16

Na sodium. 5–7, 10

NaCl sodium chloride. 41, 42, 45

OECT organic electrochemical transistor. x, 43–48

OLED organic light-emitting diode. 52, 56, 58, 59

OPD organic photodetector. ix, x, 11–21, 23–30, 33–41, 43, 45–48, 51–53, 55–59

P3HT poly(3-hexylthiophene-2,5-diyl). x, 12, 21, 25, 26, 30, 51–53

PBS phosphate buffered saline. 42

PCE power conversion efficiency. 11

PEDOT poly(3,4ethylenedioxythiophene). 12–14, 18, 36, 41, 43, 45, 52, 53

PEIE polyethylenimine ethoxylated. 15, 20, 53

PSS poly(styrene sulfonate). 12–14, 18, 36, 41, 43, 45, 52, 53

RF receptive field. 7, 8

SMU source measure unit. 46

XPL6 eXtra Large Bandgap Polymer. x, 12, 21, 33, 34, 36, 37, 41, 51

Scientific Contributions

- **Rezaei-Mazinani S.**, Ivanov A.I., Rutz, AL., Chochos, C.L., Bernard, C., Malliaras, G.G., O'Connor, R., & Ismailova E. (**2017**). Monitoring fluorescent calcium signals in brain tissue with high performance organic photodetectors. *Advanced Materials*, In prepration

- **Rezaei-Mazinani S.**, Ivanov A.I., Proctor C. M., Gkoupidenis P., Bernard C., Malliaras G. G. & Ismailova E. (**2017**). Monitoring intrinsic optical signals in brain tissue with organic photodetectors. *Advanced Materials*, Submitted

- Gkoupidenis P.*****, **Rezaei-Mazinani S.***, Proctor C. M., Ismailova E. & Malliaras G. G. (**2016**). Orientation selectivity with organic photodetectors and an organic electrochemical transistor. *AIP Advances*, 6(11), 111307 - ***** *Authors contribute equally to this work.*

- Papaiordanidou M., Takamatsu S., **Rezaei-Mazinani S.**, Lonjaret T., Martin A., & Ismailova E. (**2016**). Cutaneous Recording and Stimulation of Muscles Using Organic Electronic Textiles. *Advanced Healthcare Materials*